Copyright

by

Yida Gao

2020

The Dissertation Committee for Yida Gao Certifies that this is the approved version of the following dissertation:

Insights into Cell Loss Processes of Toxic Dinoflagellate *Karenia brevis*

Committee:

Deana L. Erdner, Supervisor

Brett Baker

Lisa Campbell

Andrew Esbaugh

Tracy Villareal

Insights into Cell Loss Processes of Toxic Dinoflagellate *Karenia brevis*

by

Yida Gao

Dissertation

Presented to the Faculty of the Graduate School of

The University of Texas at Austin

in Partial Fulfillment

of the Requirements

for the Degree of

Doctor of Philosophy

The University of Texas at Austin

December 2020

Dedication

This work is dedicated to my parents. You make me feel loved, you make me brave, you make me a better person.

Acknowledgements

First of all, I want to give my big thank to my advisor, Dr. Deana Erdner. She is such an amazing advisor who provided me invaluable guidance and support that developed my skill set, independent thinking and passion for chasing career in science. I am also really inspired by her positiveness, kindness, and resolution at work and life. I appreciate the help from every current and previous members of Erdner Lab (Yesid Lozano-Duque, Ingrid Sassenhagen, Tatiana Severin, Liz Murphy, Royoung Park, Lun Wang, Amanda Alva, Chang-Jae Choi, Taylor Krilanovich and Kylie Holt), especially thank Tatiana Severin for her instructions in photosynthetic analysis and thank Taylor Krilanovich for her help in the development of qPCR method. I am grateful to Meizhen Li from Mcgill University for her help in cell cycle analysis. I thank Dr. Lisa Campbell for providing all the *Karenia brevis* strains used in my research. I thank Dr. Tracy Villareal for giving guidance and equipment for the photosynthetic analysis. I am very grateful for the guidance and comments provided by my committee members (Drs. Brett Baker, Lisa Campbell, Andrew Esbaugh and Tracy Villareal) throughout these years. My journey of PhD study may be somehow different from some other people because of Hurricane Harvey, relocation, rebuild and the current COVID-19 Pandemic. I am very grateful to those people who gave me a hand and supported me moving forward. I thank Heather Herrick and Audrey Timkovich for generously providing me a home when I was homeless after Hurricane Harvey. I thank Dr. Paul Zimba for hosting me in his lab in TAMUCC for nine months to continue my research. I thank Bum-Soo Park and Wade Huang for helping me recover my experiments. And of course, I thank Dr. Erdner for her strong and wise leadership in our lab's rebuilding process. This dissertation work is funded by NOAA-ECOHAB (NA18NOS4780168). I am grateful

for the UTMSI departmental fellowships and the UTMSI travel awards for supporting my work and opportunities to attend scientific meetings. Last but not the least, I thank all faculties, staffs and students from UTMSI for helping me get through difficult times and creating such a warm and friendly working and living environment.

Abstract

Insights into Cell Loss Processes of Toxic Dinoflagellate *Karenia brevis*

Yida Gao, Ph.D.

The University of Texas at Austin, 2020

Supervisor: Deana L. Erdner

Karenia brevis is responsible for annual harmful algal bloom (HAB) events in the Gulf of Mexico (GoM). Although the factors regulating the initiation of *K. brevis* blooms have been extensively investigated, the mechanisms leading to bloom decline and termination are not well known. Understanding the triggers of bloom decline could enhance our ability to forecast bloom dynamics and their impact on coastal areas. Microzooplankton grazing and programmed cell death (PCD) have been recognized as important pathways for the loss of phytoplankton biomass. However, neither of these two factors has been comprehensively examined in *K. brevis*. My dissertation work describes mechanisms of intrinsic cell death in response to environmental stress and develops methods to evaluate microzooplanton grazing pressure on *K. brevis* in the field. In Chapter 2, I confirmed the existence of PCD in *K. brevis* using oxidative stress as a model trigger. Acute susceptibility to oxidative stress increased as cultures aged, while the youngest cultures showed the fastest overall rate of cell loss within the first 24 hours. In untreated cells, the prevalence of components in the PCD cascade were not related to cell death, but fluctuated not only between growth phases but also over a diel cycle. Given that *K. brevis* likely experiences

drastic environmental change during bloom season in the GoM, cell death processes in response to high light, hypo-osmotic, cooling and heat stress were described in Chapters 3 and 4. PCD in *K. brevis* only occurred at the largest light shift (50 to 1000 µmol m^{-2} s^{-1}), along with induction of non-photochemical quenching which may enable cells to resist or delay PCD. Intensity-dependent induction of PCD cascade occurred when salinity decreased by 5, 10, or 15 psu, while cell death was only evident after 15 ℃ temperature change. Lastly, in Chapter 5 I describe the development of a quantitative real-time PCR method that can be used to measure species-specific grazing pressure on *K. brevis*. Overall, this work adds to our knowledge of cell loss processes in phytoplankton in general as well as insights into the effects of abiotic and biotic factors on the decline and termination of *K. brevis* blooms specifically.

Table of Contents

List of Tables

List of Figures

Chapter 1: Introduction

Karenia brevis is responsible for frequent harmful algal bloom (HAB) events in the Gulf of Mexico (GoM). They can produce brevetoxins which are the cause of neurotoxic shellfish poisoning (NSP), a type of biological intoxication (Plakas & Dickey, 2010). NSP can result in animal death, human sickness, and local economic decline from fishery and tourism industries (Brand et al., 2012). Molluscs serve as an important vectors of NSP, because they are active filter-feeders that can ingest a large number of planktonic organisms (Landsberg et al., 2009). As a result of the constant filtration and digestion of toxic dinoflagellates, a large amount of toxin is concentrated in their fatty tissues (Landsberg et al., 2009). However, NSP contamination has also been observed in non-filter feeding molluscs (Poli et al., 2000) and fish (Naar et al., 2007). Humans become intoxicated by eating contaminated seafood, and the main symptoms are abdominal pain and vomiting (Fleming et al., 2011). Besides human illness, *K. brevis* HABs can cause mass mortalities of marine animals (i.e. fish, seabirds, invertebrates, turtles and mammals) not only by toxicity, but also via anoxia due to degradation of dense blooms (Landsberg et al., 2009).

Given *K.brevis'* detrimental effects on marine ecosystems and human beings, significant attention has been paid to understanding the initiation of *K. brevis* blooms in GoM, for example the convergent bloom hypothesis (Hetland & Campbell, 2007) and Saharan dust hypothesis (Walsh et al., 2006). In contrast, much less is known of the mechanisms of bloom decline and termination of *K. brevis*. However, this knowledge is important as they can greatly improve our forecast ability on bloom development and their impact on coastal areas. Imbalances between growth and loss processes of phytoplankton influences the dynamics of blooms, and bloom decline occurs when loss processes are more

dominant than growth (Choi et al., 2017). The factors involved in cell loss processes are diverse and still poorly understood. Before the end of the 20th century, it had been thought that phytoplankton would live an immortal life by binary fission until being consumed or sunk into deep ocean by downwelling (reviewed by Bidle & Falkowski, 2004). Indeed, grazing from zooplankton has been implicated not only in prevention of HAB initiation, but also in HAB termination in many places (reviewed by Turner, 2006). However, observations of massive cell lysis in the field indicate that multiple processes contribute to cell loss of phytoplankton (Berges & Choi, 2014; Choi et al., 2017; Vardi et al., 1999). Programmed cell death (PCD), an autocatalytic process that includes a number of genetically-regulated and self-destruction pathways, can be induced by adverse conditions like viral attack, heat shock and nutrient starvation in many marine algal species (Bidle & Bender, 2008; Bidle et al., 2007; Zuppini et al., 2007). PCD in *Alexandrium cantenalla*, a HAB species prevalent at worldwide temperate waters, could account for up to 14% of cell loss per day during bloom decline (Choi et al., 2017). In addition, increasing evidence has shown an important role of parasitic infections in controlling phytoplankton populations (Chambouvet et al., 2008; Choi et al., 2017). In HAB species with haplo-diploid life history, at least 10% of bloom decline can be attributed to sexual encystment (Brosnahan et al., 2017). Understanding the triggering conditions and mechanisms of these cell loss processes in *K. brevis* would elucidate the driving forces of bloom dynamics and strengthen our ability to forecast the end of blooms. With these purposes, in my dissertation two main cell loss processes - cell death and grazing on *K. brevis* - were investigated under environmental conditions relevant to the GoM.

CELL DEATH IN PHYTOPLANKTON

Classification of cell death within microalgae is still a matter of debate (Berges & Choi, 2014). However, most cell death events observed from previous research can be broadly categorized as either necrosis or PCD (Berges & Choi, 2014; Bidle, 2016). Necrosis is usually the direct effect of physical or mechanical stress on a cell, e.g. heat and freeze-thawing, that cause acute and irreversible cellular injury (Krysko et al., 2008; Vavilala et al., 2015). Morphologically, this cell death mode is characterized by swelling of the plasma membrane and DNA strand breaks (Golstein & Kroemer, 2007; Laporte et al., 2007). PCD is comprised by a variety of intrinsic autocatalytic pathways including *apoptosis*, *paraptosis*, *aponecrosis*, *autophagy* and *ferroptosis* which are defined by particular morphological and biochemical changes as well as occurrence under certain circumstances (reviewed by Bidle, 2016). Among them, apoptosis is the most common cell death mode observed in microalgae, and is characterized by caspase activity, DNA fragmentation and phosphatidylserine (PS) translocation in the cell membrane (Berges & Choi, 2014; Jimenez et al., 2009; Leist & Jäättelä, 2001). The benefit of PCD for phytoplankton cells is still a topic of debate. It has been hypothesized that PCD may be used as a strategy to relieve nutrient stress, limit virus attack, or maximize genetic fitness at a community level even if the consequence is the loss of individual organisms (Bidle & Falkowski, 2004; Franklin et al., 2006).

The concept and definition of the PCD pathway originated from metazoan system, prior to reports of PCD in phytoplankton, bacteria and archaea (Deponte, 2008; Taylor-Brown & Hurd, 2013; Vardi et al., 1999). In metazoan systems, all stimuli that induce apoptosis seem to do so by activating caspases (Cysteine-dependent ASPartic acid proteASES), a series of key metazoan enzymes that strengthen signaling throughout the PCD pathway (Kanduc et al., 2002; Taylor et al., 2008). Caspases have a conserved

catalytic structure containing histidine and cysteine, and cleave after aspartate residue on various substrate proteins (Boyce et al., 2004; Cohen, 1997; Nicholson & Thornberry, 1997). In metazoans, elevated caspase activities can induce apoptotic changes (Taylor et al., 2008). For example, caspase-mediated cleavage of nuclear lamins precedes DNA fragmentation and subsequent cell death (Rao et al., 1996; Taylor et al., 2008). The general patterns of PCD in metazoans and phytoplankton share similar enzymatic activities and the corresponding morphological changes. In many microalgal species, increases of caspase-like enzyme activity, measured by the cleavage rate of canonical caspase substrates, is found to be associated with cell death under environmental stress (Bouchard & Purdie, 2011; Darehshouri et al., 2008; Dingman & Lawrence, 2012; Segovia & Berges, 2009; Vardi et al., 1999; Zuppini et al., 2007). For example, Zuppini et al. (2007) reported the occurrence of cell death with caspase-like activity under heat shock in the green alga *Chlorella saccharophila*, while caspase inhibitors provided significant protection against this heat-induced cell death. Since no caspase enzymes with aspartic acid cleaving specificity have been identified in any phytoplankton species, it is still unknown about the specific executioners of the caspase-like activities (Berges & Choi, 2014; Johnson et al., 2014). A few types of metacaspases, orthologues of caspase, have been identified in phytoplankton (Choi & Berges, 2013), while they are not believed to be responsible for the caspase-like activity, as metacaspases mainly cleave after arginine and lysine (Berges & Choi, 2014).

With the development of molecular and computational tools, a PCD cascade that starts with ROS (Reactive Oxygen Species) signaling has been gradually revealed (Bidle, 2016). In this pathway, a variety of environmental stresses (e.g. temperature, salinity and high light) enhance intracellular production of ROS like hydrogen peroxide (H_2O_2), superoxide (O^{2-}) and singlet oxygen (O_2*) by disrupting homeostasis of metabolic

processes (photosynthesis and respiration; Bidle, 2016; Miller et al., 2010; Suzuki et al., 2012; Suzuki & Mittler, 2006). This stress-generated ROS and the ROS actively produced by Rboh (respiratory burst oxidative homolog) will be sensed within the cell and activate a variety of antioxidant enzymes (ROS scavengers) to restore intracellular redox balance (N. Suzuki & Mittler, 2006). Under oxidative stress the expression of a ROS scavenger-ascorbate peroxidase (APX) and the change of the ratio of its catalytic metabolite products can paradoxically weaken cells against subsequent ROS bursts and elicit PCD via caspase activity (Murik et al., 2014; Murik & Kaplan, 2009). In the dinoflagellate *Peridinium gatunense* cell death concomitant with ROS and caspase-like activity is induced by CO_2 limitation, while the addition of catalase greatly reduces mortality suggesting the role of ROS as a PCD inducer (Vardi et al., 1999). However, the detailed steps between ROS and the activation of caspase-like activity in microalgae is still far from clear.

Apart from their roles in the PCD cascade, ROS and caspase-like enzyme activity may also be involved in cellular metabolic processes in phytoplankton. Enhanced production of ROS has been observed during active growth of microalgae, which may be due to increased mitochondrial or chloroplastic activity (Kim et al., 2004; Portune et al., 2010; Twiner & Trick, 2000). A constitutive caspase-like activity has been observed in many microorganisms, and it may perform housekeeping functions including protein turnover, cell cycle progression and cell division (Jauzein & Erdner, 2013; Seth-pasricha et al., 2013). For example, in *A. tamarense* the increase of caspase-like activity in the dark phase during exponential growth suggests non-death roles in cell cycle regulation or cell proliferation (Jauzein & Erdner, 2013). Fluctuation of caspase-like activity observed in *K. brevis* under controlled conditions also supports its role in housekeeping functions (Bouchard & Purdie, 2011; Johnson et al., 2014).

PCD AND ENVIRONMENTAL STRESS

The induction of PCD in microalgae is closely related to environmental stress, and therefore it may be an important cell loss process during algal blooms. So far, external stress from irradiance, temperature, salinity and nutrients have been reported to trigger apoptosis in microalgae (Berman-Frank et a., 2004; Bidle & Bender, 2008; Vardi et al., 1999; Zuppini et al., 2007; Zuppini et al., 2010). Although Johnson et al. (2014) observed PCD in *K. brevis* after the addition of H_2O_2, it is still not clear which environmental stressors can cause cell death in *K. brevis*. During bloom season in the GoM (August to December), sea surface irradiance (> 1000 µmol m^{-2} s^{-1}) and sporadic freezing events may expose *K. brevis* surface populations to strong high light and temperature stress, respectively. Cells can also be transported between inshore and offshore areas repeatedly causing *K. brevis* populations to experience drastic salinity shifts (Errera, 2013). Since phytoplankton are in direct contact with their surroundings, variation of these environmental factors would significantly affect physiological status of cells and potentially lead to cell death (Bidle & Falkowski, 2004). Therefore, I aimed to (1) identify the types and intensities of environmental stress that can cause cell death in *K. brevis*; (2) elucidate stress-related cell death pathways; (3) gain insights into potential effects of intrinsic cell death in bloom decline and termination of *K. brevis*; (4) understand non-death roles and behavior of ROS and caspase-like activity during normal growth of *K. brevis*.

GRAZING EFFECTS ON *K. BREVIS*

While microzooplankton grazing is considered as an important cell loss process in the termination of HABs (reviewed by Turner, 2006), this top-down control has not been quantified in *K. brevis* blooms. Microzooplankton (e.g. heterotrophic dinoflagellates and

ciliates) may exert greater impact on bloom populations than the mesozooplankton community (e.g. copepods) due to the higher growth rates of microzooplankton grazers that can be comparable to those of their prey species (Strom & Morello, 1998). Many previous studies have reported the removal of more than 50% of the targeted species by microzooplankton during bloom events (Matsuyama et al., 1999; Kamiyama & Matsuyama, 2005; Nakamura et al., 1996). In the GoM, predation on *K. brevis* by heterotrophic dinoflagellate and ciliates was observed at the onset of bloom using PCR with species-specific primers (Campbell, 2012). However, *K. brevis* may be able to escape from microzooplankton grazing due to its nutritional inadequacy (Breier & Buskey, 2007) and excretion of chemical compounds (Kubanek et al, 2007; Waggett et al., 2012). In the laboratory environment the heterotrophic dinoflagellates *Protoceratium sp.* and *Noctiluca scintillans* exhibited negative growth rates when given *K. brevis* as the sole diet, while *K. brevis* experienced enhanced growth in the cultures with *Protoceratium* sp. (Campbell, 2012). Selective grazing on HAB species vs other co-occurring phytoplankton species may determine if the nascent HAB bloom is controlled by or released from top-down control (Sieracki et al., 2004; Stoecker et al., 2008; Turner, 2006). Therefore, it is necessary to compare microzooplankton grazing pressure on *K. brevis* vs. the whole phytoplankton community at different stages of blooms to evaluate the effects of this cell loss processes on bloom dynamics.

An ideal quantification method for measuring grazing pressure on *K. brevis* would have both high species-specificity and low detection limit. Quantitative real-time polymerase chain reaction (qPCR) has been used for quantification of target HAB species with high specificity and sensitivity (1 cell/L) in the field (Coyne et al., 2005; Erdner et al., 2010; Hariganeya et al., 2013; Kon et al., 2017). Given to the morphological similarities among species in genus *Karenia* and low cell densities of *K. brevis* at some stages of

blooms (Haywood et al., 2007), qPCR is a promising method that would increase the accuracy of measuring microzooplankton grazing pressure on *K. brevis* in the field.

RESEARCH OBJECTIVES

K. brevis's interactions with the abiotic and biotic environment have the potential to induce cell loss processes leading to bloom decline and termination. This work describes mechanisms of intrinsic cell death in response to environmental stress and evaluated microzooplankton grazing pressure on *K. brevis*. In chapter 2, I evaluated whether susceptibility to stress-induced PCD varies as cultures age in *K. brevis* and characterize the variability of ROS and caspase-like activity during normal growth over both the full course of culture growth and diel cycles. In chapter 3, I investigated photosynthetic performance and stress-related death processes in response to different levels of acute high light stress. In chapter 4, cell death responses to acute hypo-osmotic, cooling and heating stress in *K. brevis* were examined. Potential effects of these environmental changes on the decline and termination of *K. brevis* blooms were discussed. In chapter 5, a qPCR method was developed for sensitive and species-specific quantification of *K. brevis*, and a mock grazing experiment was conducted at the Aransas Pass Ship Channel to quantify and compare grazing pressure on *K. brevis* and the community as a whole. Ultimately, this work will lead to better understanding of cell loss process during *K. brevis* bloom and enhance our ability to predict bloom dynamics to the benefit of management agencies and coastal communities.

Chapter 2: Insights into stress-related death processes at different growth stages and variation of stress markers under normal growth in toxic dinoflagellate *Karenia brevis*

ABSTRACT

During recent years, increasing evidence suggests that programmed cell death (PCD) may play an important role in the decline and termination of phytoplankton blooms. For the toxic dinoflagellate *Karenia brevis*, the role of PCD as a response to environmental stress is still largely unknown. In the absence of exogenous stress, components of the PCD cascade may serve signaling or housekeeping functions in *K. brevis*. In this study we aimed to (1) evaluate susceptibility to stress-induced PCD during culture growth, and (2) characterize the variability of stress and death markers under replete culture conditions during both the full course of culture growth and diel cycles. Specifically, I examined the prevalence of PCD markers during 48 hours with/without the addition of the strong oxidant H_2O_2 in *K. brevis* cultures at early-log, mid-log and stationary phase. Replete cultures under either 12:12 light:dark cycle or continuous light were sampled every four hours for two consecutive days for comparing diel stress responses and cell cycle patterns. The results showed that acute susceptibility to oxidative stress increased as cultures aged, which may reflect a decrease in cell defense abilities. However, the youngest cultures showed the fastest overall rate of cell loss within the first 24 hours, hypothesized to result from cell density-dependent H_2O_2 detoxifying process. In untreated cells, the prevalence of ROS and caspase-like activity fluctuated not only between growth phases but also over a diel cycle, supporting their role in cellular metabolism and housekeeping functions. The diel pattern of ROS prevalence was under circadian control and may be due to circadian rhythm of antioxidant enzymes. This research highlights the multiple roles of ROS and caspase-like

activity in death and non-death cellular responses in phytoplankton as well as the importance of understanding mechanisms controlling their accumulation.

INTRODUCTION

The HAB-forming toxic dinoflagellate *Karenia brevis* has a profound impact on the ecosystem and economy of the coastal Gulf of Mexico (GoM; Vargo, 2009). Most studies of *K. brevis* has focused on toxicity and mechanisms of bloom development, while the processes leading to bloom decline are far less understood (Johnson et al., 2014). It had been long assumed that phytoplankton would reproduce constantly by binary fission unless consumed by zooplankton grazers or sunk into the deep ocean (reviewed by Bidle & Falkowski, 2004). However, increasing evidence suggests that programmed cell death (PCD), which refers to a variety of genetically-controlled forms of cell suicide, may play an important role in decline and termination of phytoplankton blooms (Bidle, 2016; Choi et al., 2017; Vardi et al., 1999). Among the different modes of PCD, apoptosis is characterized by involvement of caspase-like activity, DNA fragmentation, and inversion of phosphatidylserine in the cell membrane (Bidle, 2016; Kerr et al., 1972).

In marine algal species, PCD pathways are induced by various adverse conditions like CO_2 limitation, high salinity, light deprivation and iron starvation (Bidle & Bender, 2008; Franklin & Berges, 2004; Jiménez et al., 2009; Vardi et al., 2008). A common feature of these biotic and abiotic stress-induced PCD processes is an increase in intracellular reactive oxygen species (ROS) which can elicit caspase-like activity and lead to cell death (Bidle, 2016; Gechev & Hille, 2005). The most common ROS include hydrogen peroxide (H_2O_2), singlet oxygen and superoxide radical (Apel & Hirt, 2004). Various stresses cause a burst of ROS production through different mechanisms (reviewed by Bidle, 2016).

For example, decreased CO_2 during bloom development of the dinoflagellate *Peridinium gatunense* is thought to induce the transfer of photosynthetic electrons from CO_2 fixation to oxygen, causing ROS production and triggering the PCD pathway (Butow et al., 1997). The addition of catalase, which specifically detoxifies H_2O_2, inhibits cell death under the stress of CO_2 depletion, implicating H_2O_2 as an active ROS (Vardi et al., 1999).

In the laboratory environment, exogenous H_2O_2 is a classic stimulus to conveniently and controllably induce cellular stress responses, and has been widely used to trigger and characterize the PCD process in cyanobacteria, green algae and dinoflagellates (Bouchard & Purdie, 2011; Darehshouri et al., 2008; Ding et al., 2019; Jauzein & Erdner et al., 2013; Vavilala et al., 2015). The only research of stress-induced PCD in *K. brevis* was conducted by Johnson et al. (2014) who observed a small increase of mortality (less than 5%) with a drastic rise in ROS occurrence, caspase-like activity and DNA fragmentation after 10 mins incubation with 80 μM H_2O_2. Since the metabolic state and stress acclimation ability of *K. brevis* may change significantly as cultures age (Johnson et al., 2012), their cell death responses under stress may vary depending on growth stage. In addition, given the potential for a lagged cell death reaction by days to oxidative stress observed in other dinoflagellates (Jauzein & Erdner, 2013), experiments with a longer time scale would be beneficial to comprehensively understand cell death responses.

Beside their functions in PCD cascade, ROS and caspase-like activity also serve non-death roles in the cell. In plants, ROS are continuously generated from metabolic activities in chloroplasts, mitochondria and peroxisomes (Apel & Hirt, 2004; Diaz & Plummer, 2018). While it is widely known that excessive accumulation of ROS can cause severe cellular damages (i.e. alteration of lipids, proteins and DNA) and cell death, lower levels of ROS are critical for redox signaling and the maintenance of physiological function in cells (Schieber & Chandel, 2014; Suzuki & Mittler, 2006). Increasing evidence has also

shown an active involvement of caspase-like activity in proteostasis and stress acclimation in phytoplankton (Johnson et al., 2012; Johnson et al., 2014; Thamatrakoln et al., 2012) and archaea (Bidle et al., 2010; Seth-Pasricha et al., 2019). Background expression of ROS and caspase-like activity have also been observed at different growth stages in phytoplankton cultures maintained under replete conditions (Bidle & Bender, 2008; Bouchard & Purdie, 2011; Johnson et al., 2014; Thamatrakoln et al., 2012). Most previous experiments only sampled once or twice a day to analyze expression of these stress markers in untreated cultures. However, diel variation of ROS and caspase-like activity may also exist. Intracellular accumulation of ROS may be regulated by antioxidant enzymes which have shown robust diurnal rhythms in phytoplankton (Okamoto et al., 2001a); caspase-like activity is also suggested to be involved in cell proliferation which often occurs at night and is closely associated with daily cell cycle pattern (Algeciras-Schimnich et al., 2002; Jauzein & Erdner, 2013; Bouchard & Purdie, 2011; Taroncher-Oldenburg et al., 1997). Understanding diel variation of ROS and caspase-like activity in phytoplankton may provide insights into their housekeeping functions.

The objectives of this research were to: (1) confirm the existence of PCD in *K. brevis* and evaluate whether susceptibility to stress-induced PCD varies as cultures age in *K. brevis*; and (2) characterize the variability of the prevalence of ROS and caspase-like activity during normal growth over both the full course of culture growth and diel cycles. Here I examined the prevalence of ROS, caspase-like activity, and cell death during 48 hours with/without the addition of the strong oxidant H_2O_2 in *K. brevis* cultures at early-log phase, mid-log phase and stationary phase. In order to understand diel variation of these markers, *K. brevis* cultured under either 12:12 light:dark cycle (L:D) or continuous light were sampled every four hours for two consecutive days in order to compare stress responses and cell cycle patterns. Our results show that oxidative stress can trigger the PCD

cascade in *K. brevis* and that susceptibility changes as the culture ages. In untreated cells, the prevalence of ROS and caspase-like activity varied across growth and over the diel cycle. Death and non-death roles of ROS and caspase-like activity in *K. brevis* are discussed, including potential mechanisms driving the diel variations of stress markers.

METHODS

Culture conditions and experimental setup

Growth stages

K. brevis clone SP3 was isolated by Suzanne Pargee from a red tide offshore of South Padre Island, Texas in 1999 (Magaña & Villareal, 2006). On Day 1, strain SP3 was inoculated at a starting density of 300 cells/ml into 2300 ml L1 medium made from seawater collected offshore in the GoM. The seawater was filtered through 0.2 um polycap capsule filter (Whatman Inc.), adjusted to a salinity of 32 psu and autoclaved prior to the addition of sterile L1 nutrient stocks. The culture was maintained at an irradiance level of 90 µmol m^{-2} s^{-1} on a 12:12 L:D with cool white fluorescent bulbs inside a 25°C PERCIVAL incubator. When the concentration of cells reached ~1000 cells/ml, 120 ml of culture was dispensed into 18 small flasks. These flasks were designated in triplicate as "early-log treatment", "early-log control", "mid-log treatment", "mid-log control", "stationary treatment" and "stationary control". Another flask with 120 ml of culture was inoculated at the same time and maintained under controlled environment, and its cell densities were used as an indicator for the growth stages in other flasks (Fig. A1 in Appendix A). Specifically, cell densities of approximately 3000 cells/ml, 8000 cells/ml and 18000 cells/ml in this flask indicated that the batch cultures were in early-log, mid-log and

stationary stages, respectively. The cell densities corresponding to each growth stage were based on previous growth curves of SP3 cultures incubated under the same environmental conditions.

Oxidative stress was induced by addition of 180 μM H_2O_2 (calculated final concentration) to early-log treatment, mid-log treatment and stationary treatment cultures on Day 9), Day 14 and Day 21, respectively. The level of H_2O_2 addition was chosen from a preliminary test as a dose that caused death in some of cells but did not obliterate them rapidly. Since H_2O_2 is prone to decompose at room temperature, the stock solution of H_2O_2 was dispensed into aliquots immediately after opening, and the aliquots were kept in frozen until shortly before the beginning of experiment. The addition of H_2O_2 occurred at time 0h, and Treatments and their corresponding Controls were sampled at 0.5h, 6h, 24h, 30h and 48h after H_2O_2 addition for measurement of cell density and percentages of cells staining for SYTOX, ROS and caspase-like activity.

Cell cycle

K. brevis was cultured under different light cycles and sampled for cellular stress responses and cell cycle patterns. Two, 2000 ml cultures of SP3 starting at 500 cells/ml were grown as described under "Growth Stages" above with the exception of light conditions: one was under 12:12 L:D, the other one was under continuous light. For each of them, when the concentration of cells reached ~2000 cells/ml, 50 ml of algal liquid was dispensed into 36, 100 ml tissue flasks. Flasks were grouped into 12 sets of 3, allowing triplicate samples to be taken at every 4 hours during two diel cycles. When cultures were in log phase under 12:12 light cycle, the first sample was taken at 2 hours after the beginning of light phase (time 2h). For "continuous light experiment", sampling started after being exposed to continuous light for 7 days, and their sampling time shared the same

clock hours with the ones in "12:12 L:D" experiment. In these two experiments, we measured cell density, percentages of cells with SYTOX, ROS and caspase-like activity as well as the percentages of cells in each cell cycle phase at every sampling point.

Measurement of stress and cell death markers

Three cellular parameters were measured by fluorescent dyes as described below: SYTOX, ROS and caspase-like activity. All reagents produced green fluorescence which was observed under the epifluorescent microscope with an excitation wavelength of 450–490 nm and emission of 523 nm. More than 50 cells were counted and examined, in replicate from each culture vessel, by using a Sedgewick Rafter chamber under a fluorescent microscope.

Cell death detection

Integrity of the cell membrane, which is an indicator of cell death, was determined using SYTOX-green dye (S7020, Invitrogen). This reagent has high affinity with nucleic acid and can only penetrate compromised plasma membranes. An aliquot of stock solution (5 mM in DMSO) was diluted into Phosphate-Buffered Saline (PBS) to prepare a 100 μM working solution. A 2.5 μl aliquot of the working solution then added directly to 500 μl of algal culture sample, making the final concentration of SYTOX-green dye 0.5 μM. Observations of SYTOX-stained cells were conducted after 60 min of dark incubation at room temperature. SYTOX percentages were calculated as: the number of cells with green fluorescence/ total cell number.

ROS production

Intracellular ROS was detected by using carboxy-H_2DCFDA (C400, Invitrogen). For preparing stock solution, 2 mg of carboxy-H_2DCFDA were dissolved in DMSO to yield a concentration of 10 mM. Before the experiment, PBS was used to prepare working solution by diluting an aliquot of stock solution to 100 μM. The working solution then mixed with algal sample at a 1:10 ratio, for a 10 μM final concentration of carboxy-H_2DCFDA. Green fluorescence generating from the oxidation of carboxy-H_2DCFDA was examined after 20 min dark incubation at room temperature. Percentages of cells with ROS were calculated as: the number of cells with green fluorescence/ total cell number.

Activity of caspase-like enzymes

A distinctive feature of PCD is the activation of caspase-like enzyme activity. Caspase-like activity was examined with Image-iT LIVE Green Poly Caspases Detection Kit (I35104, Invitrogen), which is based on a fluorescent inhibitor of caspases (FLICA). This FLICA reagent is able to detect activities of most caspases including caspase-1, -3, -4, -5, -6, -7, -8, and -9. *Karenia* cells were harvested by centrifugation at 500 g for 5 min, and then resuspended in 1X FLICA working reagent, and incubated for 60 min at room temperature in darkness. The FLICA reagent was then removed by centrifuge (500 g, 5 min), and then cells were resuspended in wash buffer before being observed on the epifluorescence microscope. Percentage of cells with caspase-like activity were calculated as: the number of cells with green fluorescence/ total cell number.

Cell Density

The densities of total morphologically intact cells were estimated in replicate from each culture vessel and counted under the microscope using a Sedgewick Rafter chamber

after Lugol's preservation. Single measurement was only applied on flasks in the "stationary control". Prior observations have revealed that *K. brevis* cells can show membrane permeability i.e. be inviable, yet still maintain their structure for some period of time. Because light microscope counts include all morphologically distinguishable cells, densities of live cells from each triplicate flask were calculated as: averaged total morphologically intact cells per ml × (1- averaged SYTOX proportion). Then the value of these densities were averaged among triplicates. The specific growth rate of the cultures in each growth stage was calculated as: Ln $(N_2/N_1)/(t_2 - t_1)$, where N1 and N2 = live cell densities at time 1 (t_1) and time 2 (t_2).

Flow cytometric cell cycle analysis

A 30 ml sample from each culture bottle was harvested by centrifugation (500g, 5 min), and the resultant pellets were fixed in 2% glutaraldehyde and stored at 4°C for at least 12 h. Fixed samples were centrifuged (500g, 5 min) to pellet the cells, and then resuspended in 1 mL ice cold absolute methanol and stored at -20°C to extract cellular pigments. This step was used to inhibit the interference of pigment's autofluorescence on DNA stain fluorescence. Before flow cytometry analysis, samples were pelleted by centrifugation (500g, 5 min). Their DNA was stained by addition of 10 ug/mL propidium iodide (PI) in 500 µl PBS containing 10 mg/ml RNase and 0.5% Tween 20 for at least 12 h at 4°C. DNA analysis of the PI-stained cells was conducted on a Becton Dickinson Accuri C6 flow cytometer with the emitted wavelength at 488 nm for excitation. Fluorescence of the DNA-bound PI stain was detected at 585 nm with "FL2 90% attenuation filter" (BD Biosciences, 653175), and then data were collected with 2-min fast inflow for each sample. Based on the flow cytometric data, the percentages of cells in each stage (G1, S, and

G2+M) of the cell cycle in each flask were calculated and analyzed using Flowjo 7.6 software. Since cells in the G2 or M phase have similar DNA content, flow cytometric analysis cannot distinguish these two phases; therefore, the two phases are categorized as G2+M.

Statistical analysis

Two-way repeated measures ANOVA (RM-ANOVA) was used to evaluate differences of PCD markers' prevalence between treatments and controls during the "growth stages" experiment. Bonferroni post hoc test was used to determine significance of the differences. The original α is equal to 0.05. All statistical analysis was performed using SigmaPlot 14.

RESULTS

Growth stages

Oxidative stress caused by 180 μM H_2O_2 induced extensive cell death responses at all growth stages. During the 48-h experiment the control cultures in early-log phase, mid-log phase and stationary phase were growing at rates of -0.17 ± 0.037, 0.048 ± 0.058 and -0.024 ± 0.021 d^{-1} respectively. In order to compare stress responses right before and after the addition of H_2O_2, the data from controls measured at time 0.5h were used as a proxy for time 0h in Treatments, representing the cellular status right before the induction of oxidative stress.

Within 30 mins after the addition of H_2O_2, sharp decreases in live cell densities and drastic increases in stress and cell death markers were generally observed at all of growth

stages (Fig. 2.1). During this short period of time, proportions of cells with ROS increased by 64% in early-log phase, and 40% in mid-log phase (Fig. 2.1A & 2.1B). In contrast, ROS prevalence did not change significantly in stationary phase (80.68 ± 5.73% vs. 87.15 ± 2.59%; $p = 0.372$) as background levels were already high at time 0h (Fig. 2.1C). The baseline prevalence of ROS before H_2O_2 treatment increased with aging of the cultures (Fig 2.1A, 2.1B, 2.1C). Significant increases in the proportion of cells expressing caspase-like activity were observed in all growth stages after the addition of H_2O_2 ($p < 0.05$). Almost 100% of cells displayed caspase-like activity after 30 mins of treatment in stationary phase, which was even higher than the ROS prevalence (Fig. 2.1F). Proportions of cells with caspase-like activity and ROS were similar to each other in early-log phase (~70%), and mid-log phase (~80%) at time 0.5h (Fig. 2.1A, 2.1B, 2.1D, 2.1E). Mortality was also induced rapidly within 30 mins of the treatment in all growth stages (Fig. 2.1G, 2.1H, 2.1I). Although early-log phase and stationary phase shared similar percentages of cells displaying permeable membranes at time 0.5h (~30%; SYTOX-positive; Fig. 2.1G, 2.1I), their vulnerability to oxidative stress was very different: approximately 2% vs 65% of the cells were lysed within the first 30 mins in early-log phase and stationary phase, respectively. In contrast, mid-log phase exhibited the highest cell death percentages (52.62 ± 7.22%; Fig. 2.1E) with a moderate cell lysis percentage of 25%.

After the initial 30-minute acute response phase, *K. brevis* cultures from all growth stages continued to lose cells but at different rates. In early-log phase (Fig. 2.1J), despite cells experiencing the lowest cell lysis percentages (2%) during the initial acute phase, more than 95% of cells counted at time 0h were lost by time 24h, with accompanying prevalence of caspase-like activity and heavy ROS load (Fig. 2.1A, 2.1D). In contrast, live cell densities in mid-log and stationary phase steadily decreased over a 48-hour period (Fig. 2.1K, 2.1L). This slower culture crash pattern was also reflected in the changes of

mortality, as cell death percentages in these two phases were lower than early-log phase and tended to level off after the initial acute shock (Fig. 2.1G, 2.1H, 2.1I). Although the prevalence of cells with ROS and caspase-like activity was somewhat variable after time 0.5h, the expression of these two stress markers was generally significantly higher in treatments vs controls across all growth stages ($p < 0.05$), except ROS prevalence in stationary phase ($p = 0.57$; Table 2.1).

While H_2O_2-treated cells showed a high prevalence of all three of the stress markers, cells in untreated control cultures also expressed ROS and caspase activity (Fig. 2.1, Table 2.1). Caspase-like activity was found in 23.89 ± 8.40% to 55.72 ± 9.78% of control cells at all three growth stages (Table 2.1). ROS was detected in roughly half of the cells at mid-log phase (48.93 ± 7.55%) and stationary phase (52.67 ± 14.89%) cells, compared to only 8.87 ± 3.64% of cells in early-log phase (Table 2.1). Little or no SYTOX labeling was observed at any of the growth stages with continuing increased live cell densities (Table 2.1).

Diel cycle

Cellular stress responses and cell cycle patterns of *K. brevis* were determined during 2 diel cycles under 12:12 L:D and continuous light, respectively.

Cellular stress responses

Cell death percentages remained very low (less than 10%) under both light conditions throughout the two-day monitoring period (data not shown). However, ROS prevalence under 12:12 L:D was highest during the dark phase, and generally lower during the light phase (Fig. 2.2). A similar pattern of ROS prevalence was observed in the cultures

grown under continuous light, with ROS percentages also peaking during circadian night, and reaching the lowest levels during circadian daytime hours. However, the daily amplitude of ROS variation under 12:12 L:D was higher than under continuous light. In contrast, the prevalence of caspase-like activity did not correlate with the light:dark cycle or circadian timing during the two diel cycles (Fig. 2.3). The proportion of cells showing caspase-like activity ranged from 3.20 ± 1.52% to 32.57 ± 3.02% (average 18.70 ± 4.57%) under 12:12 light cycle and from 10.83 ± 7.56 to 45.44 and 4.44% (average 28.12 ± 4.92%) under continuous light (Fig. 2.3).

Cell cycle patterns

At the beginning of both light phases under 12:12 L:D, more than 85% of cells were in G1 phase (Fig. 2.4A: time 2h, time 26h). The proportion of cells undergoing DNA synthesis (S phase) was highest during the light phase, peaking at around 10 h into light (time 10h, time 34h). Peaks in the proportion of S phase cells corresponded to minima in the proportion of cells in G1. No consistent diel pattern was observed for G2+M phase during the two-day experiment. After being exposed to continuous light for seven days, the diel patterns for all cell cycle phases seemed to be reversed or lost (Fig. 2.4B). On the first day, the proportion of cells in G1 and S phase were highest at the beginning of the "circadian day" and "circadian night" respectively, which were opposite the patterns observed under 12:12 L:D. For the second day, there was little to no variation for any of the cell cycle stages, exhibiting a loss of synchronization of the cell cycle.

DISCUSSION

This study investigated how cell death responses to external stress vary as the cultures grow and age as well as how baseline ROS and caspase-like activity change with growth, both at the short-term (diel) scale and the long-term (growth cycle) scale. In response to oxidative stress, the classic PCD cascade was observed in *K. brevis*, as ROS and caspase activity increased along with cell death. Acute susceptibility to oxidative stress increased as cultures aged, while the youngest stage (early-log phase) showed the highest overall rate of cell loss within the first 24 hours. In untreated control cells, ROS and caspase-like activity were common throughout growth but did not correlate with cell death. Observations of untreated cells over diel cycles suggested that while light may play an important role in determining cell cycle patterns in *K. brevis*, neither light cycles nor cell cycles were correlated with ROS diel variations.

Stress responses at different growth stages

PCD could be induced by oxidative stress in *K. brevis* at all growth stages, as prevalence of cell death, ROS and caspase-like activity in treatments were significantly higher than controls after H_2O_2 addition. PCD triggered by exogenous H_2O_2 has been documented in many microorganisms (Berman-Frank et al., 2004; Bouchard & Purdie, 2011; Darehshouri et al., 2008; Vavilala et al., 2015). In the green alga *Micrasterias* addition of 5000 uM H_2O_2 caused up to 20% mortality in 6 hours with the appearance of caspase-like activity, chromatin condensation and ultrastructural changes in mitochondria, indicating the role of H_2O_2 inducing PCD (Darehshouri et al., 2008). For *K. brevis*, Johnson et al. (2014) observed a cell death pathway that exhibited heavy ROS load, caspase-like activity, DNA fragmentation, and specific morphotypes after 10 mins of the addition of 80

μM H_2O_2. Caspase-like proteases have been suggested as PCD executioners in phytoplankton (Varidi, 1999; Bidle & Bender, 2008; Bidle et al., 2007; Jiménez et al., 2009). For example, Vardi et al (1999) found that caspase inhibitors blocked PCD in *P. gatunense* under oxidative stress triggered by CO_2 limitation, indicating the involvement of caspase-like enzymes in cell death and bloom decline process. However, cell death responses to oxidative stress may be diverse and species-specific in dinoflagellates. Jauzein & Erdner (2013) reported that in *Alexandrium tamarense* PCD was not activated in response to 400 μM H_2O_2, while the mortality observed here may result from the added oxidant directly causing cell damage.

Short-term stress responses were similar at different growth stages; all showed sharp increases in both ROS, caspase, and cell death prevalence after the first 30 minutes following exposure. While the baseline cell death prevalence was low at all growth stages, the baseline level of ROS and the extent of rapid cell lysis increased with aging of cultures. This increasing acute cell mortality may be related to biochemical changes in physiology as cultures age. Genes responsible for cell defense and stress acclimation including DNA repair, heat shock proteins, and pentatricopeptide repeat proteins are significantly downregulated during stationary phase in *K. brevis*, which may translate to increased vulnerability to external stress (Johnson et al., 2012; Miller-Morey & Van Dolah, 2004). A comparison of gene expression before/after the induction of acute oxidative stress at different growth stages may help further explain the change of susceptibility as cultures age, and the connection between reduced defense response and oxidative-stress-induced mortality.

Although acute susceptibility to oxidative stress increased with the ages of cultures in *K. brevis*, the youngest cultures (early-log phase) show the highest overall rate of cell loss. After the initial phase (30 minutes), the cultures in early-log phase showed continued

increases in the prevalence of caspase activity and SYTOX labelling, with an almost complete loss of cells during the first 24 hours. In contrast, *K. brevis* cells in mid-log and stationary phase experienced decreases in caspase prevalence and a more gradual increase in cell death percentages compared to early-log cells. This translated to a slower PCD process which continued over 48 hours. The observed delayed culture crash and slower PCD progression at the latter two growth phases may be related to cell density-dependent H_2O_2 detoxifying processes. Previous research has suggested that rate of decrease of extracellular H_2O_2 concentration increases with cell densities, due to stronger intracellular ROS scavenging from denser cells (Gülden et al., 2010; Uhl & Dukan, 2016). Therefore, after the acute initial phase the surviving cells from the cultures with higher starting cell densities may experience much lower external H_2O_2 concentrations, which would lead to a slower cell death progression (Houot, 2001; Vavilala et al., 2015). Density-dependent cell death was observed in C6 glioma cells under oxidative stress, as viability after 24 hours of H_2O_2 addition was higher in the cultures with higher initial cell densities (Gülden et al., 2010). In addition, just as kelps can secrete iodide under oxidative stress to detoxify external oxidants (Kupper et al., 2008), *K. brevis* may also have some mechanisms to produce antioxidants in response to elevated surrounding H_2O_2 concentrations. With more live cells producing antioxidants in a similar culture volume during acute initial phase, the concentrations of oxidant in the culture of mid-log and stationary phase would be lower, therefore effectively delaying the break-down of cultures.

Untreated cells showed evidence of ROS and caspase-like activity which varied along the growth curve but was not associated with cell death. This supports roles for both ROS and caspase-like activity in a variety of cellular metabolism processes and housekeeping functions. ROS percentages in untreated *K. brevis* cultures were low in early-log phase and increased with culture age. On average about half of the cells in mid-log and

stationary cultures had detectable ROS, although the underlying causes may be different. The observation of extensive ROS prevalence in mid-log phase may be a consequence of enhanced cellular metabolic processes. Significant production of ROS in exponential growth phase has been observed in the dinoflagellate *Margalefidinium polykrikoides* (Kim et al., 1999) and some raphidophyte species including *Heterosigma akashiwo* (Portune et al., 2010; Twiner & Trick, 2000), *Chattonella antiqua* (Kim et al., 2004) and *Chattonella marina* (Kawano et al., 1996; Liu et al., 2007; Oda et al., 1995). The ROS observed during rapid exponential growth is generally attributed to increased mitochondrial or chloroplastic activity depending on the specific species (Kim et al., 2004; Portune et al., 2010; Twiner & Trick, 2000). The high levels of ROS prevalence in stationary phase agrees with the results of Johnson et al. (2014) who observed ROS staining in more than 65% of stationary phase *K. brevis* cells. *K. brevis* in stationary phase may experience tremendous change of metabolic and physiological status which are reflected in a major restructuring of the transcriptome for stress responses including repression of ROS detoxification pathways (Johnson et al., 2012) that may enhance ROS prevalence in cultures.

In our experiment constitutive prevalence of caspase-like activity in more than 20% of cells from all the control samples was observed. Bouchard & Purdie (2011) and Johnson et al. (2014) examined temporal variation of caspase-like activity (protein cleavage rate) in *K. brevis* under normal conditions. Both of these studies revealed baseline cleavage activity of caspase-like enzyme along the growth curve which reflected similar background caspase-like activity with our study. Among these three reports only Bouchard & Purdie (2011) observed significant non-induced cell death (about 15% of cells) which was independent of caspase-like activity.

Caspase activity has been associated with non-death functions in both multicellular and unicellular organisms. In metazoans, caspases are involved in diverse processes including cellular survival, differentiation, proliferation and so on (Algeciras-Schimnich et al., 2002). Increasing evidence of housekeeping functions of caspase-like activity later emerged for unicellular organisms (Bidle et al., 2010; Bidle & Bender, 2008; Jimenez et al., 2009; Seth-Pasricha et al., 2019; Thamatrakoln et al., 2012). In the diatom *Thalassiosira pseudonana* a constitutive presence of caspase-specific activity is found during log phase in non-stressed cultures (about 14% of total cells; Bidle & Bender, 2008; Thamatrakoln et al., 2012). A high basal level of caspase activity was observed in exponentially growing archaeal cells, where it may be responsible for cellular proteolytic activities that prevent accumulation of damaged proteins during active growth (Seth-Pasricha et al., 2019). As algal cells approach quiescence, caspase-like activity may be involved in the cellular response to ambient stress. For example, genomic and biochemical analyses of *T. pseudonana* show higher caspase-specific activity and up-regulation of gene expression associated with some types of metacaspases (homologues of caspase) during stationary phase (Bidle & Bender, 2008). This is hypothesized to assist in acclimation to iron and photosynthetic stress (Bidle & Bender, 2008; Thamatrakoln et al., 2012).

Diel cycle

The presence of stress markers in untreated control cells and their possible association with physiological processes led us to investigate these same markers in untreated cells over a finer growth scale, that of the diel cycle. This included cultures grown under 12:12 L:D and continuous light, in order to examine the relationships between light cycles, cell cycles, and expression of intracellular ROS and caspase-like protease activity.

Very little cell death (less than 10%) was detected in diel samples, which supports a general housekeeping role for these PCD components.

ROS prevalence exhibited a diel phasing pattern that does not correlate with light cycle or cell cycle. Since the ROS variation pattern observed under 12:12 L:D did not change under continuous light, the ROS diel pattern appears to be under circadian control. To our knowledge, there are no reports of diel variation of intracellular ROS prevalence in phytoplankton. It is well known that in dinoflagellates the cell cycle often follows a diel pattern (Li et al., 2015), so perhaps ROS diel variation may closely connect with active cell division. In this study, the observed peak of cell division and ROS prevalence both occurred during night phase under 12:12 L:D in *K. brevis*. However, the rhythm of cell cycle phasing was lost in continuous light which indicates a loss of concentrated time for cell division. The peak of ROS prevalence at circadian night hours persisted under continuous light, which suggests that cell division does not drive the observed ROS diel rhythm in *K. brevis*.

The observed diel variation of ROS prevalence may be attributable to the circadian rhythm of antioxidant enzymes previously reported in dinoflagellates and other algae. In phytoplankton, ROS production occurs at several sites including the chloroplasts (photosynthesis) and mitochondria (respiration; Diaz & Plummer, 2018; Møller, 2001), and the maximal production of ROS generally occurs during the day as a result of active photosynthesis (Foyer et al., 1994). In order to deal with the oxidative stress resulting from photosynthesis, many microalgae exhibit a diel cycle of antioxidants peaking at daytime (Bucciarelli et al., 2007; Dupont et al., 2004; Jensen et al., 2011; Levy et al., 2006; Mella-flores et al., 2012; Okamoto & Colepicolo, 2001; Sigaud-Kutner et al., 2005). For example, in cyanobacteria gene expression associated with ROS detoxification (i.e. superoxide dismutase (SOD) and catalase) is remarkably upregulated during the day (Jensen et al.,

2011; Mella-flores et al., 2012). However, studies have also implicated an endogenous circadian clock, rather than light levels, in controlling different antioxidants in algae, mainly focusing on the dinoflagellate *Lingulodinium polyedrum* (Okamoto & Colepicolo, 2001b) and cyanobacteria (Edgar et al., 2012; Toepel et al., 2008). Okamoto & Colepicolo (2001) tracked the diel change of antioxidant Mn-SOD (the main ROS scavenger in mitochondria) and Fe-SOD (the main ROS scavenger in chloroplasts) activity under 12:12 L:D and continuous light, and observed a solid circadian rhythmicity that increased and peaked at circadian early day hours and then decreased to the lowest value during circadian dark phase. This circadian time-keeping behavior may be beneficial for phytoplankton to deal with predictable challenges from daily variation of light conditions (Okamoto & Colepicolo, 2001). The generation of ROS during dark hours under 12:12 L:D would mainly be from mitochondrial activity, while both photosynthesis and respiration are sources of ROS in circadian dark hours under continuous light. Therefore, ROS generated from these metabolic processes may be effectively removed by antioxidant enzymes like Mn-SOD and Fe-SOD during circadian light hours, while those ROS produced during circadian dark hours would remain in cells. Toepel et al. (2008) also suggested similar circadian regulation of oxidative stress in the cyanobacterium *Cyanothece sp.*, as the expression of genes responsible for SOD and catalase remain low in circadian dark hours under continuous light. Peroxiredoxin, a family of antioxidant proteins that are involved in controlling intracellular redox levels, are also reported to exhibit a conserved circadian rhythm persisting for days under constant light in *Synechococcus* and archaeal cells (Edgar et al., 2012). Therefore, it is possible that circadian rhythm of different antioxidants would explain the observed diel variation of ROS prevalence in microalgae.

Light does control cell cycle patterns in *K. brevis*, as exposure to continuous light for seven days remarkably "erased" the cell cycle pattern shaped by growth under 12:12

L:D. Diel variation of the cell cycle has been well documented in *K. brevis* (Brunelle et al., 2007; Dolah & Leighfield, 1999; Van Dolah et al., 2008). Van Dolah et al. (2008) cultured multiple *K. brevis* strains under 16:8 L:D and recorded cell cycle patterns which were generally similar to the patterns observed here (12:12 L:D) in terms of the relationship with light and dark phases. Brunelle et al. (2007) transferred *K. brevis* cultures from 16:8 L:D to continuous light and monitored cell cycle patterns for three consecutive days, finding that the cell cycle of *K. brevis* was under circadian control as the pattern behaved similarly as observed in 16:8 L:D. However, based on our results it seems exposure to continuous light for seven days is enough to significantly disturb the previous cell cycle pattern. A similar effect was reported from dinoflagellate *Prorocentrum donghaiense*, as the amplitude of each cell cycle phase generally tended to decrease after 22 hours under continuous light (Shi et al., 2013).

Caspase-like activity does not appear to be involved in cell cycle regulation in *K. brevis*, as the caspase-like activity showed a random fluctuation under different light environments. In metazoans, caspases are believed to serve as one of the checkpoints to make sure only healthy cells can proceed and complete cell cycle (Algeciras-Schimnich et al., 2002). If caspase-like activity plays a role in quality control of cell cycle progression in *K. brevis*, coherent peaks would be expected under the synchronized cell cycle pattern in 12:12 L:D. The absence of peaks may be due to the expression of multiple housekeeping functions which act as a "noise" in the diel expression of caspase-like activity in *K. brevis*.

CONCLUSIONS

Our results show that oxidative stress triggers the classic PCD cascade in *K. brevis*. Acute susceptibility to oxidative stress increased as cultures aged, which may reflect a

decrease in cell defense abilities with time in culture. However, the youngest cultures showed the highest overall rate of cell loss within the first 24 hours, hypothesized to result from cell density-dependent H_2O_2 detoxifying process. In untreated cells, the prevalence of ROS and caspase-like activity fluctuated not only between growth phases but also over a diel cycle, supporting their role in cellular metabolism and housekeeping functions. The diel pattern of ROS prevalence was under circadian control, and not related to light-regulated cell cycle patterns. Circadian rhythm of antioxidant enzymes may be able to explain the diel variation of ROS prevalence based on the dynamics of ROS generation and removal processes. Our results highlight the multiple roles of ROS and caspase-like activity in death and non-death cellular responses in phytoplankton as well as the importance of understanding mechanisms controlling their accumulation.

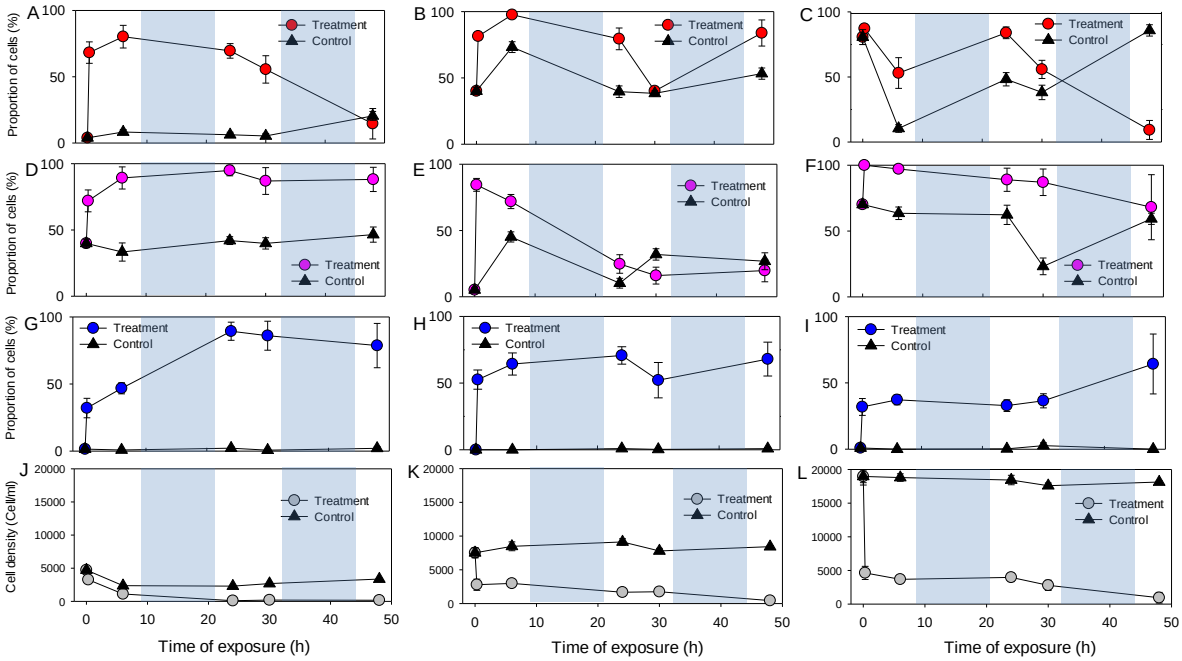

Figure 2.1: Cellular stress responses to 180 μM H_2O_2 and the control environment in *K. brevis* cells at early log phase (A, D, G, J), mid-log phase (B, E, H, K) and stationary phase (C, F, I, L). (A, B, C) Variations in the proportion of cells showing reactive oxygen species (ROS). (D, E, F) Variations in the proportion of cells showing caspase-like activity. (G, H, I) Variations in the proportion of cells stained with SYTOX. (J, K, L) Variations in live cell density. Data points show average values obtained from triplicate cultures, and error bars show standard deviation of the replicates (n = 3). Blue shades indicate dark phase.

Table 2.1: Average live cell densities and percentages of cellular parameters in treatments and controls from all sampling time points during the 48-hour experiment at early-log, mid-log and stationary phase.

	ROS (%)		Caspase-like activity (%)		Cell death (%)		Live cell density (cells/ml)
	Treatment	Control	Treatment	Control	Treatment	Control	Control
Early log	57.64 ± 14.35	8.87 ± 3.64	86.24 ± 8.58	40.34 ± 4.99	66.60 ± 14.94	1.42 ± 0.89	3094 ± 510
Mid log	76.54 ± 11.30	48.93 ± 7.55	43.38 ± 15.86	23.89 ± 8.40	61.59 ± 10.10	0.39±0.41	8310 ± 885
Stationary	57.86 ±15.78	52.67 ± 14.89	88.26 ± 13.00	55.72 ± 9.78	40.84 ± 11.92	0.75 ± 1.05	18533 ± 1537

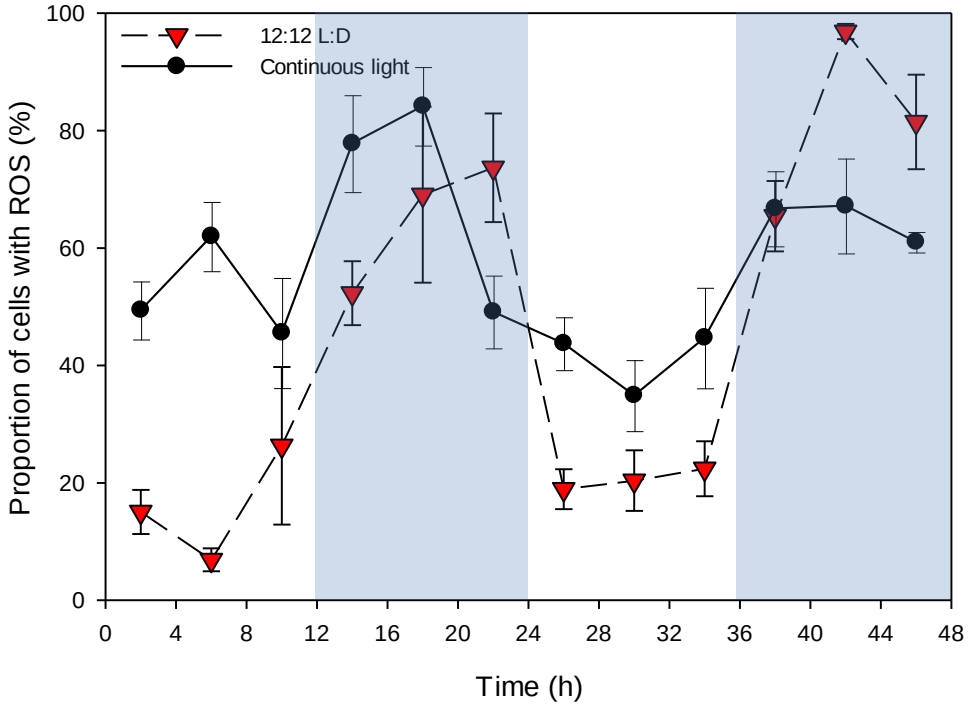

Figure 2.2: Temporal variations in the proportion of cells showing ROS during two diel cycles under 12:12 light cycle and continuous light. Data points show average values obtained from triplicate cultures, and error bars show standard deviation of the replicates (n = 6). Blue shades indicate dark phase for 12:12 L:D, and circadian dark hours under continuous light.

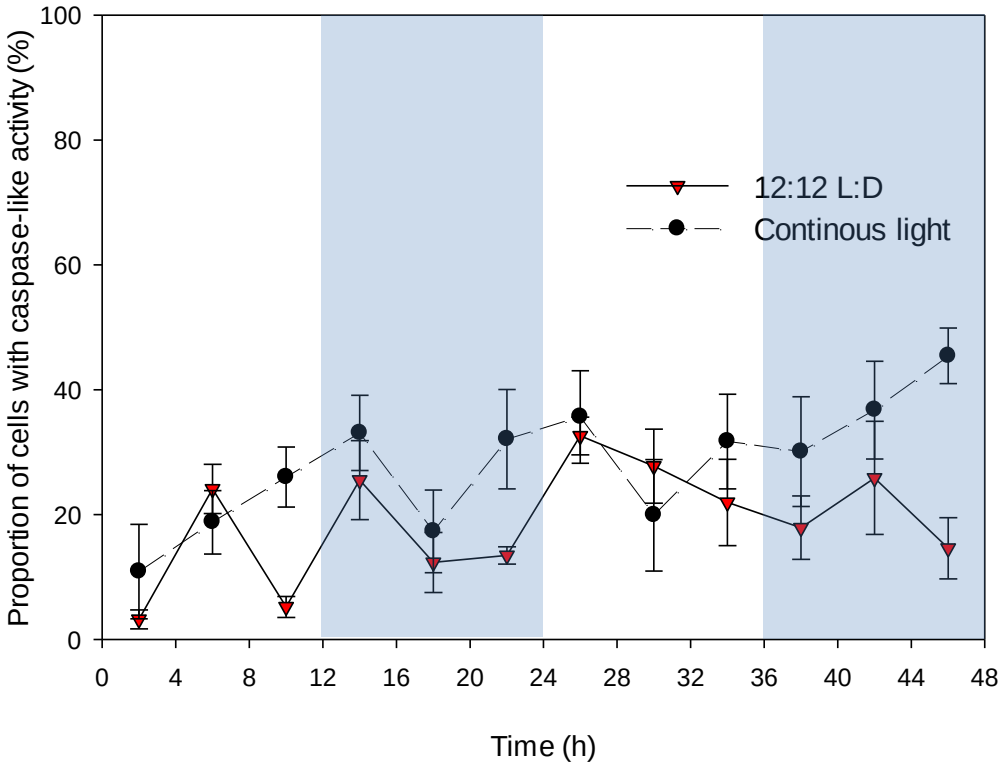

Figure 2.3: Temporal variations in the proportion of cells showing caspase-like activity during two diel cycle under 12:12 L:D and continuous light. Data points show average values obtained from triplicate cultures, and error bars show standard deviation of the replicates (n = 6). Blue shades indicate dark phase for 12:12 L:D, and circadian dark hours under continuous light.

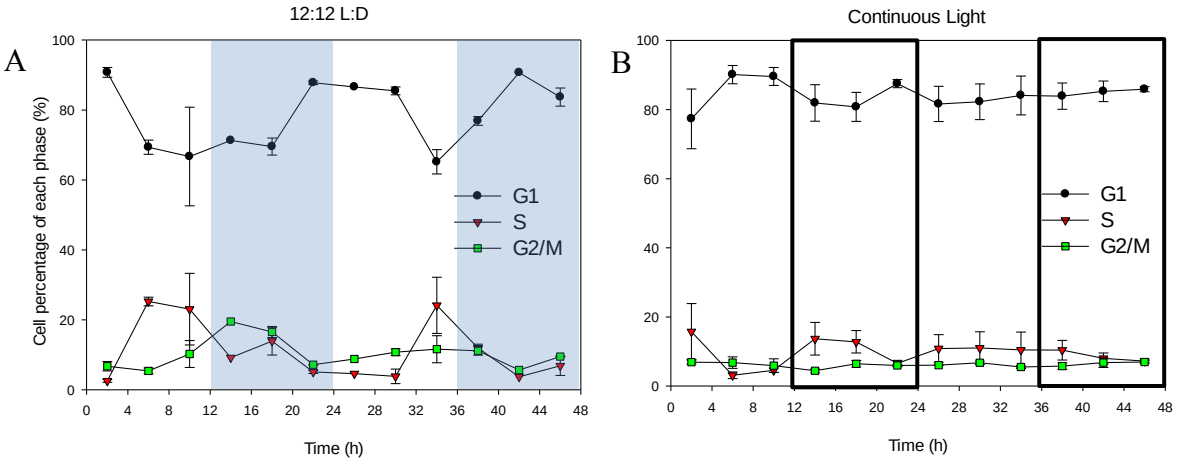

Figure 2.4: Percentages of cells in each cell cycle phase during two diel cycles under 12:12 L:D (A) and continuous light (B). Data points show average values obtained from triplicate cultures, and error bars show standard deviation of the replicates (n = 3). Blue shades indicate dark period of 12:12 L:D, and bold black rectangles indicate circadian dark hours under continuous light.

Chapter 3: Cell death responses to acute high light mediated by photosynthetic reactive oxygen species balance in toxic dinoflagellate *Karenia brevis*

ABSTRACT

Programmed cell death (PCD) can be induced in marine phytoplankton by many biotic and abiotic challenges, potentially leading to significant cell loss in the field. These organisms live in a highly intense and variable light environment, yet the potential for excess photosynthetically available radiation (PAR) to trigger PCD has not been investigated. In the Gulf of Mexico, populations of toxic dinoflagellate *Karenia brevis* can experience light irradiance of more than 1000 µmol m^{-2} s^{-1} at the surface during bloom season. The main objective of this study is to elucidate photosynthetic and stress-related death processes in response to acute high light stress in *K. brevis*. Here, cultures maintained under 50 µmol m^{-2} s^{-1} were transferred to 500, 750 or 1000 µmol m^{-2} s^{-1} for two light periods. I used stress and cell death markers as well as a series of photosynthetic parameters to characterize high-light-induced death responses and their relationship with photosynthesis. PCD in *K. brevis* only occurred at the largest light shift (50 to 1000 µmol m^{-2} s^{-1}). Although depressed photosynthetic capacities and oxidative stress were apparent across the stress gradient, they did not necessarily lead to cell death. Non-photochemical quenching (NPQ) exhibited dose-dependent activation with increasing light stress, which may enable cells to resist or delay PCD. These results highlight the important role of the balance between ROS generation and NPQ activation on determining cell fates in *Karenia* under acute irradiance stress. This research also provides insights into potential survival strategies and mechanisms of cell loss under the changeable light environment in the field.

INTRODUCTION

Karenia brevis is responsible for frequent harmful algal bloom (HAB) events in the Gulf of Mexico (GoM). *K. brevis* produces potent neurotoxins called brevetoxins, and blooms can result in animal death, human sickness, and significant loss in fishing and tourism industries (Brand et al., 2012). While the mechanisms of *K. brevis* bloom initiation have been intensively investigated (Hetland & Campbell, 2007; Liu et al., 2001; Walsh et al., 2006), the causes of bloom decline in *K. brevis* remain poorly understood. During the past two decades, the development of molecular and computational tools have revealed the impact of programmed cell death (PCD) in causing lysis of many cosmopolitan algal species (Bidle, 2015). PCD refers to a variety of genetically-controlled and self-destruction pathways (Bidle, 2015). PCD can be induced by a variety of biotic and abiotic challenges such as viral attack, CO_2 limitation, and iron starvation, potentially leading to decline of algal blooms (Bidle & Bender, 2008; Bidle et al., 2007; Vardi et al., 1999; Zuppini et al., 2007).

Marine phytoplankton live in a highly variable light environment, yet the potential for excess photosynthetically available radiation (PAR) to trigger PCD in phytoplankton has not been investigated. Most algal cell-death research relating to irradiance has focused on ultraviolet (UV) exposure and dark deprivation (Britt, 1996; Jiménez et al., 2009; Moharikar et al., 2006). However, high light can be damaging to cells, perhaps to the point of PCD. Absorption of light energy beyond photosynthetic capacity results in excessive excitation of electrons from chlorophyll (Li et al., 2009; Niyogi, 1999). One fate of these over-excited electrons is the generation of singlet oxygen, an extremely damaging reactive oxygen species (ROS), as a consequence of photoinhibition (Apel & Hirt, 2004; Muller et al., 2001). In the PCD cascade, ROS serves as an intracellular signal to activate caspase-like activity in phytoplankton cells and thus lead to cell death (reviewed by Bidle, 2016).

It is clear that high light can induce photoinhibition in *K. brevis* (McKay et al., 2006; Miller-morey & Dolah, 2004; Tilney et al., 2019; Yuasa et al., 2019), potentially producing ROS and triggering PCD. Given the fact that *K. brevis* can experience huge variation in light over short time scales in the GoM (Evens et al., 2001; Heil et al., 2014; Tilney et al., 2019), understanding their cell death responses to light can inform our understanding of bloom development and decline. On the other hand, in order to mitigate intracellular accumulation of ROS and induction of PCD, a photoprotective non-photochemical quenching (NPQ) pathway may be induced to dissipate excessive excitation energy as heat (Krause & Jahns, 2004). However, under high light the NPQ pathway in *K. brevis* has not yet been characterized.

This study investigated photosynthetic and stress-related death processes in response to different levels of acute high light stress in *K. brevis*. I hypothesized that NPQ would be induced to prevent ROS production and therefore mitigate cell death under high light stress in *K. brevis*. Cultures maintained under 50 µmol m^{-2} s^{-1} were transferred to 500, 750 or 1000 µmol m^{-2} s^{-1} for two light periods. We used stress and cell death markers (ROS, caspase-like enzyme activity and SYTOX) to characterize high-light-induced death responses. Since ROS production is closely linked to photoinhibition in dinoflagellates, photosynthetic status was characterized by non-photochemical quenching (NPQ), Fv/Fm, and rapid light curves (RLC). Results showed that cell death only occurred at the largest light shift (50 to 1000 µmol m^{-2} s^{-1}) and was accompanied by caspase-like activity. Oxidative bursts and depressed photosynthetic measures were observed at lower light levels but did not necessarily lead to cell death. Induction of NPQ may mitigate the damaging effects of ROS and therefore delay cell death under certain levels of acute light stress. These results highlight the important roles of the production and removal of ROS

on determining cell fates under acute irradiance stress, providing insights into how high light may affect maintenance and decline of *Karenia* blooms.

METHODS

Strains and culture conditions

K. brevis clone SP3 was isolated by Suzanne Pargee from a red tide bloom near South Padre Island, Texas in 1999 (Magaña & Villareal, 2006). An inoculum culture (1100 ml) was started at 1200 cells/ml and grown in L1 medium (Guillard & Hargrave, 1993) made from seawater collected offshore in the GoM. The seawater was filtered through 0.2 um polycap capsule filter (Whatman Inc.), adjusted to a salinity of 32 psu and autoclaved prior to the addition of sterile L1 nutrient stocks. The culture was maintained at an irradiance level of 50 µmol m^{-2} s^{-1} on a 12:12 hour light:dark cycle with cool white fluorescent bulbs at 25°C. When the concentration of cells in the flasks reached early log phase (~2300 cells/ml), 60 ml of algal culture was dispensed into each of 18, 125 ml flasks, and maintained under the same environmental conditions. Among these 18 flasks, sets of 3 flasks were designated as "treatment 500", "treatment 750", "treatment 1000", "control 500", "control 750" and "control 1000".

Experimental setup and sampling

Experimental high light intensities of 500, 750 and 1000 µmol m^{-2} s^{-1} were achieved by using two sets of light banks with a number of dimmable small cool white lights (Bozily Aquarium Lights LED). The light intensities were confirmed by LI-192 quantum sensor connected to an LI-1400 DataLogger (LI-COR Biosciences). During the log phase of the

K. brevis cultures, the 3 treatment 500 flasks were moved to 500 µmol m^{-2} s^{-1} at the beginning of a light period (time 0h), while the 12:12 hour light:dark cycle was remained. Meanwhile, the 3 control 500 flasks were kept at 50 µmol m^{-2} s^{-1} with the same light:dark cycle as the treatments. During the experiment, cultures were sampled from both treatments and controls at time 0.5h, 6h and 24.5h. The experiments for 750 and 1000 µmol m^{-2} s^{-1} were set up in the same way, except that the sets of treatment 750 and treatment 1000 flasks were transferred to their corresponding light conditions. Experiments for these three light treatments were conducted on different but consecutive days (Day 1 and Day 2 for treatment 500; Day 3 and Day 4 for treatment 750; Day 5 and Day 6 for treatment 1000), so a separate control set was used and sampled together with each treatment set.

Measurement of stress and cell death markers

Three PCD-related parameters were determined by fluorescent labeling as described below: the prevalence of cells showing cell death, ROS and caspase-like activity. All reagents produced green fluorescence which was observed under the epifluorescent microscope with an excitation wavelength of 450–490 nm and emission of 523 nm. More than 50 cells were counted and examined, in replicate from each culture vessel, using a Sedgewick Rafter under a fluorescent microscope.

Cell death detection

Integrity of the cell membrane, which is an indicator of cell death, was examined using SYTOX-green dye (S7020, Invitrogen). This reagent has high affinity with nucleic acid and can only penetrate compromised plasma membranes. An aliquot of stock solution (5 mM in DMSO) was diluted into phosphate-buffered saline (PBS) to prepare a 100 µM

working solution. A 2.5 µl aliquot of the working solution then added directly to 500 µl of algal culture sample, resulting in a final concentration of 0.5 µM SYTOX-green dye. At room temperature SYTOX-stained cells were counted after 60 min dark incubation. SYTOX percentages were calculated as: the number of cells with green fluorescence/ total cell number.

ROS production

Intracellular ROS was detected by using carboxy-H_2DCFDA (C400, Invitrogen). For preparing the stock solution, 2 mg of carboxy-H_2DCFDA were dissolved in DMSO at a concentration of 10 mM. Before the experiment PBS was used to prepare the working solution by diluting an aliquot of stock solution to 100 µM. The working solution was then mixed with algal culture sample at a 1:10 ratio, resulting in a 10 µM final concentration of carboxy-H_2DCFDA. Green fluorescence generating from the oxidation of carboxy-H_2DCFDA was examined after 20 min dark incubation at room temperature. Percentages of ROS were calculated as: the number of cells with green fluorescence/ total cell number.

Activity of caspase-like enzymes

A distinctive feature of PCD is the activation of caspase-like enzymes. In order to detect caspase-like activity in *K. brevis* cells, CellEvent in situ caspase 3/7 Green Detection Reagent (C10423, Invitrogen) was diluted by a subsample of *K. brevis* cultures to a final concentration of 10 µM. Observations of stained cells were performed after at least 30 mins of room temperature incubation. Percentage of cells with caspase-like activity were calculated as: the number of cells with green fluorescence/ total cell number.

Cell Density

The number of total morphologically intact cells was estimated in replicate from each culture vessel via microscope using a Sedgewick Rafter counting chamber after Lugol's preservation. Densities of live cells from each flask were calculated as: total morphologically intact cells per ml × (1- averaged SYTOX proportion). Then these densities were averaged among triplicate control/treatment flasks.

Photosynthetic parameters

At each sampling time 2 ml of algal culture were collected from each flask and placed in the dark for 30 min. Fast Repetition Rate fluorometry (FRRf) on a FastTRACKA instrument (Chelsea Technologies Group Ltd.) was used to measure the photosynthetic efficiency of photosystem II (Fv/Fm), where Fm is the maximal fluorescence excited by saturating pulse of light from a dark-adapted sample and Fv is the difference between minimal fluorescence (F_0) and Fm. In addition, Rapid Light Curves (RLC) were also collected by FRRf to derive the potential maximum relative electron transport rate (potential rETRmax, an approximation of the potential maximum rate of electrons pumped through the electron transfer chain; dimensionless) and the efficiency of photosynthesis (alpha, initial slope of the rETR vs. irradiance curve; $\mu mol^{-1}\ m^2\ s$). RLC measurements were conducted with a stepped actinic irradiation of 10 s duration from 0 to ~1000 µmol $m^{-2}\ s^{-1}$. RLC data were analyzed in R software using the package phytotools (Silsbe & Malkin, 2015). The FRRf was conducted with single turnover (ST) acquisition. An ST sequence is composed of 100 saturation flashes of 1 µs duration with an interval of 1 µs in between. For each acquisition twelve sequences were performed with an interval of 100 ms between each sequence (Severin & Erdner, 2019). In order to calculate non-

photochemical quenching (NPQ), another 2mL sample was collected from each flask at each sampling time, and then maximum fluorescence yield of a light-adapted samples (F'm) was measured by FRRf. NPQ was calculated by the following equation:

NPQ = (Fm - F'm)/F'm),

and if F'm >Fm then NPQ = 0 (Ralph & Gademann, 2005).

Statistical analysis

Two-way repeated measures ANOVA (RM-ANOVA) was used to evaluate differences of some cellular parameters between treatments and controls at each sampling time point. The Bonferroni post hoc test was used to determine significance of the differences. The original α is equal to 0.05. All statistical analysis was performed using SigmaPlot 14.

RESULTS

Photosynthetic function in *K. brevis* cells generally decreased with increasing light intensities (Fig. 3.1). The Fv/Fm in treatments was characterized by a dose-dependent decrease with increasing irradiance and was significantly lower than controls at each time point ($p < 0.05$, Fig. 3.1a). From RLC measurements, maximum photosynthetic rates (rETRmax) and the efficiency of photosynthesis (alpha) showed similar patterns as they both decreased as light stress increased (Fig. 3.1b, 3.1c). One exception is the rETRmax under 500 µmol m^{-2} s^{-1}, which was not reduced during the first 6 hours after stress compared with the controls (Fig. 3.1b).

No significant caspase-like activity and cell death were observed under acute light stress at 500 µmol m^{-2} s^{-1} (10-fold increase) and 750 µmol m^{-2} s^{-1} (15-fold increase) at each time point in this 24-hour experiment ($p > 0.05$; Fig. 3.2a, 3.2b). However, ROS prevalence in *K. brevis* varied under these two stress levels. After exposure to 500 µmol m^{-2} s^{-1}, ROS prevalence was not significantly higher than control until time 24.5h ($p < 0.001$; Fig. 3.3a). In contrast, ROS prevalence in treatment 750 showed an immediate increase ($p < 0.001$; Fig. 3.3b) at time 0.5h, after which it was reduced relative to the controls ($p < 0.01$; Fig. 3.3b). There was little to no cell loss under these two non-lethal irradiance stress levels. In treatment 500 live cell numbers increased from 4,032 ± 314 to 6,238 ± 655 cells/ml, while in treatment 750 cell numbers increased from 7,136 ± 1275 to 10,804 ± 876 cells/ml during the 24 hours of the experiment (Fig. 3.2c).

Under 1000 µmol m^{-2} s^{-1} a self-catalyzed cell death was observed at time 24.5h. SYTOX florescence was detected in 29.27 ± 7.40% of cells (Fig. 3.2b) and 33.92 ± 6.59% of cells showed caspase-like activity (Fig. 3.2a). The mortality was severe, as 60% of live cells were lysed between time 6h and time 24.5h (14,713 ± 1840 to 4,275 ± 542 live cells/ml; Fig. 3.2c). In comparison, no evidence of caspase-like activity (Fig. 3.2a) or cell death (Fig. 3.2b) were observed during the first 6 hours. The percentages of cells showing an intracellular accumulation of ROS were not significantly different between treatments and controls at any point during the experiment at 1000 µmol m^{-2} s^{-1} even when there was conspicuous mortality ($p > 0.05$, Fig. 3.3c).

NPQ also varied under different levels of light stress (Fig. 3.4). At 500 µmol m^{-2} s^{-1} NPQ remained very weak at all the sampling time points (Fig. 3.4a) even when the increase of ROS prevalence occurred at time 24.5h (Fig. 3.3a). At 750 µmol m^{-2} s^{-1}, NPQ increased from 0 to 0.29 ± 0.13 between time 0.5h and time 6h before dropping to 0.072 ±

0.062 at time 24.5h (Fig. 3.4b). In contrast, NPQ at 1000 µmol m^{-2} s^{-1} remained high at all sampling time points (Fig. 3.4c).

DISCUSSION

This study investigated cell death processes in response to acute high light stress as well as the dissipation of extra light energy by NPQ in *K .brevis*. Cell death only occurred at the largest light shift (50 to 1000 µmol m^{-2} s^{-1}) with concomitant increase of caspase-like activity. This is the first report of high-light induced PCD in a dinoflagellate. Our results also support strong light-tolerance in *K. brevis*, as no significant mortality or caspase-like enzyme activity were induced at an increase of irradiance up to 700 µmol m^{-2} s^{-1}. Oxidative stress and decreased photosynthetic capacities, however, were observed at lower light levels, but did not lead to cell death. The induction of NPQ may mitigate ROS production and therefore delay or prevent cell death under most levels of acute light stress. Our results highlight the important role of the balance between ROS production and removal on determining cell fates in *Karenia* under acute irradiance stress.

Light energy absorbed by chlorophyll is dissipated via three main pathways: fluorescence emission, photochemistry and non-photochemical quenching (NPQ; Fig. 3.5; Apel & Hirt, 2004; Muller et al., 2001). When a cell is acclimated to its ambient light level, the vast majority of energy is used to fuel photosynthesis by pumping electrons through PS II and PS I, while NPQ and intracellular ROS remain at very low levels (Fig. 3.5; Krause & Jahns, 2004; Müller et al., 2001; Suzuki & Mittler, 2006). Meanwhile, a small amount of the energy absorbed by chlorophyll is released as fluorescence; the yield of fluorescence is 0.6% - 3% (Krause & Weis, 1991; Müller et al., 2001). With increasing light intensity, the flux of electrons in the electron transport chain (ETC) increases. When the electron flux

exceeds the capacity of CO_2 assimilation, the extra electrons can be shunted to the reduction of oxygen by PSI (Mehler reaction) and the photorespiratory pathway, to protect the ETC against photoinhibition (Fig. 3.5; Apel & Hirt, 2004). Toxic H_2O_2 can be generated by these two processes and can be converted to H_2O efficiently by antioxidant enzymes (Fig. 3.5; Apel & Hirt, 2004). However, continuing strong electron flux will eventually lead to overreduction of ETC in PSII and formation of singlet oxygen (ROS) which cannot be scavenged (Figure 3.5; Apel & Hirt, 2004; Muller et al., 2001). Accumulation of ROS can trigger PCD by eliciting caspase-like activity (Bidle, 2016; Gechev & Hille, 2005; Vardi et al., 1999). In plant cells, another main source of ROS is respiration in mitochondria, but its contribution to cellular ROS load is very low at daytime as a result of efficient scavenging (Apel & Hirt, 2004; Miller et al., 2010; Purvis, 1997). Therefore, I focus on ROS generated from photosynthesis in this chapter.

Beside transferring electrons to O_2, excessive excitation energy in chlorophyll can be dissipated as heat by thermal inactivation of chlorophyll (Krause & Jahns, 2004), a process called non-photochemical quenching (NPQ; Fig. 3.5). In dinoflagellates, the major type of NPQ is the pH- or energy- dependent component (qE) characterized by rapid induction and relaxation (Cui et al., 2017). This rapid type of NPQ has been observed in *K. brevis* under stepped actinic irradiation (Cassell et al., 2015). The activation of qE pathway is determined by lumen pH which is affected by the splitting of H_2O in light reaction ($2H_2O \rightarrow 4H^+ + O_2 + 4e^-$; Fig. 3.5) (Krause & Jahns, 2004). NPQ plays an important role in photoprotection, as it accounts for the fate of 75% of absorbed light energy in plants (Niyogi, 1999; Rev, Demmig-Adams & Adams III, 1992). In order to gain insights into the effects of ROS production and NPQ-driven ROS inhibition on determining cell death under high light in *K. brevis*, the dynamics of photosynthetic parameters, ROS

prevalence and NPQ expression were analyzed and compared to understand their interrelationships under different levels of light stress.

NPQ-ROS regulation processes under different levels of high light

Acute light increase to 500 µmol m^{-2} s^{-1}

At 500 µmol m^{-2} s^{-1} photoinhibition appeared to be cumulative, as photosynthetic efficiency showed immediate decreases, but ROS generation and a reduction in electron transport capacity (rETRmax) only occurred after at least 6 hours of exposure. These observations indicated that *K. brevis* is able to manage this level of acute light stress for at least 6 hours, but by 24.5h ETC could not keep up with the high flow of energy and therefore could not resist the accumulation of oxidative stress. However, 500 µmol m^{-2} s^{-1} irradiance is insufficient to induce significant NPQ (0 to 0.027 ± 0.0118) in *K. brevis*. Other strains of *K. brevis* showed some induction of NPQ (0.1 and 0.05) under 363 µmol m^{-2} s^{-1} which is lower than the light level we used (Cassell et al., 2015). The light intensity needed to trigger NPQ is also highly variable among algal species. In the green alga *Chlamydomonas reinhardtii*, NPQ reaches to more than 0.2 immediately after light shift from darkness to 350 µmol m^{-2} s^{-1} (Elrad et al., 2002), while the dinoflagellate *Karlodinium veneficum* shows even stronger sensitivity of NPQ induction as the NPQ is higher than 1 after light shock from 0 to 200 µmol m^{-2} s^{-1} (Cui et al., 2017). Moreover, since the culture responses were only examined for the first 24 hours after exposure, it is unknown if NPQ would be activated later to balance the oxidative burst.

Acute light increase to 750 µmol m^{-2} s^{-1}

Under acute stress of 750 µmol m^{-2} s^{-1} we observed an immediate and sustained reduction in photosynthetic parameters. ROS prevalence increased within the first 30 minutes, indicating that the light shock rapidly overwhelmed the capacity of some cells to channel the additional light energy. High light-induced ROS have been reported in microalgae including cyanobacteria and diatom. In cyanobacteria *Trichodesmium* high light remarkably enhanced the production of ROS (Berman-Frank et al., 2001), while rapid light-induced ROS was detected in the diatom *Thalassiosira weissflogii* under changing light (30-500 µmol m^{-2} s^{-1}; Milne et al., 2009). While NPQ activity was not evident at 30 minutes, it was induced during the next 6 hours. Induction of NPQ was accompanied by a disappearance of ROS staining, suggesting that excess energy was diverted into the NPQ pathway and away from the damaged ETC (Apel & Hirt, 2004; Triantaphylides et al., 2008; Muller et al., 2001). A balancing relationship between NPQ and ROS has been reported in *K. brevis*, as a strain that was deficient in NPQ produced ROS at twice the rate of the strain with high NPQ activity (Cassell et al., 2015). Previous research has also suggested that conversion of xanthophyll cycle in NPQ activation can offer significant protection under partially cloudy and sunny days by down-regulating photosynthesis in *K. brevis* (Evens et al., 2001). Therefore, photoprotection regulated by NPQ may play a key role in cellular survival in *K. brevis* under sudden light increase. This is evident from the increase in cell densities at time 6h, as no significant mortality occurred despite the clear impacts on photosynthetic function. After the dark period, we see a repeat of the ROS/NPQ pattern from the day before. Within 30 minutes of the 750 µmol m^{-2} s^{-1} light exposure, ROS prevalence spikes without induction of NPQ, which presumably relaxed during the preceding 12 hours of dark. An increase in ROS in the control culture was also observed,

but this corresponds to the diel fluctuation of ROS described in Chapter 2, which is evident in all of the control cultures in Figure 3.3.

Acute light increase to 1000 µmol m^{-2} s^{-1}

Cell death was observed under 1000 µmol m^{-2} s^{-1}, but rapid induction of the NPQ pathway may have delayed the mortality for a limited period of time. Immediately after the transfer to 1000 µmol m^{-2} s^{-1}, photochemistry was severely reduced by photoinhibition and/or photodamage, as shown by tremendously depressed photosynthetic parameters. NPQ was also markedly induced within 30 minutes of exposure. This induction of NPQ likely reduced the potential for ROS production, thereby delaying the activation of the PCD cascade for at least six hours. Rapid NPQ activation (within 30 mins) triggered by intensive acute light stress (over 1000 µmol m^{-2} s^{-1}) has been observed in rice, diatom, green algae and cyanobacteria (Xu et al., 2012; Yamori et al., 2016). Nonetheless, the 1000 µmol m^{-2} s^{-1} eventually overwhelmed the *K. brevis* cells and 60% of them died over the next 18 hours. The high prevalence of STYOX staining and caspase-like activity at time 24.5h indicate autocatalytic cell death. ROS prevalence increased from time 6h to time 24.5h in the treatments, likely because there were far fewer live cells. Dead cells have permeable membranes which would not retain small intra-cellular ROS molecules, so ROS detection may be restricted to the few remaining live cells.

Cell death and tolerance under high light stress in *K. brevis*

Significant cell death was only observed at the highest light levels in *K. brevis,* and it was a self-catalytic process. Although no research of high-light-induced PCD has been reported from dinoflagellates, cell death pathway with PCD features was reported in

cyanobacteria species under high light. Berman-Frank et al. (Berman-Frank et al., 2004) studied the demise of the marine cyanobacterium *Trichodesmium* in response to 450 µmol m^{-2} s^{-1} and found that within 3 hours of light exposure a large proportion of cells showed low levels of DEVD cleavage (a substrate for caspase), while extended exposure (> 7 hours) caused stronger DEVD cleavage and death in cells. Our research is the first report of high-light-induced PCD in a dinoflagellate, revealing the effects of short-term light shock on the viability of *K. brevis* populations.

Our results support the hypothesis that *K. brevis* is a high-light-tolerant species (Tilney et al., 2019). No significant cell death and caspase-like activity were observed after light shift from 50 to 500 or 750 µmol m^{-2} s^{-1}, instead the cell densities continued to increase. The cells remained viable despite severe depression of photosynthetic capacities under acute light stress. In a previous study that investigated physiological responses of *K. brevis* transferred from 150 to 825 µmol m^{-2} s^{-1} for 4-8 hours, there was no difference in viability even though Fv/Fm declined significantly (Miller-Morey & Dolah, 2004). Tilney et al. (2019) reported dose-dependent decreases of Fv/Fm without growth inhibition from 43 to 1340 µmol m^{-2} s^{-1} in *K. brevis*, leading to the idea that PSII photoinactivation may not affect photosynthesis to an extent that would significantly suppress growth. In addition, *K. brevis* are apparently insensitive to UV in the field, because photosynthetic responses between "PAR-only" and "PAR + UV" treatments from natural sunlight were very similar, and the level of photoinhibition due to high PAR irradiance was significantly higher than the level of inhibition from UV (Evens et al., 2001). These characteristics described above may be beneficial for the formation and development of *K. brevis* blooms in GoM, because swimming behavior and upwelling can keep algal cells at sea surface where the noon incident radiation can be as high as 1200 µmol m^{-2} s^{-1} (Evens et al., 2001; Walsh et al., 2006).

While cell death of *K. brevis* did occur at 1000 µmol m^{-2} s^{-1} it happened only after at least 6 hours of exposure. In this case, dose-dependent NPQ expression may have played a key role in preventing or delaying the occurrence of cell death by mitigating ROS production that could trigger the PCD cascade. The timing of NPQ induction varied by light intensity and exposure time, and it was preceded by an increase in ROS prevalence. At the 500 µmol m^{-2} s^{-1} exposure level, significant ROS prevalence was only detected at the last time point in the absence of NPQ induction. At the 750 µmol m^{-2} s^{-1} level, immediate increase in ROS was followed by a later induction of NPQ, decrease in ROS, and no evidence of cell death. At the highest light exposure, NPQ induction was immediate, and widespread cell mortality occurred after 6 hours exposure. In the field, different intensities and timing of NPQ expression may help *K. brevis* cope with natural fluctuations of light intensity, maintaining the viability and development of the population. On the other hand, the occurrence of significant PCD and cell lysis after 6 hours of 1000 µmol m^{-2} s^{-1} also revealed the limitations of photoprotection from NPQ as well as the potential effects of extreme high light on the sustainability of *K. brevis* populations.

CONCLUSIONS

This is the first report of high-light induced PCD in a dinoflagellate. Cell death in *K. brevis* only occurred at the largest light shift (50 to 1000 µmol m^{-2} s^{-1}) and was associated with an increase of caspase-like activity. This research supports strong light-tolerance in *K. brevis*, as no significant mortality and caspase-like activity were shown under 700 µmol m^{-2} s^{-1} increase of irradiance. However, depressed photosynthetic capacities and oxidative stress were apparent, but did not necessarily lead to cell death. NPQ exhibited dose-dependent activation with increasing light stress and duration; it

enables cells to resist or delay PCD by mitigating ROS production under certain levels of acute light stress. These results highlight the important role of the balance between ROS generation and NPQ activation on determining cell fates in *Karenia* under acute irradiance stress. They also provide insights into potential survival strategies and mechanisms of bloom decline under the changeable light environment in the field.

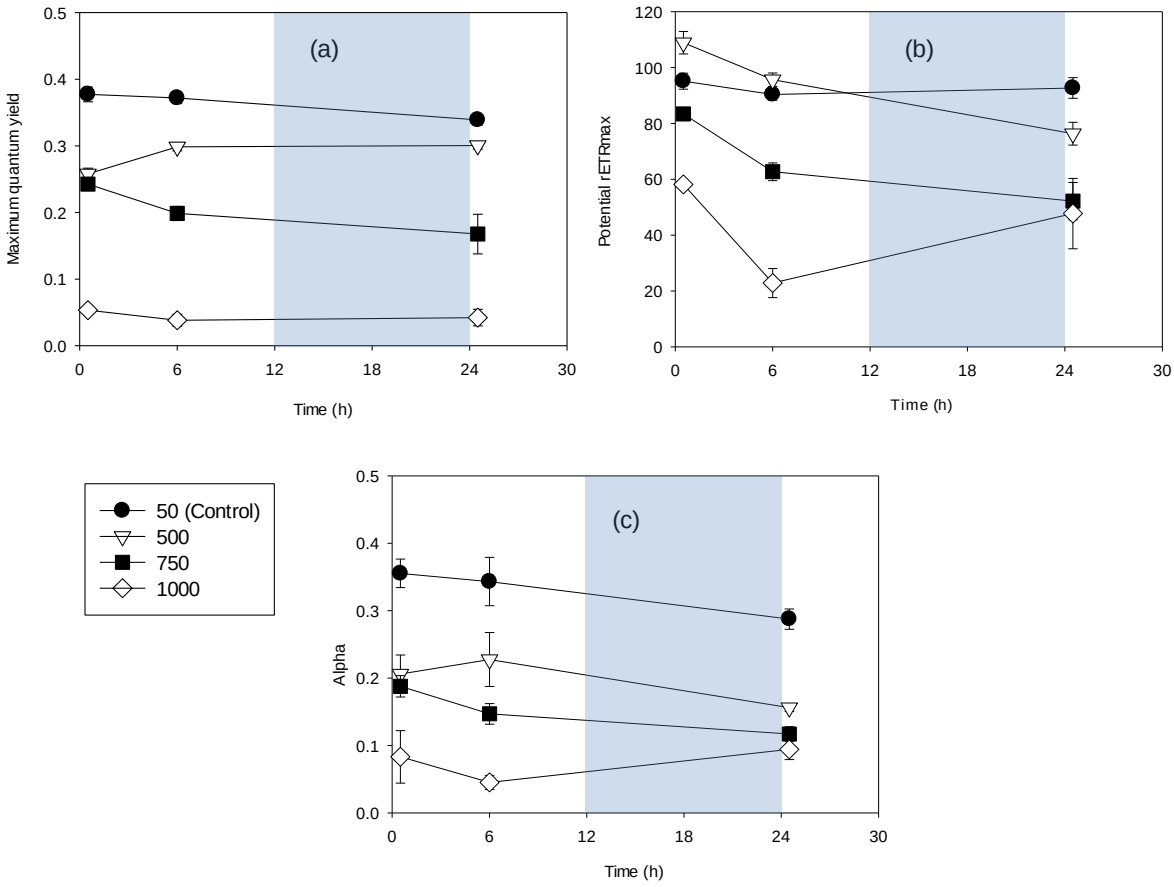

Figure 3.1: Fv/Fm (a), potential rETRmax (b) and alpha (c; μmol^{-1} m^2 s) in *K. brevis* cells transferred from 50 to 500, 750 and 1000 µmol m^{-2} s^{-1} and the controls (50 µmol m^{-2} s^{-1}). Blue shading indicates dark phase. Note: patterns of Fv/Fm, rETRmax and alpha among the control sets were very similar, so only the data from the control 500 set are shown in the figure. Data points show average values of triplicate treatment/control, and error bars show standard deviation of the replicates (n = 3).

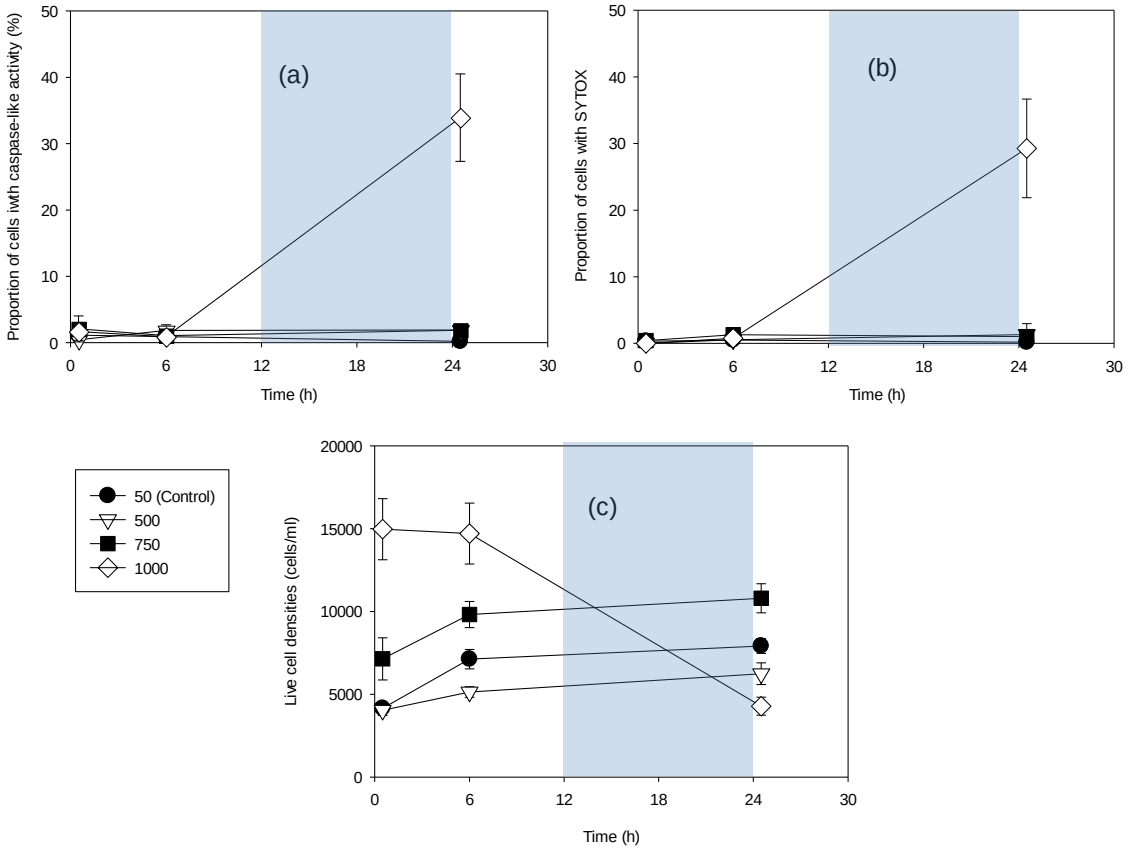

Figure 3.2: Caspase-like activity (a), cell death (b) and live cell densities (c) in *K. brevis* cells transferred from 50 to 500, 750, and 1000 µmol m^{-2} s^{-1} and the controls (50 µmol m^{-2} s^{-1}). Blue shading indicates dark phase. Note: the data for control were obtained from control 500 cultures. Data points show average values of triplicate treatment/control, and error bars show standard deviation of the replicates (n = 6).

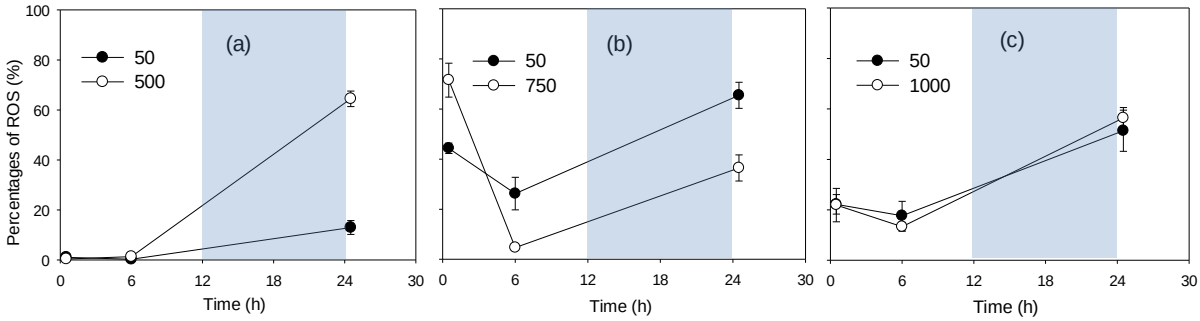

Figure 3.3: The temporal changing patterns of ROS percentages in *K. brevis* cells transferred from 50 to 500 (a), 750 (b) and 1000 (c) µmol m^{-2} s^{-1} and their corresponding controls (50 µmol m^{-2} s^{-1}). Blue shades indicate dark phase. Data points show average values of triplicate treatment/control, and error bars show standard deviation of the replicates (n = 6).

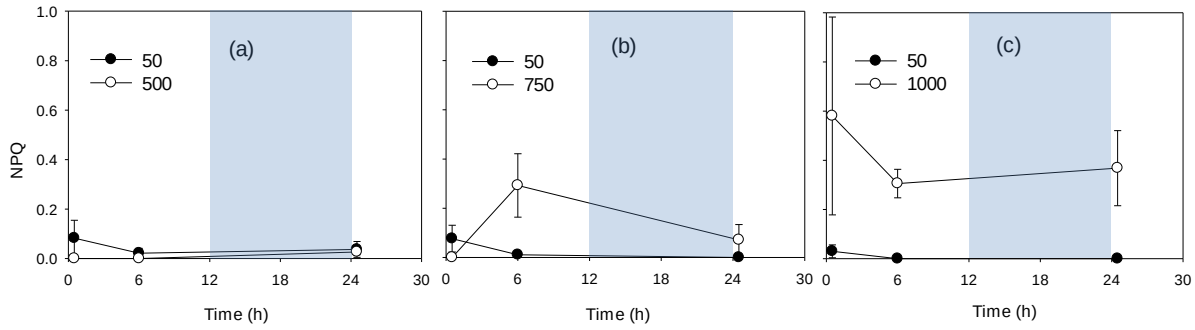

Figure 3.4: The temporal changing patterns of NPQ in *K. brevis* cells transferred from 50 to 500 (a), 750 (b) and 1000 (c) µmol m^{-2} s^{-1} and their corresponding controls (50 µmol m^{-2} s^{-1}). Blue shades indicate dark phase. Data points show average values of triplicate treatment/control, and error bars show standard deviation of the replicates (n = 3).

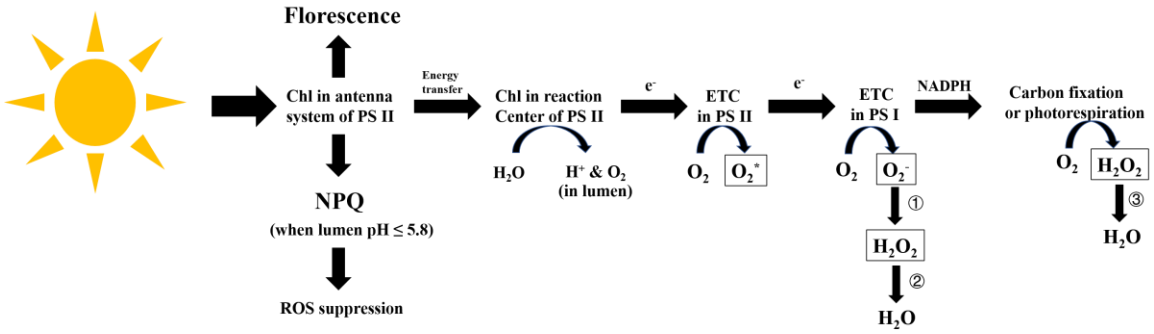

Figure 3.5. Possible fates of energy absorbed by chlorophylls in microalgae: fluorescence emission, photochemistry and non-photochemical quenching (NPQ). When Chl in antenna system is excited by light absorption, some energy can be relaxed via fluorescence emission. Some other energy will be transferred to Chl in reaction center and enter ETC in a form of electrons. Meanwhile, oxygen and hydrogen ions would be generated by the split of H_2O in lumen. Under low light, electrons would be transferred through ETC and attend carbon fixation. Under high light, in order to sustain high level of electron flux, excessive electrons would be transferred to oxygen: (a) the reduction of oxygen by PSI that generates superoxide (O_2^-) and H_2O_2, and (b) the photorespiratory pathway that generates H_2O_2 within the peroxisome. These ROS species can be converted to H_2O by (1) superoxide dismutase, (2) ascorbate peroxidase and (3) catalase. Singlet oxygen (O_2*), a species of ROS, are increasingly generated when ETC are over-reduced due to high light. Accumulation of ROS (in black boxes) would trigger PCD pathways. On the other hand, when pH in lumen is lower than 5.8 by split of H_2O, NPQ would be activated to dissipate excitation energy in Chl as heat for the suppression of ROS production.

Chapter 4: Do acute osmotic and temperature stress trigger cell death responses in the harmful dinoflagellate *Karenia brevis*?

ABSTRACT

During *K.brevis* bloom season in the Gulf of Mexico (August to December), algal populations may experience drastic temperature and salinity changes as a result of freeze events and transport between coastal and offshore areas. Given the close relationship between environmental stimuli and algal cell death, understanding cellular stress responses to acute hypo-osmotic stress, cooling and heat stress in *K. brevis* could provide insights into potential cell loss processes during bloom dynamics. Here I used established cell death and stress markers to characterize the short-term (6 hours) cellular response to a gradient of each environmental stimulus (hypoosmotic stress: 35 psu → 30, 25 and 20 psu; cooling stress: 30℃ → 25, 20 and 15 ℃; heat stress: 20 ℃ → 25, 30 and 35℃). Intensity-dependent apoptotic cell death occurred when salinity decreased by 5, 10, or 15 psu. It was accompanied by increases in reactive oxygen species, which may also interact with photosynthesis to further decrease photosynthetic efficiency. Acute heating and cooling stress within 10 ℃ did not induce cell death in *K. brevis* cells, revealing a strong thermal tolerance. Cell death processes were only evident after 15 ℃ temperature change without induction of caspase-like activity, suggesting that cell death modes vary with different environmental stimuli in *K. brevis*. Comparing our experimental results with hydrographic data from the western GoM, *K. brevis* populations are not likely to encounter sufficient acute temperature or salinity stress in isolation to result in appreciable mortality.

INTRODUCTION

During the past two decades programmed cell death (PCD), a series of genetically controlled self-destruction pathways, have been revealed to trigger cell lysis of many cosmopolitan phytoplankton species, potentially playing an important role in rapid termination of harmful algal blooms (HABs; reviewed by Bidle, 2015). Therefore, it is necessary to understand physiological characteristics of HAB species that link to cell death/PCD under environmental stress. In the coastal Gulf of Mexico (GoM) the HAB-forming dinoflagellate *Karenia brevis* has profound impacts on the ecosystems, economy and human health (Brand et al., 2012; Vargo, 2009). During its bloom season in the GoM (August to December), *K. brevis* may experience chilling events and be transported between coastal and offshore areas repeatedly, which would expose algal cells to drastic salinity and temperature changes (Errera, 2013; Reyna et al., 2017; Steidinger, 1998). Given the occurrence of PCD induced by various adverse environmental conditions in many microalgal species (Bidle & Bender, 2008; Bidle et al., 2007; Jiménez et al., 2009), understanding cell death responses to acute hypo-osmotic stress, cooling and heating stress in *K. brevis* could provide insights into potential mechanisms of bloom decline and termination.

To the best of our knowledge, no research has investigated cell death responses under hypo-osmotic and cooling stress in unicellular algae, leaving a gap in our understanding of the effects of these two ecologically-relevant stimuli on algal mortality. Previous research on salinity-induced cell death in microalgae mostly focused on high salt addition in freshwater algae, and diverse PCD cell death modes have been reported in different species. For example, apoptosis was observed under hyper-osmotic stress in the cyanobacterium *Anabaena* (Ning et al., 2002) and the chlorophyte *Chlorella saccharophila* (Zuppini et al., 2010) including the hallmarks of caspase-like activity and DNA

fragmentation. The unicellular chlorophyte *Dunaliella viridis* exhibited morphological features of paraptosis, which is a type of PCD that lacks caspase-like activity (Jimenez et al., 2009). In the unicellular green alga *Micrasterias denticulata*, high KCl and NaCl induced a special form of PCD - autophagy - that was also independent of caspase-like activity but genetically controlled and involved lysosomes to engulf cellular content (Affenzeller et al., 2009; Denton et al., 2012). Similarly, cell death modes reported after heat shock include apoptosis (Durand et al., 2011; Bouchard & Yamasaki, 2009; Zuppini et al., 2007), apoptosis-like (Leu & Hsu, 2005) and necrosis (Jimenez et al., 2009), which is acute and irreversible cellular injury featuring loss of membrane integrity, swelling and lysis (Bidle, 2016; Dingman & Lawrence, 2012). Different intensities of heat shock can induce different types of cell death within the same microalgal species (Dingman & Lawrence, 2012; Dunn et al., 2004). Thus, cell death modes in response to environmental stresses can be both species-specific and dose-dependent.

The objectives of this research were to: (1) define stress-related death processes in response to acute hypo-osmotic, cooling and heating stress in *K. brevis*; (2) evaluate the existence of non-apoptosis cell death induced by environmental stimuli in *K. brevis*; (3) gain insights into the potential effects of low salinity and temperature changes on the decline and termination of *K. brevis* blooms. Here we used established cell death and stress markers to characterize the short-term (6 hours) cellular response to a gradient of each environmental stimulus. Hypo-osmotic stress resulted in intensity-dependent apoptotic cell death, marked by increases in reactive oxygen species (ROS) prevalence and caspase-like activity. In contrast, a non-apoptotic cell death was observed only under the greatest (15 ℃) temperature increase or decrease, indicating that cell death modes may vary depending upon the environmental stimulus. Acute heating and cooling stress within 10 ℃ did not induce cell death responses in *K. brevis* cells, revealing their strong thermal acclimation

ability. The potential effects of hypo-osmotic and temperature on cell death in *K. brevis* populations were discussed based on annual hydrographic data from western GoM.

METHODS

Culture conditions and experiment setup

Osmotic stress:

K. brevis clone SP3 was isolated by Suzanne Pargee from a red tide offshore of South Padre Island, Texas in 1999 (Magaña & Villareal, 2006). SP3 was inoculated at a density of 950 cells/ml into 1100 ml of L1 medium (Guillard & Hargrave, 1993) made from seawater collected offshore in the GoM. For medium preparation, seawater was filtered through 0.2 um polycap capsule filter (Whatman Inc.), adjusted to a salinity of 35 psu and autoclaved prior to the addition of sterile L1 nutrient stocks. The culture was maintained at an irradiance of ca. 120 µmol m^{-2} s^{-1} on a 12:12 hour light:dark cycle with cool white fluorescent illumination at 25°C. When the concentration of cells reached early log phase (~3500 cells/ml), 60 ml of culture was dispensed into each of 18, 125 ml flasks. Sets of triplicate flasks were designated as "S-Treatment 30", "S-Treatment 25", "S-Treatment 20", "S-Control 30", "S-Control 25" and "S-Control 20".

After 3-5 days, when cultures were in mid-log phase (~8000 cells/ml), hypo-osmotic stress was induced in S-Treatment 30, S-Treatment 25 and S-Treatment 20 by diluting the cultures to a salinity of 30, 25 and 20 psu respectively, via the addition of MilliQ water enriched with L1 nutrients. Controls received the same volume of L1 medium (salinity 35 psu) at the same time. Salinity in each flask was verified with a refractometer (Magnum Media Salinity). The experiments were conducted on 3 successive days in the

order of 30, 25, then 20 psu. The introduction of hypo-osmotic stress occurred at time 0h which was 3 hours into the light cycle. Treatments and their corresponding controls were sampled at time 0.5h and time 6h for measurement of cell density, Fv/Fm and percentages of cells with cell death, ROS and caspase-like activity.

***Cooling stress**:*

SP3 was inoculated at a starting density of 3000 cells/ml into 1100 ml of L1 medium of salinity 32 psu and maintained at an irradiance of ca. 120 µmol m^{-2} s^{-1} on a 12:12 light:dark cycle at 30 °C. When the concentration of cells reached early log phase (~3500 cells/ml), 60 ml of culture were dispensed into each of 18, 125 ml flasks. Sets of triplicate flasks were designated as "C-Treatment 15", "C-Treatment 20", "C-Treatment 25", "C-Control 15", "C-Control 20" and "C-Control 25". After 3-5 days, when cultures were in mid-log phase (~10000 cells/ml), C-Treatment 15, C-Treatment 20 and C-Treatment 25 were moved from 30 °C to 15, 20 or 25 °C respectively, while their corresponding controls remained at 30 °C. The experiments were conducted on 3 successive days in the order of 15, 20 and 25 °C. The move to a cooler incubator occurred at time 0h which was 3 hours into the light cycle. Treatments and their corresponding controls were sampled at time 0.5h and time 6h for measurement of cell density, Fv/Fm and percentages of cells with cell death, ROS and caspase-like activity. During the period between time 0.5h to time 6h in the experiment at 25 °C, a system fault in the incubator triggered by power outage caused severe temperature fluctuation and therefore the loss of samples at time 6h.

Heating stress:

SP3 was inoculated at a starting density of 2100 cells/ml into 1100 ml of L1 medium of salinity 32 psu and maintained at an irradiance of ca. 120 µmol m^{-2} s^{-1} on a 12:12 light:dark cycle at 20°C. When the concentration of cells reached early log phase (~3500 cells/ml), 60 ml of culture was dispensed into each of 18, 125 ml flasks. Sets of triplicate flasks were designated as "H-Treatment 25", "H-Treatment 30", "H-Treatment 35", "H-Control 25", "H-Control 30" and "H-Control 35". After 3-5 days, when cultures were in mid-log phase (~9000 cells/ml), H-Treatment 25, H-Treatment 30 and H-Treatment 35 were moved from 20 °C to 25, 30 or 35°C respectively, while their corresponding controls remained at 20 °C. The experiments were conducted on 3 successive days in the order of 25, 30 and 35 °C. The move to a warmer incubator occurred at time 0h which was 3 hours into the light cycle. Treatments and their corresponding controls were sampled at time 0.5h and time 6h for measurement of cell density and percentages of cells with cell death, ROS and caspase-like activity.

Measurement of stress and cell death markers

Three cellular parameters were measured by fluorescent dyes as described below: SYTOX, ROS and caspase-like activity. All reagents produced green fluorescence which was observed under the epifluorescent microscope with an excitation wavelength of 450–490 nm and emission of 523 nm. More than 50 cells were counted and examined, in replicate, from each culture vessel using a Sedgewick Rafter chamber under a fluorescent microscope.

Cell death detection

Integrity of the cell membrane, which is an indicator of cell death, was assessed using SYTOX-green dye (S7020, Invitrogen). This reagent has high affinity with nucleic acid and can only penetrate compromised plasma membranes. Stock solution (5 mM in DMSO) was diluted into Phosphate-Buffered Saline (PBS) to prepare a 100 μM working solution. Samples were stained by adding 2.5 μl of the working solution directly to 500 μl of culture, for a 0.5 μM final concentration of SYTOX-green dye. At room temperature SYTOX-positive cells were counted after 60 min dark incubation. SYTOX percentages were calculated as: the number of cells with green fluorescence/ total cell number.

ROS production

Intracellular ROS was detected using carboxy-H_2DCFDA (C400, Invitrogen). A 10mM stock solution was prepared by dissolving 2 mg of carboxy-H_2DCFDA in 376 μl DMSO. Before the experiment a 100 μM working solution was prepared by diluting an aliquot of stock solution in PBS. The working solution was then mixed with the culture sample at a 1:10 ratio, resulting in a 10 μM final concentration of carboxy-H_2DCFDA. Green fluorescence generating from the oxidation of carboxy-H_2DCFDA was examined after 20 min dark incubation at room temperature. Percentages of ROS were calculated as: the number of cells with green fluorescence/ total cell number.

Activity of caspase-like enzymes

A distinctive feature of PCD is the activation of caspase-like enzyme activity. In order to detect caspase-like activity in *K. brevis* cells, CellEvent *in situ* caspase 3/7 Green Detection Reagent (C10423, Invitrogen) was diluted in a subsample of *K.brevis* cultures to a final concentration of 10 μM. Observations of stained cells were performed after at least

30 mins of room temperature incubation. Percentage of cells with caspase-like activity were calculated as: the number of cells with green fluorescence/ total cell number.

Cell Density

The number of total morphologically intact cells was estimated in replicate from each culture vessel via microscope using a Sedgewick Rafter counting chamber after Lugol's preservation. Single measurement was applied on the flasks in the controls of osmotic stress. Densities of live cells from each flask were calculated as: total morphologically intact cells per ml × (1- averaged SYTOX proportion). Then these densities were averaged among triplicate control/treatment flasks.

Photosynthetic parameters

At each sampling time of the hypo-osmotic stress and cooling stress experiments, 2mL of sample were collected from each flask and placed in the dark for 30min. Fast Repetition Rate fluorometry (FRRf) on a FastTRACKA instrument (Chelsea Technologies Group Ltd.) was used to measure the photosynthetic efficiency of photosystem II (Fv/Fm), where Fm is the maximal fluorescence excited by a saturating pulse of blue light from a dark-adapted sample and Fv is the difference between minimal fluorescence of a dark-adapted sample (Fo) and Fm.

Statistical analysis

Two-way repeated measures ANOVA (RM-ANOVA) was used to evaluate differences of live cell densities, Fv/Fm and prevalence of PCD markers in treatments and

controls at each sampling time point. The Bonferroni post hoc test was used to determine significance of the differences. The original α is equal to 0.05. All statistical analysis was performed using SigmaPlot 14.

RESULTS

Osmotic stress:

Acute hypo-osmotic stress (5, 10 and 15 psu decrease) induced intensity-dependent cell death and photosynthetic responses within 6 hours.. Percentages of cellular parameters (ROS, caspase-like activity and cell death) in treatments and controls arer shown in Table B1 in Appendix B.

Within 30 mins after the introduction of hypo-osmotic stress (Fig. 4.1A, 4.2A), cellular responses of *K. brevis* ranged from minor oxidative stress to population crash. Rapid cell lysis occurred under the largest salinity change (15 psu decrease), where total cell densities (live + dead cells) in the treatments were about 25% lower than controls (data not shown). ROS prevalence in all salinity treatments was higher than in controls ($p < 0.05$), increasing from 10.39 ± 3.11% to 78.00 ± 6.26% as salinity was reduced (Fig. 4.1A). At the lowest stress level (5 psu decrease), all other measures - caspase-like activity, SYTOX, and Fv/Fm - were not different from the controls ($p > 0.05$; Fig. 4.1A, 4.2A). In contrast, the 10 and 15 psu reductions showed rapid activation of the apoptosis cascade and significant depression of Fv/Fm, in an intensity-dependent manner (Fig. 4.1A, 4.2A). Specifically, after 10 psu decrease the percentages of cells with caspase-like activity and SYTOX were higher than controls by 50 ± 9.62% and 32.84 ± 4.93% respectively ($p < 0.001$), while the differences under 15 psu decrease were even higher, about 80% ($p <$

0.001; Fig. 4.1A). Fv/Fm (Fig. 4.2A), a common proxy of cellular stress, was reduced to 0.027 ± 0.024 (25 psu) and 0.011 ± 0.0095 (20 psu).

By time 6h, intensity-dependent cell death responses to hypo-osmotic stress were observed in all treatments (Fig. 4.1B). Significant apoptosis cascade remained under 10 and 15 psu decrease. Although cell death percentages under decrease of 5 psu was observed to be significantly higher than controls (higher by 7.67 ± 3.56%; $p < 0.02$; Fig. 4.1B), Fv/Fm and live cell densities did not change from the control levels at this time point ($p > 0.05$; Fig. 4.2B). In contrast, cell death percentages under 10 and 15 psu decrease remained high and Fv/Fm was extremely low (Fig. 4.1B, 4.2B). The difference of live cell densities between treatments and controls under decrease of 10 psu continuedly increased, while this difference under 15 psu decrease remained similar from time 0.5h to time 6h (Fig. 4.2A, 4.2B).

Cooling stress:

Cellular responses of *K. brevis* to cooling stress were studied through culture transfer from 30 °C to 25°C, 20°C or 15°C. Percentages of cellular parameters (ROS, caspase-like activity and cell death) in treatments and controls were shown in Table. B2 in Appendix B.

Only the greatest decrease in temperature (-15 °C) induced significant stress and cell death responses during the 6 hours of monitoring (Fig. 4.3). Under decrease of 5 °C and 10 °C, percentages of cells with ROS, caspase-like activity and SYTOX were not significantly higher than controls during the 6-hour experiment ($p > 0.05$; Fig. 4.3). Meanwhile Fv/Fm and live cell densities in treatments and controls were not different from each other under these two cooling stress levels ($p > 0.05$; Fig. 4.4). After the introduction

of acute temperature decrease of 15 °C, rapid cell death responses were observed (Fig. 4.3), but in the absence of significant cell lysis. Percentages of cells with ROS or SYTOX labeling at time 0.5h were higher than controls by 61.20 ± 2.62% ($p < 0.001$) and 44.32 ± 6.70% ($p < 0.001$), respectively (Fig. 4.3A). Fv/Fm was reduced to 0.13 ± 0.010 from 0.32 ± 0.0010 in controls (Fig. 4.4A). However, percentages of cells with caspase-like activity in treatments and controls were not different (36.78 ± 2.09% vs. 30.69 ± 5.53%; $p > 0.05$). At time 6h the difference in percentages of cells with ROS and SYTOX between treatments and controls grew to 77.80 ± 3.34% and 65.53 ± 7.28%, respectively (Fig. 4.3B). Caspase-like activity was not induced by any of the low temperature treatments, and in two cases its prevalence was higher in control cultures than in treatments (Fig. 4.3B).

Heating stress:

Cellular responses of *K. brevis* to heat stress were studied through culture transfer from 20 °C to 25°C, 30°C or 35°C. Percentages of cellular parameters (ROS, caspase-like activity and cell death) in treatments and controls were shown in Table B3 in Appendix B

Cell death responses were only observed under the greatest increase in temperature (+15 °C) during the 6 hours of monitoring (Fig. 4.5). With increase of 5 °C and 10 °C prevalence of components in apoptosis cascade were generally not significantly higher than controls except some small increases in ROS percentages with statistical significance in these experiments ($p < 0.02$; Fig. 4.5A). Pronounced mortality was induced by increase of 15 °C at time 6h, as percentages of cells with SYTOX were higher than controls by 27.24 ± 3.99% ($p < 0.001$; Fig. 4.5B) with increased ROS prevalence ($p < 0.001$; Fig. 4.5B) and much lower live cell densities ($p < 0.001$; Fig. 4.6B). In contrast, percentages of cells with caspase-like activity were lower than controls by 14.31 ± 6.98% ($p < 0.02$; Fig. 4.5B). It is

noteworthy that drastic cell lysis occurred from time 0.5h to time 6h under the greatest temperature increase, as approximately 4000 cells/mL disappeared.

DISCUSSION

In this study, we used established cell death and stress markers to define short-term cellular responses to different levels of acute hypo-osmotic, heating and cooling stress in *K. brevis*. Our results indicate that temperature and salinity stress induce death by different pathways. Intensity-dependent apoptosis was clearly observed with decreasing salinity. In contrast, only the largest change in temperature (15 ℃) caused significant mortality, and it was not accompanied by caspase-like activity.

Cell death responses to hypo-osmotic stress

This research represents the first report of apoptosis in response to hypo-osmotic stress in unicellular algae. Our results showed that salinity reductions $\geqslant$5 psu induced cell death that was characterized by intensity-dependent increases in the prevalence of ROS and caspase-like activity. The smallest decrease in salinity used here (35 to 30 psu) triggered slight mortality after 6 hours of exposure, whereas a significant apoptosis response and Fv/Fm depression were observed within 30 minutes when the salinity decreased by 10 or 15 psu. Most previous research regarding the relationships between salinity change and cell death in microalgae focused on freshwater species and therefore high salt stress (Affenzeller et al., 2009; Ning et al., 2002; Vavilala et al., 2015; Zuppini et al., 2010), whereas in saline microalgae hyper-osmotic stress has only been examined in *Dunaliella viridis* (Jimenez et al., 2009). A variety of PCD types are found in green algae

(Affenzeller et al., 2009; Jimenez et al., 2009; Zuppini et al., 2010) and cyanobacteria (Ning et al., 2002) in response to increased salinity, while non-PCD cell death modes may also occur in microalgae, as necrosis was caused by ionic stress of NaCl in the unicellular green alga *Chlamydomonas reinhardtii* (Vavilala et al., 2015). The cell death pattern observed here under hypo-osmotic stress in *K. brevis* was categorized as apoptosis because of the accompanying induction of caspase-like activity. Although there are no reports of hypo-osmotic stress and PCD in marine phytoplankton, apoptosis is triggered by hyper-osmotic stress in the cyanobacterium *Anabaena* (Ning et al., 2002) and the Chlorophyte species *Chlorella saccharophila* (Zuppini et al., 2010), both of which exhibited caspase-like activity. To date, the specific executioners of caspase-like activities in phytoplankton have not been identified, while these caspase-like activities were evidenced to correlate with apoptosis in many algal species under a variety of environmental stresses (Bidle & Bender, 2008; Bidle et al., 2007; Jiménez et al., 2009; Vardi et al., 1999; Zuppini et al., 2010).

In *K. brevis* hypo-osmotic stress clearly triggers ROS production which can induce PCD and interact with photosynthetic activity. The main source of ROS accumulated in photosynthetic cells is the blockage of electron transfer flow in chloroplast which leads to photoinhibition and generation of singlet oxygen (Apel & Hirt, 2004). In our experiment a significant decline of Fv/Fm was observed with increasing ROS prevalence along with stress gradient in *K. brevis*. However, since they were measured at the same time, it is difficult to assign the cause-and-effect. Excessive production of ROS is a feature of instant responses to various abiotic stresses in unicellular algae, where ROS can act as a signal in transduction pathways for activation of PCD (Bidle, 2016; Vardi et al., 1999; Zuppini et al., 2010). In *K. brevis* hypo-osmotic-induced apoptosis pathway, we found significant increase of ROS prevalence during the first 30 mins after the stress, supporting a rapid

involvement of ROS in responses to decreasing salinity in phytoplankton. Beside leading to PCD in phytoplankton, the generated ROS under hypo-osmotic stress may interact with photosynthesis to further decrease its capacity directly and indirectly. Many previous studies have suggested a close correlation between oxidative stress and photosynthesis under salinity change. In *Dunaliella salina* ROS production induced by hypo-osmotic stress activates significant decline of carbonic anhydrase and therefore decrease of Fv/Fm and photosynthetic carbon fixation (Liu et al., 2012). In addition, ROS is believed to have regulatory roles on the expression of chloroplast genes that involve in decrease of photosynthetic efficiency (Pfannschmidt, 2003). Apart from acting as a signal, ROS itself would exert detrimental effects on photosynthetic apparatus by the pre-oxidation of lipids in thylakoids (Lu & Vonshak, 1999). On the other hand, in order to prevent ROS hyper-accumulation, non-photochemical quenching (NPQ) would be induced to further downregulated photosynthesis. Azzabi et al. (2012) observed activation of NPQ in Bryophyte as a response to high salt stress against photooxidation. In *K. brevis* Daugherty (2017) noted increase of NPQ concomitant with decline of Fv/Fm when cultures transferred from salinity 35 to 27 psu, suggesting a role of NPQ induction in photoprotection and osmo-acclimation in chloroplast. However, this ability to adjust photosynthesis via ROS and NPQ may be varied among *K. brevis* strains depending on individual's toxicity (Cassell et al., 2015; Daugherty, 2017). In order to understand the effects of hypo-osmotic stress on productivity of *K. brevis*, our results highlight the needs to further investigate the stepwise interactions between ROS and photosynthesis under low salinity.

Cell death responses under temperature stress

Cell death was only observed under the most severe temperature changes. When the temperature decreased by 15 °C, cell death occurred rapidly, within the first 30 minutes, whereas after 15 °C heating stress it was not apparent until the 6-hour time point. The increases in cell death percentages and the reductions in live cell densities in *K. brevis* were not accompanied by induction of caspase-like activity, indicating a non-apoptotic death pathway. Caspase-independent cell death induced by temperature stress was reported in microalgal species including *Alexandrium tamarense* (Jauzein & Erdner, 2013) and *Duneliella viridis* (necrosis, Jiménez et al., 2009). The observed increase of ROS prevalence in *K. brevis* cultures may result from disruption of membrane-based processes such as photosynthesis which are very sensitive to thermal stress (N. Suzuki & Mittler, 2006). Comparable extent of mortality and widespread ROS prevalence was reported in *A. tamarense* after acute heat shock from 16 °C to 32 °C at which the extent of temperature change was similar to the one in our study (Jauzein & Erdner, 2013). The occurrence of necrosis is possible, as it is considered as a consequence of severe physiochemical stress such as heat or freeze-thawing in some microalgae (Vavilala et al., 2015). Since data of cellular structure change from stressed cells were not available in our experiment, it is impossible to categorize the specific cell death mode observed under cooling stress in *K. brevis*. In addition, the percentages of cells with caspase-like activity revealed strong background level and diel variation in *K. brevis,* which is discussed in Chapter 2 and may explain the negative value in Fig. 4.3 and Fig. 4.5.

In this study *K. brevis* revealed impressive acclimation ability to acute temperature changes. Similar cellular responses to heat stress were observed in *Karenia mikimotoi,* as robust photosynthesis with no mortality was noted under acute heat shock from 16 to 28 °C for at least 6 hours (Shen et al., 2016). In contrast, *A. tamarense* isolated from Japan

exhibited 40% cell death after 1 hour heat shock from 20 °C to 30 °C (Kobiyama et al., 2010), which may reflect a lower heat tolerance than *K. brevis* and the species' characteristic temperature ranges. Under heat stress, heat shock protein (hsp) can alleviate proteotoxic effects by holding protein structures and repairing denatured proteins (Bierkens, 2000; Sanders et al., 1994). The heat acclimation ability in *K. brevis* may partially result from rapid induction of hsp which was detected within 1.5 hours after temperature increase from 25 °C to 30 °C in Miller-Morey & Van Dolah (2004). In addition, fluctuating but low prevalence of ROS was observed in both *K. brevis* (this study) and *A. tamarense* under non-lethal heat stress (Jauzein & Erdner, 2013), indicating some potential non-death roles of ROS. Previous research on higher plants have revealed a signaling role of ROS for activating ROS defense (ROS-scavenging enzymes) and temperature defense (i.e. hsp and heat shock transcription factors) in the process of cellular protection (Suzuki & Mittler, 2006). Non-death housekeeping roles of ROS are discussed in Chapter 2.

Cell death modes varying by stimuli

It has been proposed that cell death mode induced in an algal species may be determined by the type of environmental stimulus (Jiménez et al., 2009; Leist & Jäättelä, 2001; Papucci et al., 2004). Our results support this hypothesis based on the induction of cell death responses with and without caspase-like activity under hypo-osmotic stress and temperature stress respectively. The existence of diverse cell death pathways in response to various environmental stress in microalgae were exhibited in *Dunaliella viridis*, as treatment of heat shock, UV, high salt and nitrogen starvation triggered cellular structures that fitted morphological characteristics of necrosis, aponecrosis, paraptosis and

autophagy, respectively (Jimenez et al., 2009). Interestingly, in our research it seems different cell death modes share the characteristic of being mediated by ROS as the primary signal. ROS production has been observed to accompany non-apoptotic cell death like autophagy (Affenzeller et al., 2009) and necrosis (Laporte et al., 2007), whereas the specific mechanisms that decide the types of subsequent cell death pathway still remain unclear in microalgae. Besides the effects of different abiotic stress on cell death modes, an environmental stimulus with different intensity may also induce different types of cell death modes in a population of microalgae. Dingman & Lawrence (2012) examined heating stress responses of the raphidophyte *Heterosigma akashiwo* from 20 °C to 35, 37, 40 and 50 °C, respectively. Their results revealed a recovery from 35 °C and a switch of cell death mode from apoptosis (37 °C and 40 °C) to necrosis (50 °C). Although it is not clear about the existence of apoptosis with temperature change > 15 °C in *K. brevis*, cell death induced by temperature change within an ecologically relevant range is non-apoptotic.

Ecological implication of environmental-stress-induced cell death in *K. brevis*

From this study, only acute salinity reductions greater than 10 psu and temperature changes of 15 degree or more are likely to induce significant cell death in *K. brevis* populations along the coast of the western GoM. As populations of *K. brevis* in the GoM move into coastal or estuarine waters with inshore flow during bloom season, they would experience a gradual decrease in salinity (Steidinger, 1998). From our results *K. brevis* could acclimate to a reduction in salinity from 35 to 30 psu with minimal mortality, while acute salinity decreases by more than 5 psu may trigger rapid apoptosis and significant cell loss. In the coastal areas of the western GoM intensive storm events during the bloom season could lower salinity in estuaries by up to 10 psu on a timescale of 1 or 2 weeks

(Reyna et al., 2017), which might be problematic for populations in coastal embayment. In our study, *K. brevis* cells exhibited strong thermal tolerance with no significant cell death occurrence after 10 ℃ of acute heating or cooling stress, which is similar to the heat tolerance level of *H. akashiwo* and *A. tamarense* (Dingman & Lawrence, 2012; Jauzein & Erdner, 2013). A drastic water temperature change of more than 10 ℃ in such a short time scale is very uncommon in the western GoM (Reyna et al., 2017). Predictions based on lab studies need to be tested using field observations, and the effects of multiple environmental stressors need to be considered. For example, deterioration of oxidative damage by high-light stress during temperature stress has been reported in many higher plants (Jeong et al., 2002; Larkindale & Knight, 2002; Suzuki & Mittler, 2006), which may also apply to marine phytoplankton in the field.

CONCLUSIONS

Intensity-dependent apoptotic cell death occurred when salinity decreased by 5, 10, or 15 psu. Acute heating and cooling stress within 10 ℃ did not induce cell death in *K. brevis* cells, revealing their strong thermal tolerance. Cell death processes were only evident after 15 ℃ temperature change without induction of caspase-like activity, suggesting that cell death modes vary with different environmental stimuli in *K. brevis*. Comparing our experimental results with hydrographic data from western GoM, *K. brevis* populations are not likely to encounter sufficient acute temperature or salinity stress in isolation to result in appreciable mortality. Further studies should consider the effects of multiple stressors to better relate the field environment to cell death responses and therefore bloom decline processes.

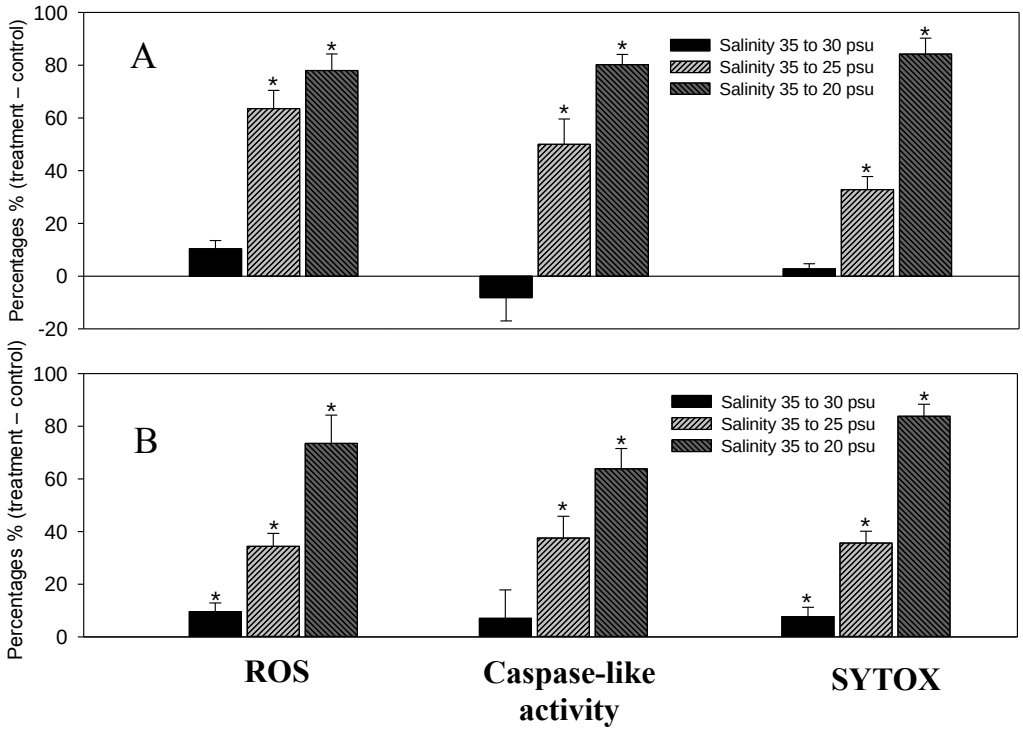

Figure 4.1: Osmotic stress. Difference between treatment and control in the proportion of cells showing reactive oxygen species (ROS), caspase-like activity, or SYTOX labeling at time 0.5h (A) and time 6h (B). Data points show average values of difference between triplicate treatment and control, and error bars show standard deviation of the differences (n = 36). An asterisk denotes a significant difference of absolute percentages between treatments and controls ($p < 0.05$ after Bonferroni correction).

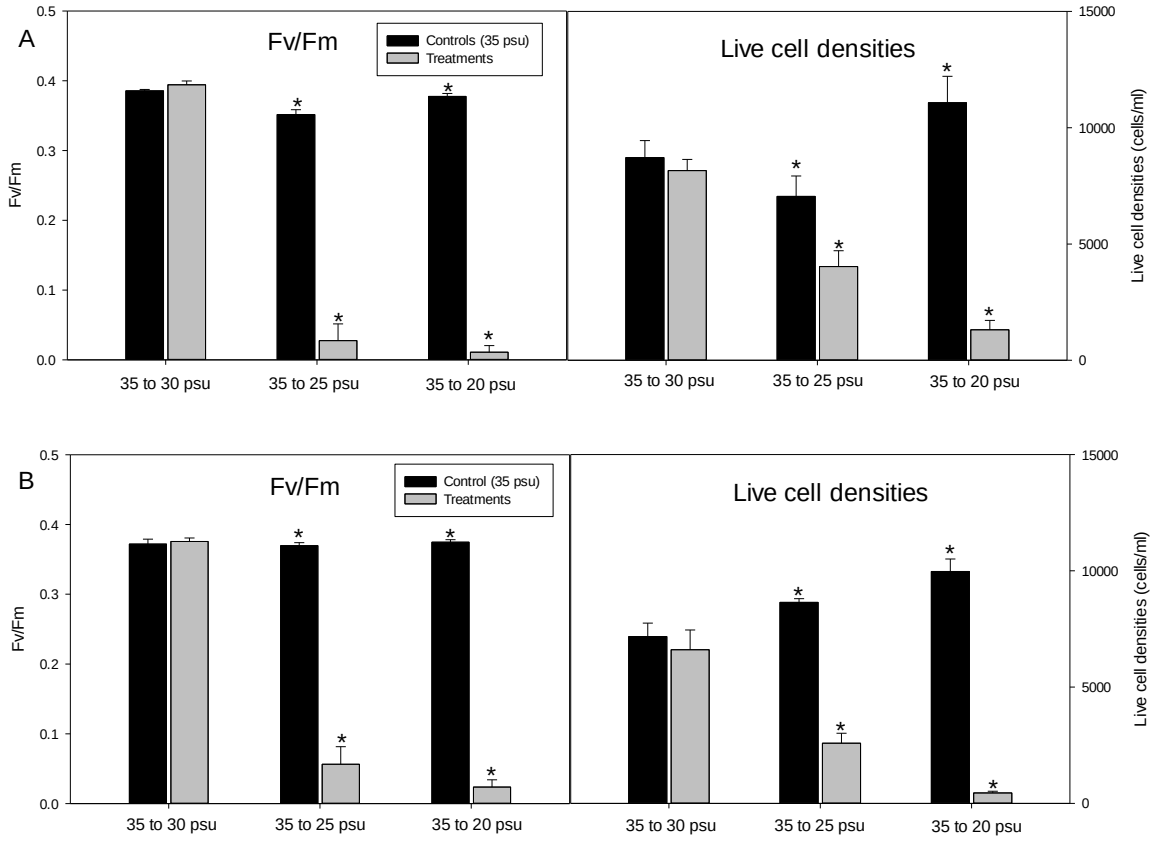

Figure 4.2: Osmotic stress. Treatments and controls in Fv/Fm and live cell densities at time 0.5h (A) and time 6h (B). Data points show average values obtained from triplicate cultures, and error bars show standard deviation of the replicates (n = 3). An asterisk denotes a significant difference of Fv/Fm or live cell densities between treatments and controls ($p < 0.05$ after Bonferroni correction).

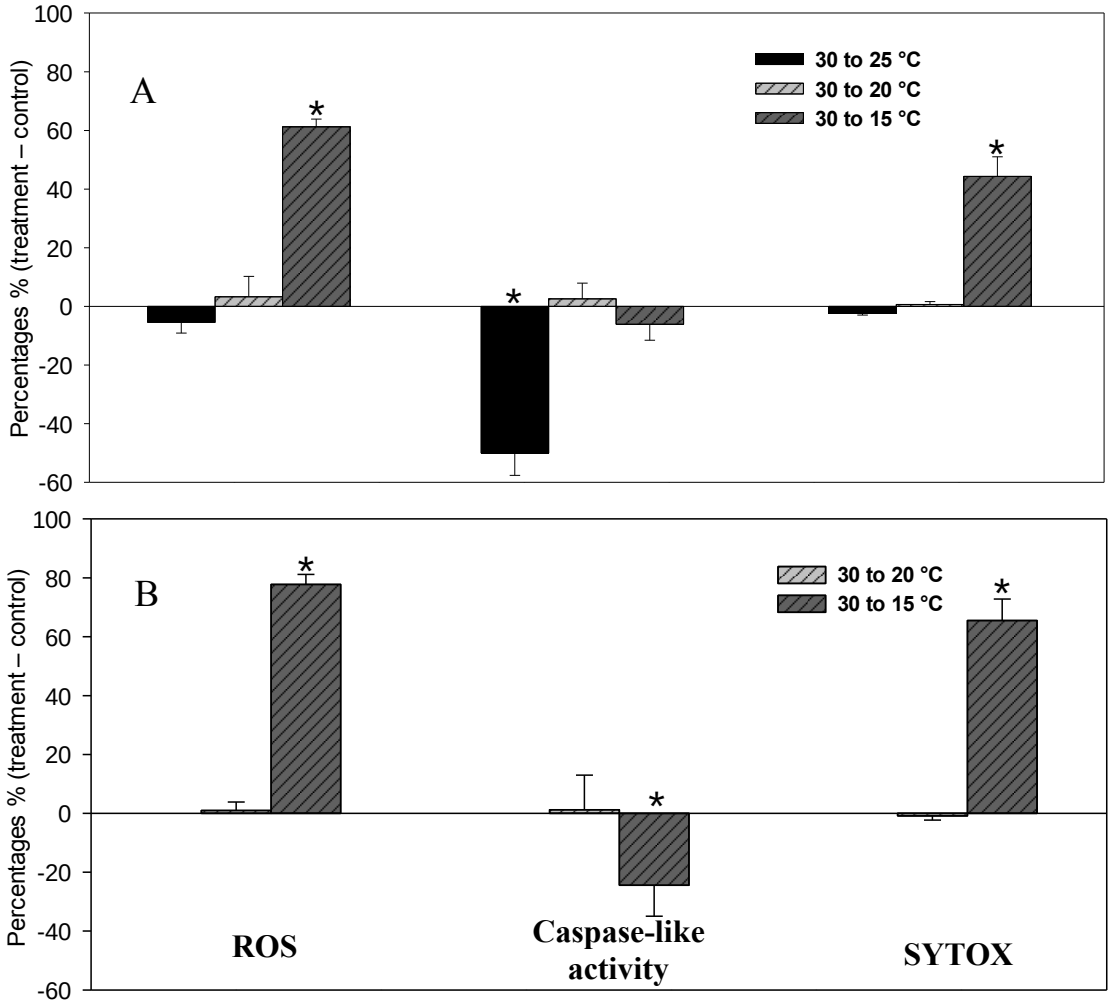

Figure 4.3: Cooling stress. Difference between treatment and control in the proportion of cells showing reactive oxygen species (ROS), caspase-like activity, or SYTOX labeling at time 0.5h (A) and time 6h (B). Data points show average values of difference between triplicate treatment and control, and error bars show standard deviation of the differences (n = 36). An asterisk denotes a significant difference of absolute percentages between treatments and controls ($p < 0.05$ after Bonferroni correction).

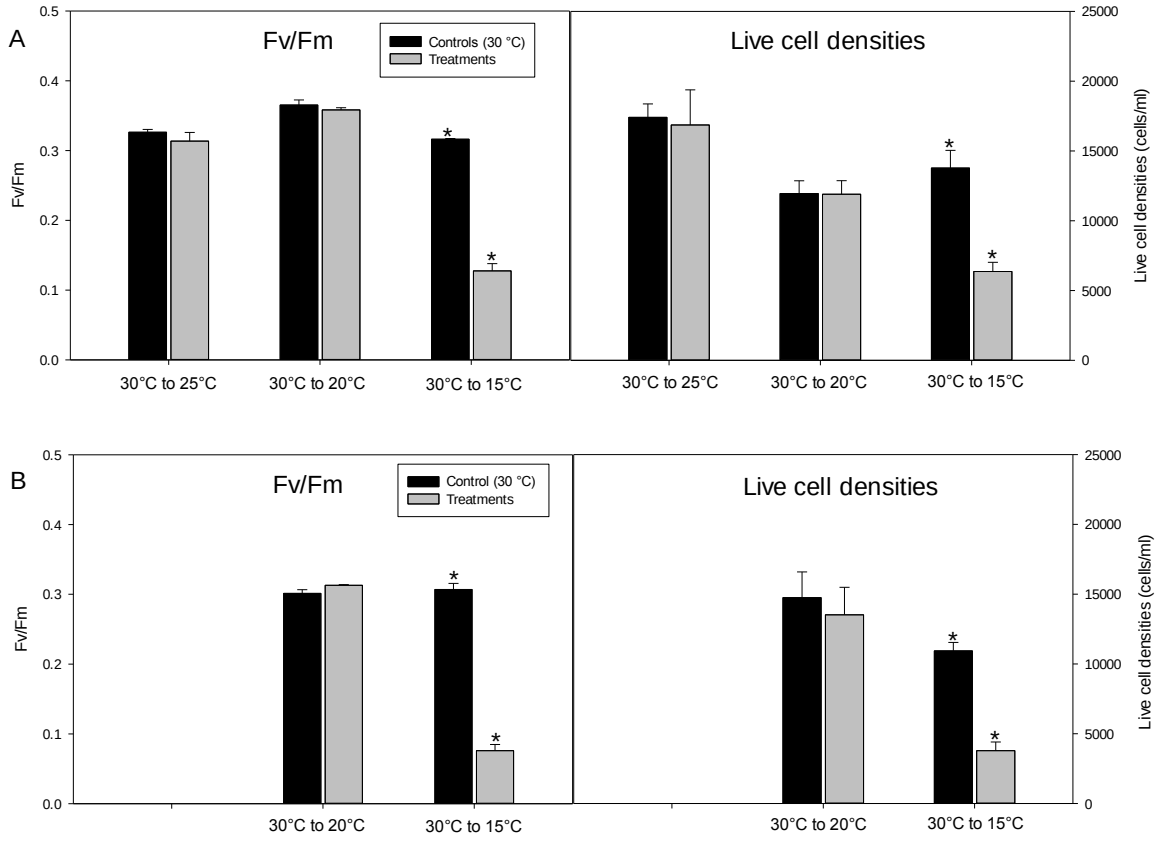

Figure 4.4: Cooling stress. Treatments and controls in Fv/Fm and live cell densities at time 0.5h (A) and time 6h (B). Data points show average values obtained from triplicate cultures, and error bars show standard deviation of the replicates (n = 3 for Fv/Fm; n = 6 for live cell densities). An asterisk denotes a significant difference of Fv/Fm or live cell densities between treatments and controls ($p < 0.05$ after Bonferroni correction).

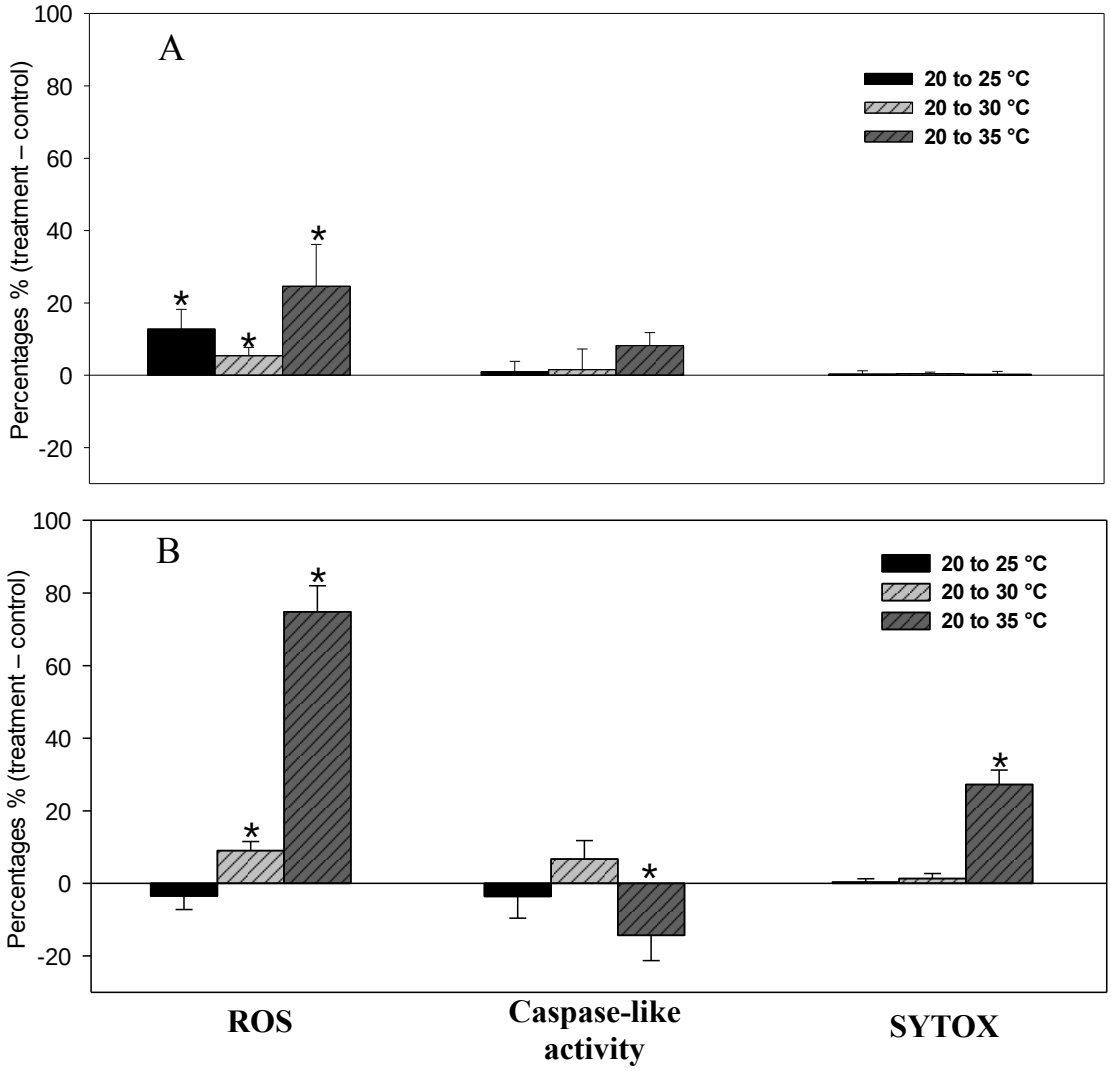

Figure 4.5: Heat stress. Difference between treatment and control in the proportion of cells showing reactive oxygen species (ROS), caspase-like activity, or SYTOX labeling at time 0.5h (A) and time 6h (B). Data points show average values of difference between triplicate treatment and control, and error bars show standard deviation of the differences (n = 36). An asterisk denotes a significant difference of absolute percentages between treatments and controls ($p < 0.05$ after Bonferroni correction).

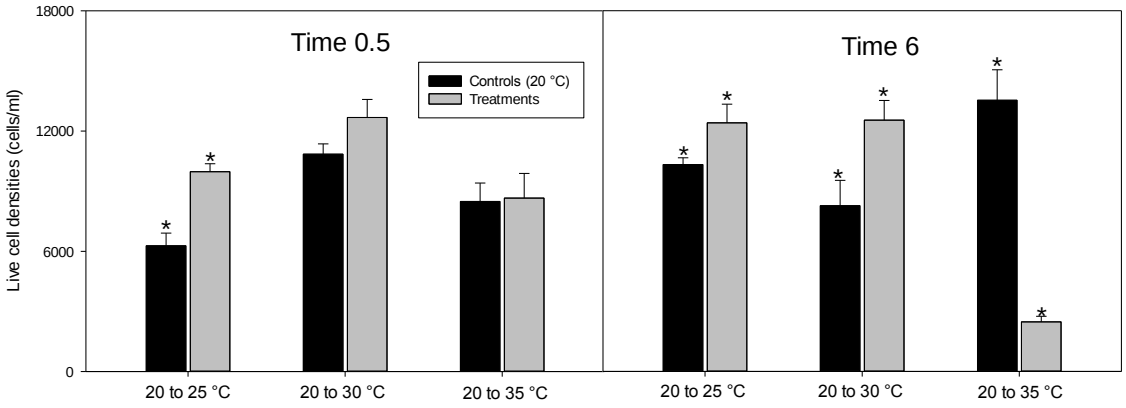

Figure 4.6: Heat stress. Treatments and controls in live cell densities at time 0.5h and time 6h. Data points show average values obtained from triplicate cultures, and error bars show standard deviation of the replicates (n = 6). An asterisk denotes a significant difference of live cell densities between treatments and controls ($p < 0.05$ after Bonferroni correction). Note: Fv/Fm was not measured due to technical problems in FRRF.

Chapter 5: Development of a quantitative real-time PCR method for the quantification of species-specific grazing on the toxic dinoflagellate *Karenia brevis*

ABSTRACT

While top-down control from microzooplankton grazers on phytoplankton has been implicated in both bloom initiation and termination, grazing pressure on toxic dinoflagellate *Karenia brevis* has not yet been quantified in the field. Understanding differential grazing on *K. brevis* specifically vs. the community as a whole can provide insights into the potential of top-down control of bloom dynamics. Quantification of *K. brevis* in the field can be challenging given their morphological similarity with other *Karenia* species and low densities at the beginning and end of blooms. A new quantitative real-time polymerase chain reaction (qPCR) method for accurate quantification of *K. brevis* from environmental samples was developed which exhibits high sensitivity and specificity to *K. brevis* cells. This method does not require morphological inspection and has better sensitivity than microscopic cell counts. A mock grazing experiment was conducted at Aransas Pass ship channel by mixing cultured *K. brevis* cells with the natural community. Microzooplankton grazing, measured by the dilution method, was greater than the growth of the phytoplankton community. High mortality of the introduced *K. brevis* cells prevented the quantification of species-specific grazing rates on *K. brevis*, but this grazing rate is expected to be lower than that on the whole community given the potential chemical defense and nutritional inadequacy of *K. brevis.*

INTRODUCTION

Grazing can be involved not only in bloom initiation by releasing certain algal species from predation pressure (Irigoien et al, 2005; Sieracki et al., 2004; Stoecker et al., 2008), but also in bloom prevention or termination by active removal of bloom species from water column (reviewed by Turner, 2006). Microzooplankton (20 - 200 um; e.g. heterotrophic dinoflagellates and ciliates) has been shown to cause significant cell loss during dinoflagellate blooms as the growth rates of these grazers could keep up with those of algal species (Johnson et al., 2003; Matsuyama et al., 1999; Kamiyama & Matsuyama, 2005; Nakamura & Suzuki, 1996; Strom & Morello, 1998). In contrast, grazing pressure from mesozooplankton (e.g. copepods) is considered to exert a comparatively lower impact on phytoplankton populations (Calbet et al., 2003; Campbell et al., 2005; Kozlowsky-suzuki et al., 2006; Jansen et al., 2006). For example, consumption by the copepod community on *Alexandrium minutum* only accounted for about 0.007% of the cell loss, while grazing losses from microzooplankton exceeded *A. minutum* growth rates (Calbet et al., 2003).

For the brevetoxin-producing dinoflagellate *Karenia brevis*, grazing research has mainly focused on interactions with copepods in terms of ingestion rates (Breier & Buskey, 2007; Waggett et al., 2012; Walsh & O'Neil, 2014), egg production (Speekmann et al., 2006; Waggett et al., 2012) and toxic effects on predators (Cohen et al., 2007; Huntley et al., 1986; Lauritano et al., 2013; Sykes & Huntley, 1987; Waggett et al., 2012). In contrast, less is known about the grazing effects of microzooplankton on *K. brevis*. Predation on *K. brevis* by heterotrophic dinoflagellate and ciliates was observed at the onset of a bloom (Campbell, 2012), while chemical defense from *K. brevis* can deter grazing of microzooplankton (Kubanek et al., 2007). However, there are no published grazing rates of microzooplankton on *K. brevis* in the field, leaving a blank for estimating the primary

grazing pressure on *K. brevis* blooms in the GoM. Since differential grazing on HAB species vs. co-occurring taxa can potentially drive both bloom initiation and termination (Sieracki et al., 2004; Stoecker et al., 2008; Turner, 2006), comparing grazing pressure on the community as a whole vs. *K. brevis* specifically in the field can provide insights into the potential for top-down control of bloom dynamics. In addition, more accurate estimates of grazing rates can be incorporated into bloom models to better predict the development and loss of *K. brevis* populations (Henrichs et al., 2015).

The standard dilution method for grazing can be coupled with species-specific quantification to understand differential grazing pressure. The dilution method of Landry and Hassett (1982) has been widely used to measure microzooplankton grazing on many phytoplankton species (Calbet et al., 2003; Caron et al., 2004; Gobler et al., 2004; Gobler et al., 2002). This method requires minimal manipulation of planktonic organisms which is particularly beneficial to fragile algal cells like *K. brevis* (Demir et al., 2008). Changes in the phytoplankton community as a whole can be determined by measuring chlorophyll *a* concentration, while quantification of *K. brevis* specifically in the field can be challenging. The cell densities during bloom initiation, termination, or the end of a grazing incubation can be lower than the lower limit of detection (LLD) for light microscopy (about 10^3 cells/L) and may therefore cause underestimation of cell densities (Haywood et al., 2007). Taxonomic expertise is needed to identify and distinguish closely related *Karenia* species due to their morphological similarities (Haywood et al., 2004). The GoM is home to at least four *Karenia* species - *K. brevis, K. mikimotoi*, *K. selliformis*, and *K. papilionacea* - and the concurrent presence of the superficially-similar toxic and nontoxic species (i.e. *K. brevis* and *K. papilionacea*) has been reported (Haywood et al., 2007). Ideally, a quantification method for measuring grazing pressure on *K. brevis* would have strong species-specificity and low LLD.

Quantitative real-time polymerase chain reaction (qPCR) is an effective method to determine species-specific biomass in natural communities. qPCR methods have been developed and applied to non-*K. brevis* species in genus *Karenia* (Smith et al., 2014; Yuan et al., 2012) and other HAB genera including *Alexandrium* (Dyhrman et al, 2006; Erdner et al., 2010; Kon et al., 2015), *Karlodinium* (Kon et al., 2017), *Heterosigma* (Coyne et al., 2005), *Gambierdiscus* (Vandersea et al., 2012) and *Aureococcus* (Popels et al., 2003). In this method, the target species is identified and quantified by amplification of a target gene from field DNA using species-specific primers and fluorescent dyes without the need for morphological inspection. In addition, the sensitivity of qPCR can be as low as 1 cell/L (Coyne et al., 2005; Hariganeya et al., 2013) which allows the measurement of cell densities at the earliest stages of bloom initiation.

The objectives of this research are to (1) develop a qPCR method for sensitive, accurate and species-specific quantification of *K. brevis* from environmental mixed samples; and (2) measure grazing rates of the natural microzooplankton community on *K. brevis* populations as compared to the phytoplankton community as a whole. In this chapter, I designed qPCR primer sets for the D1-D2 region of the 28S ribosomal RNA gene in *K. brevis* and tested their specificity on multiple species of *Karenia.* In order to correct for DNA loss during the extraction process, exogenous pGEM-3Z plasmid was used as a reference gene. The qPCR program for both the target and reference genes have been optimized for high amplification efficiency. A mock grazing experiment was conducted to compare growth and grazing rates on *K. brevis* and the whole phytoplankton community.

METHODS

Assay Development

Primer choice and testing

The nucleotide sequences of D1-D2 region of 28S ribosomal RNA (rRNA) gene from *K. brevis* and *K. mikimotoi*, *K. selliformis* and *K. papilionacea* were retrieved from GenBank nucleotide database (Table 5.1) and aligned using Geneious (Drummond et al., 2011). Potential species-specific primer sites within the D1-D2 region were chosen by visual inspection to contain at least two unique nucleotides for *K. brevis*. Sequences and melting temperature (T_m) of candidate primers are shown in Table 5.2. DNA from one strain each of *K. brevis* (SP3, Texas), *K. mikimotoi* (ARC164, Texas), *K. selliformis* (ARC356, Delaware) and *K. papilionacea* (ARC275, Texas) were extracted using the DNeasy Blood & Tissue Kit (Qiagen) following the manufacturer's instructions. In order to evaluate the species-specificity of primer candidates, PCR amplification was conducted on these four strains with five different primer combinations: Kb-F1 & Kb-R1, Kb-F1 & Kb-R2, Kb-F1 & JCR, Kb-F1 & D2C and Haywood-F & Kb-R2. Annealing temperatures tested for each primer combination are shown in Table 5.3. PCR reactions contained 10 ng of template DNA, 0.25 mM of total dNTPs, 0.2 μM of each primer, 1× DreamTaq Buffer, and 0.8 μl of DreamTaq™ polymerase (Thermo Fisher Scientific Inc.) in 20 μL total reaction volume. Two PCR additives were also tested: 0.4 μl of TMAC (10 mM final concentration) and 2.8 μl of Betaine (0.7 M final concentration). The PCR cycling conditions were as follows: 2 min at 94 °C, 30 cycles of 1 min at 94 °C, 45 s at the primer-specific annealing temperature and 1 min at 72 °C, followed by a final elongation for 5 min at 72 °C. The primer sets showing specificity to *K. brevis* were used for PCR on the DNA from another five strains of *K. brevis* (Wilson, Tb90, SP1, SP2 and nSP3). Strain Wilson

was originally isolated from offshore Florida (eastern GoM), while others were collected from the Texas coast (western GoM).

Preparation of standards for qPCR

PCR was conducted using genomic DNA of strain SP3 with primers D1R and D2C to amplify the D1-D2 region for use as *K. brevis* qPCR standards. The sequences of this primer set are listed in Table 5.2 (Scholin et al., 1994). The same PCR program and PCR reaction mix without additives described above was used, setting 56 °C as annealing temperature. The D1-D2 PCR product was purified by using PCRExtract Mini Kit (5 PRIME Inc.) and then quantified with Qubit™ (Invitrogen) following the protocol of dsDNA HS Assay Kit (Invitrogen). DNA quantification was performed on six sub-samples from the purified PCR product, and the readings were averaged for the next step. The copy number of D1-D2 gene fragment per μl was calculated as:

[amplicon Conc. (ng/μl) × 6.022E23 (molecule/mol)]／[molecular weight (g/mol) × 1E9 (ng/g)]

The purified D1-D2 PCR product was then diluted to 5×10^7 gene copies/μl, followed by 10-fold serial dilutions (5×10^3 to 5×10^7 gene copies/μl) to create the standards.

Addition of an exogenous DNA, pGEM-3Z plasmid (Promega) was employed to correct for loss of DNA during the extraction process (Hariganeya et al., 2013). Since linear plasmid standards have exhibited better reliability and accuracy (Hou et al., 2010), the plasmid was linearized by digestion with the restriction enzyme ScaI (Thermo Fisher Scientific Inc), and the success of linearization was verified by electrophoresis using 1.5% agarose gel. The quantification and calculation of copy number of linearized pGEM-3Z solution was conducted as described above. Then, the pure linearized pGEM-3Z solution

was diluted to 5×10^7 gene copies/µl, followed by 10-fold serial dilutions (5×10^3 to 5×10^7 gene copies/µl) for making pGEM-3Z standard curve.

qPCR assay

The optimized 20 µl qPCR reaction contained 10 µl PowerUp™ SYBR™ Green Master mix (Applied Biosystems Inc.), 0.2 µM of each primer, 7.2 µl of DNAse-free H_2O and 2 µl of DNA template. Assays were performed using QuantStudio 3 (Applied Biosystems Inc.). For qPCR reactions with *K. brevis*-specific primers, the following cycling protocol was used: 2 min at 94 °C followed by 40 cycles of 1 min at 94 °C, 30 s at primer-specific annealing temperatures (Table 5.3) and 1 min at 72 °C, and then a final elongation for 5 min at 72 °C. For qPCR reactions with pGEM-3Z primers (M13-F & pGEM-R; Table 5.2), the qPCR cycling conditions were as follows: 2 min at 94 °C followed by 45 cycles of 1 min at 94 °C, 45 s at primer-specific annealing temperatures (Table 5.3) and 1 min at 72 °C, and then an elongation for 5 min at 72 °C. A subsequent melting curve analysis (MCA) was performed to evaluate the specificity of amplification processes. All samples were run in triplicate in qPCR including no template controls (NTCs) which used distilled water as DNA template to examine the existence of contamination. During the qPCR process the amount of fluorescence (F) from DNA molecule is measured by the qPCR cycler after each cycle of amplification. When F reaches to the florescence thresholds, the corresponding number of cycle (Ct) will be recorded. Data acquisition and analysis were performed using the QuantStudio™ Design & Analysis software (Applied Biosystems Inc.), and florescence thresholds and C_t values were determined using the default settings.

The standard curves were built by plotting triplicate C_t values from standard solutions versus their log-transformed copy numbers ($\log X_0$). A linear regression was

applied to determine the R^2 value and the linear equation: $Ct = -k \times \log X_0 + b$. Amplification efficiency (AE) was calculated as $AE = [10^{(1/k)} - 1] \times 100\%$. AE values higher than 90% are generally considered an indication of reliable qPCR amplification.

Mock grazing experiment

In the absence of a *K. brevis* a bloom along Texas coast, a mock grazing experiment was conducted. This consisted of lab-grown *K. brevis* cells added to a natural field population from the usual bloom time and location and incubated under ambient temperature and light conditions.

Inoculum preparation

Six *K. brevis* strains (SP1, SP2, SP3, Wilson, Tb90 and TXB4) were cultured separately in L1 medium with a salinity of 32 psu on a 12:12 hour light:dark cycle (120 µmol m^{-2} s^{-1}) at 25°C in a PERCIVAL incubator. To reduce nutrient carryover into the mock grazing incubations, a stepwise decrease of nutrient concentrations was done during the transfer of these cultures until a concentration of L1/160 for N & P and L1/40 for Trace Metal & Vitamin was reached. Cell concentrations were adjusted to approximately 600 cells/ml after the last transfer of cultures.

Dilution assay

The mock grazing experiment was conducted on a pier in the Aransas Pass ship channel in Port Aransas, Texas on Oct 25th and 26th, 2019. An 800 ml volume of each *K. brevis* strain, at a density of about 1500 cells/ml, was added to a 10L glass container. This mixed *K. brevis* culture was divided into three parts (about 1600 ml each) and transferred to three 20 L polycarbonate carboys.

Seawater was collected from 2 m depth by 5L Beta sampling bottle (Wilco Inc.) and added into each carboy, diluting the mixed *K. brevis* culture to 18 L final volume, creating a "mock bloom". At this point, the *K. brevis* cell densities in the mock bloom mixture were ca. 130 cells/ml, which is a moderate concentration for *K. brevis* blooms (Haywood et al., 2007). Another 10 L of sea water were collected by Beta sampling bottle and filtered through a 0.2 um polycap capsule filter (Whatman Inc.) by gravity. This filtered seawater was measured into sterile 1.1 L polycarbonate bottles (grazing bottles) at 0%, 0%*, 25%, 50%, 75% and 100% of the total volume, in triplicate. After being pre-filtered through a 153 μm sieve to remove macro- and meso-zooplankton, the mock bloom mixture was added to completely fill each grazing bottle. All grazing bottles except the triplicate 0%* bottles received 1 ml of master nutrient stock, providing 0.5 μM NO_3^-, 1 μM NH_4^+ and 0.1 μM PO_4^{3-}. This ensured that nutrients would not limit phytoplankton growth during the 24-hour incubations. Grazing bottles were placed in a deck incubator on the pier with constantly flowing seawater provided by submerged pump, maintaining the ambient seawater temperature. Ambient light at the 2 m sampling depth and above the water surface was measured using LI-1400 DataLogger connected by LI-192 underwater quantum sensor (LI-COR Biosciences), and the plastic bin was fully covered with window screen to match the light at the sample collection depth. The incubation lasted for 24 hours. At time 0h and time 24h, samples for chlorophyll *a* extraction and qPCR analysis were collected using 25 mm GF/F glass microfiber filter (Whatman Inc.) and 25 mm, 5 μm pore size PVDF Durapore filters (Millipore Inc.), respectively. Volumes of filtrate were recorded for later normalization. Another sample aliquot (50 ml) was fixed with Lugol's iodine solution for later microscopic cell counting. Samples at time 24h were collected from all bottles, while samples at time 0h were only collected from the mock bloom mixture in triplicate, which

was equal to 0 % dilution. Lugol's preserved and filter samples were stored at 4 °C and -80 °C, respectively.

Sample processing

Before DNA extraction, the filters were submerged in 2ml of ATL buffer (Qiagen) to which 1×10^8 copies of linearized pGEM-3Z plasmid had been added. Subsequent steps of DNA extraction were performed based on the protocol of DNeasy Blood & Tissue Kit, with a final elution volume of 20 µl. For quantifying the gene copy numbers of D1-D2 region in the testing samples, qPCR was conducted on two plates. On Plate A, *K. brevis* species-specific primers were applied to both the assay samples and the standard dilution series of purified D1-D2 PCR products. On Plate B, pGEM-3Z primers were applied to both the assay samples and the dilution series of linearized pGEM-3Z plasmid. Copy numbers of pGEM-3Z (a) were calculated by interpolation of C_t into the standard curve of pGEM-3Z. Since 2 µl (10%) of DNA template was used for qPCR, the theoretical copy number of pGEM-3Z in grazing samples entering qPCR reaction should be 1×10^7. Therefore, DNA recovery efficiency (RE) was calculated as: $RE = (a) / (1 \times 10^7)$. Similarly, the copy number of D1-D2 region (T) of *K. brevis* in the assay was calculated by interpolation of Ct into the D1-D2 standard curve. The "Corrected" copy number of D1-D2 region (C) was calculated as: $C = (T) / RE$, as RE is considered the same for these two DNA fragments. After normalization by the volumes of filtrate and DNA template used for qPCR, gene copy numbers of D1-D2 region per liter of water filtered were determined.

Cell densities of *K. brevis* from each sample were counted under the microscope using a Sedgewick Rafter. Since no natural *Karenia* cells were detected from unfiltered sea water by Imaging FlowCytobot at the day of the sampling, the *Karenia* cells observed in samples would be *K. brevis* introduced for this mock grazing experiment.

Chlorophyll *a* from the total phytoplankton community was extracted by extracting each GF/F filter in 5 ml of methanol at -20 °C for 30 hours. The RFU value from each sample was measured by fluorometer (10-AU, Turner Designs) and converted to chlorophyll *a* concentration using a calibration curve. Chlorophyll *a* concentrations (μg/L) at time 0h and time 24h were determined after correcting for the volume of sample collected and the methanol extract volume.

Apparent growth rates (k) were calculated as the natural log of the ratio of time 24h and time 0h concentrations under each dilution fraction, $k = \ln(Conc._{T24}/Conc._{T0})$ (Landry & Hassett, 1982). The concentrations of total community were represented by chlorophyll *a* concentration, while gene copies/L and cell densities were used for *K. brevis* concentrations. The time 0h values for each dilution treatment were calculated by adjusting the values measured in the mock bloom mixture by the dilution fraction. The resulting k values were then plotted against the corresponding fractions of the mock bloom mixture, and the slope and the intersection with y axis of the resulting line are the grazing rate (d^{-1}) and growth rate (d^{-1}) respectively.

RESULTS

Primer specificity

In order to develop a *K. brevis* species-specific quantification method, several candidate primer sets for qPCR were designed, all targeting the D1-D2 region of the 28S rRNA gene of *Karenia* (Table 5.1). They were tested for specificity against four *Karenia* species: *K. brevis, K. mikimotoi*, *K. selliformis* and *K. papilionacea*. Haywood-F/Kb-R2 was the only primer set that did not show cross-reactivity with DNA templates from non-*K.brevis* species (Fig. 5.1). An additional five strains of *K. brevis* were examined with this

primer set, and all showed successful PCR amplifications under a range of annealing temperatures (Fig. 5.2).

Standard curves and AE

qPCR on the serial dilution of purified D1-D2 fragment in *K. brevis* was conducted with annealing temperatures of 58 °C, 60 °C and 62 °C, obtaining AE of 93%, 95% and 98% respectively. The LLD based on this qPCR standard curve is approximately 10^4 copies per reaction. Amplification of the serial dilution of linearized pGEM-3Z plasmid was conducted with annealing temperatures of 55 °C, 56 °C and 57 °C, obtaining AE of 95%, 88% and 92% respectively. Subsequent qPCR assays used the annealing temperatures that showed the highest AE values (Fig. 5.3). In addition, only one peak was observed in the melting curves of qPCR on purified D1-D2 fragment and pGEM-3Z plasmids respectively (data not shown), which indicated the specificity of amplification on targeted DNA fragments.

Microzooplankton grazing pressure on total phytoplankton community and *K. brevis*

The ambient sea water salinity and temperature were approximately 31 psu and 24°C respectively. The grazing rate on *K. brevis* was determined by cell counts of this species but not by qPCR due to a technical fault during the DNA extraction process. The mock-grazing experiment for qPCR testing was scheduled to repeat in March 2020 but had to be delayed due to the pause in research during COVID-19 pandemic.

In the dilution experiment, the grazing rate and growth rate of the total community were 0.98 d^{-1} and 0.65 d^{-1} respectively ($p = 0.0031$; Fig. 5.4). At time 0h the average

chlorophyll *a* concentration under 0% dilution was 4.75 μg/L, while at time 24h this concentration with and without nutrient addition decreased to 3.67 and 2.00 μg/L, respectively. For *K. brevis* specifically, the grazing rate was not significantly different from zero ($R^2 = 0.073$, $p = 0.40$), and cell numbers drastically decreased (growth rate -0.88 day^{-1}; Fig. 5.5).

DISCUSSION

The objectives of this study were to develop a qPCR method that can accurately identify and quantify *K. brevis* from natural samples without the necessity of microscopic cell counts and apply this method to investigate microzooplankton grazing pressure on *K. brevis* in the field. The primer set and assay conditions described here provide a quantification method that is both species-specific and sensitive. A mock grazing experiment was conducted at Aransas Pass ship channel to quantify and compare grazing pressure on *K. brevis* and the community as a whole. Validation of this qPCR method on field samples has not been completed due to COVID-19 delays and technical fault.

The primer set of Haywood-F & Kb-R2 exhibited strong specificity for the detection of *K. brevis* from lab cultures. The results of specificity test showed that only the DNA from *K. brevis* can be amplified regardless of original collection sites in GoM. High AE and R^2 value were derived from the standard curve of *K. brevis* D1-D2 gene starting at 1×10^4 gene copies. The LLD of this method is likely to be lower than 1×10^4 copies per reaction, but the standard curve did not test lower concentrations. In dinoflagellates, gene copy numbers per cell have been reported to be higher than 1×10^4 in many genera including *Alexandrium* (Galluzzi et al., 2010), *Gambierdiscus* (Vandersea et al., 2012), *Ostreopsis* (Hariganeya et al., 2013) and *Karlodinium* (Kon et al., 2017). With the high AE

value, it is reasonable to hypothesize that this qPCR method can reliably detect *K. brevis* even if only one cell is contained in the sample.

qPCR can quantify target-species by "relative" (Δ Ct) and "absolute" methods, and the latter one is used in this study. The Δ Ct method measures the difference in the relative abundance of cells between the field samples and a calibrator sample (Coyne et al., 2005). The calibrator sample is chosen from amongst the field samples, and its cell density is determined independently, e.g. by microscope count (Coyne et al., 2005). An advantage of this method is that it eliminates the concern of potential different AEs for field samples and the laboratory cultures used for the standard curve (Coyne et al., 2005). However, the applicability of this method relies on a microscope cell count of calibrator samples, which has the disadvantage of high LLD and requires taxonomic skill to distinguish morphologically similar species. Furthermore, in order to make this method valid, the AEs of the target genes and the exogenous plasmid from field samples must be equal (Livak & Schmittgen, 2001). In contrast, the "absolute" qPCR method used in this study does not require any cell counts from field samples and is considered to be suitable for quantification of cryptic or morphologically indistinct species (Fong et al., 2015; Hariganeya et al., 2013; Perini et al., 2011). Absolute quantification uses standard curves generated by the amplification of a dilution series of pure target genes (Hariganeya et al., 2013). Therefore, an important prerequisite of this method is that environmental DNA does not have significant inhibitory effects on qPCR amplification. Previous research has validated the use of absolute quantification qPCR methods for dinoflagellate species in the field. For example, Hariganeya et al. (2013) proved that AEs of qPCR on target species with/without environmental DNA were not significantly different in *Ostreopsis spp*. For *K. brevis*, this potential inhibitory effect needs to be evaluated as described below.

Although the logic and principle of the "absolute" method is comparatively straightforward, some studies have reported low precision of cell counts with this method in dinoflagellates, which may be mainly due to variation in gene copy numbers per cell of target species from both lab cultures and environmental samples (Galluzzi et al., 2010; Godhe et al., 2007). In order to obtain a value for cell density, the calculated gene copy numbers/L from qPCR need to be divided by gene copy numbers per cell of the target species. Galluzzi et. (2010) noted overestimation of cell counts of *Alexandrium taylori* and *Alexandrium catenella* blooms by qPCR method when using a value of rRNA gene copies per cells from one lab strain for each species. They further found that rRNA gene content per cell varies greatly among different strains and growth stages, which may result from the existence of unstable rRNA pseudo-genes (Scholin et al., 1993; Yeung et al., 1996) as well as different culture conditions including temperature, light cycle and medium types (Galluzzi et al., 2010). In *Ostreopsis cf. ovata* a difference of rRNA gene copies per cell between field samples and cultured samples was also observed (Perini et al., 2011). Thereafter, Hariganeya et al. (2013) suggested using averaged gene copy numbers per cell obtained from single cells isolated from environmental samples to calculate cell numbers of targeted species, which exhibited better consistency with microscopic cell counts. However, in our study only the ratio of the *K. brevis* densities at time 0h and time 24h are needed for quantifying grazing pressure. Since the average gene copy number per cell is not expected to change significantly between the beginning and end of a 24-hour period, the calculated gene copy numbers/L serve as a direct proxy for cell densities in the calculation of apparent growth rates.

The observed negative growth rate of the added *K. brevis* may indicate a stressful ambient environment for the survival of these cells, which were cultured in the lab. Negative phytoplankton growth rates are not uncommon from previous research (Liu et al.,

2002; Loebl & Van Beusekom, 2008; Sherr et al., 2009; Strom & Fredrickson, 2008; Suzuki et al., 2002; Zhou et al., 2011). Some contributing factors may be low nutrient conditions (Zhou et al., 2011), senescence (Sherr et al., 2009), contamination (H. Liu et al., 2002), temperature and light (K. Suzuki et al., 2002). Although efforts were made to pre-acclimate the lab-cultured *K. brevis* strains to field temperature, light, and nutrient conditions, the loss of over half of the added cells indicates that there was some essential mismatch between the culture and field conditions. On other hand, the absence of natural blooms during the bloom season may indicate an existing adverse environment for the growth of *K. brevis*. For example, bacteria or viruses isolated from sea water during a *K. brevis* bloom in the GoM have been suggested to induce lysis of *K. brevis* cultures (Paul et al., 2002), which would potentially control their growth in the field.

The unmeasurable grazing rate on *K. brevis* may result from their negative growth and/or their physiological characteristic that are not favored by predators. Given the loss of *K. brevis* population in grazing bottles, possibilities of encounter between microzooplankton grazers and *K. brevis* cells may be lower than that for other phytoplankton, which may cause underestimation of the grazing pressure on *K. brevis*. However, it is reasonable that microzooplankton grazing pressure on the whole phytoplankton community is higher than that on *K. brevis*. Campbell (2012) found that when given *K. brevis* as the sole diet, the heterotrophic dinoflagellates *Protoceratium sp.* and *Noctiluca scintillans,* which are widely distributed in GoM, exhibit negative growth rates. This suggests that these microzooplankton species are unable to effectively control established bloom conditions (Campbell, 2012). Previous research showed that the rejection of *K. brevis* by two species of microzooplankton rotifers may result from low nutritional content and chemical deterrence (Kubanek et al., 2007). Similar mechanisms may also exist in the interactions between *K. brevis* and copepods. Breier & Buskey (2007)

observed lower ingestion rates and offspring production in copepods that were fed with a sole diet of *K. brevis* compared to a mixed diet of *K. brevis* and *Peridinium foliaceum*, indicating the nutritional inadequacy of *K. brevis* for offspring production in copepods. In addition, *K. brevis* may use brevetoxins as chemical defense against copepod grazing, as non-toxic strains of *K. brevis* were grazed at significantly higher rates than those toxic strains (Waggett et al., 2012). Among six strains of *K. brevis* used in this mock-grazing experiment, at least three of them (Wilson, TXB4 and SP1) have been reported as brevetoxin producers (Daugherty, 2017). Therefore, it is possible that toxin production of *K. brevis* may also be used to deter grazing from microzooplankton community.

Due to the shutdown of research facility amid COVID-19 pandemic, two following experiments have been postponed: (1) examining and minimizing inhibitory effects of environmental DNA on qPCR to further validate applicability of the absolute qPCR method on quantifying field samples; (2) conducting another grazing experiment to measure grazing pressure on *K. brevis* populations.

CONCLUSIONS

In this research, I aimed to quantify grazing pressure on *K. brevis* and co-occurring taxa to gain insights into the roles of top-down control on dynamics of *K. brevis* blooms. With this purpose, a new qPCR method for accurate quantification of *K. brevis* from environmental samples was developed in which exhibits high sensitivity and specificity to *K. brevis* cells. This method does not require morphological inspection and has better sensitivity than microscopic cell counts when applied on quantification of grazing pressure. In the mock grazing experiment the lab-grown *K. brevis* cells exhibited negative growth, indicating adverse ambient environment and/or differences between laboratory and field

conditions. The grazing pressure on *K. brevis* may be underestimated here, but this grazing rate is expected to be lower than that on the whole community considering the potential chemical defense and nutritional inadequacy of *K. brevis.*

Table 5.1: List of 28S rDNA sequences of *Karenia* species retrieved from GenBank nucleotide database.

Species	**Strain name**	**Origin**	**Accession**
Karenia brevis	Texas B5	South Padre Island, Texas, USA	AY355455
	SP3	South Padre Island, Texas, USA	AY355456
	PNS	Pensacola, Florida, USA	AY355457
	CAWD08	John's Pass, Florida, USA	U92248
Karenia mikimotoi	GATIN95	Brest Bay, France	KJ508362
	IFR559	Concarneau Bay, France	KJ508363
Karenia selliformis	HKS01	Honk Kong, China	KY580784
	HKS02	Honk Kong, China	KY580785
Karenia papilionacea	SKLMP_J011	Honk Kong, China	MG914087
	SKLMP_J012	Honk Kong, China	MG914088

Table 5.2: Primer sequences for *K. brevis* and pGEM plasmid.

Primers	**Sequence (5'-3')**	**Tm (°C)**	**Reference**
Kb-F1	AAGGTGATAGCTTGCCACTTCAAC	57.6	This study
Haywood-F	CGGGCGACTGAATGTCCCCA	62.3	Haywood et al. 2007
Kb-R1	GCACACGGAGCAGTGCG	60.0	This study
Kb-R2	GGCACTAGCAACCTTCATGCCAAG	60.6	This study
JC-R	AAGATTGCAAGCAAGCACACGGAG	60.4	Campbell 2012
D2C	CCTTGGTCCGTGTTTCAAGA	55.1	Scholin et al., 1994
D1R	ACCCGCTGAATTTAAGCA	52.0	Scholin et al., 1994
M13-F	CCCAGTCACGACGTTGTAAAACG	58.3	Coyne et al., 2005
pGEM-R	TGTGTGGAATTGTGAGCGGA	56.9	Coyne et al., 2005

Table 5.3: Annealing temperatures tested for each primer set in regular PCR and qPCR.

Primer set	Annealing temperature (°C)	
	Regular PCR	qPCR
Haywood-F & Kb-R2	60-65	58, 60 ,62
Haywood-F & D2C	51	\
Kb-F1 & Kb-R1	53-60	\
Kb-F1 & Kb-R2	53, 54	\
Kb-F1 & JCR	55-60	\
M13-F & pGEM-R	\	55-57

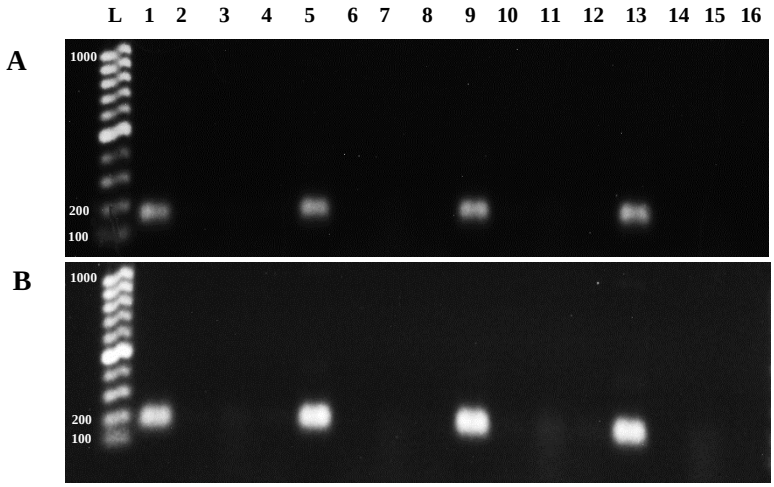

Figure 5.1: Assay of amplification specificity of Haywood-F & Kb-R2 on *Karenia* species. In each gel picture, 100-bp PCR DNA ladder (Lane L), *K. brevis* (Lane 1, 5, 9, 13), *K. mikimotoi* (Lane 2, 6, 10, 14), *K. selliformis* (Lane 3, 7, 11, 15) and *K. papilionacea* (Lane 4, 8, 12, 16). Samples loaded on Lane 1-4 & Lane 9-12 were from PCR aliquot with additives (Betain & TMAC); samples loaded on Lane 5-8 & Lane 13-16 were from standard PCR aliquot. In (A), annealing temperature 61 °C (Lane 1-8), 62 °C (Lane 9-16). In (B), annealing temperature 64 °C (Lane 1-8), 65 °C (Lane 9-16).

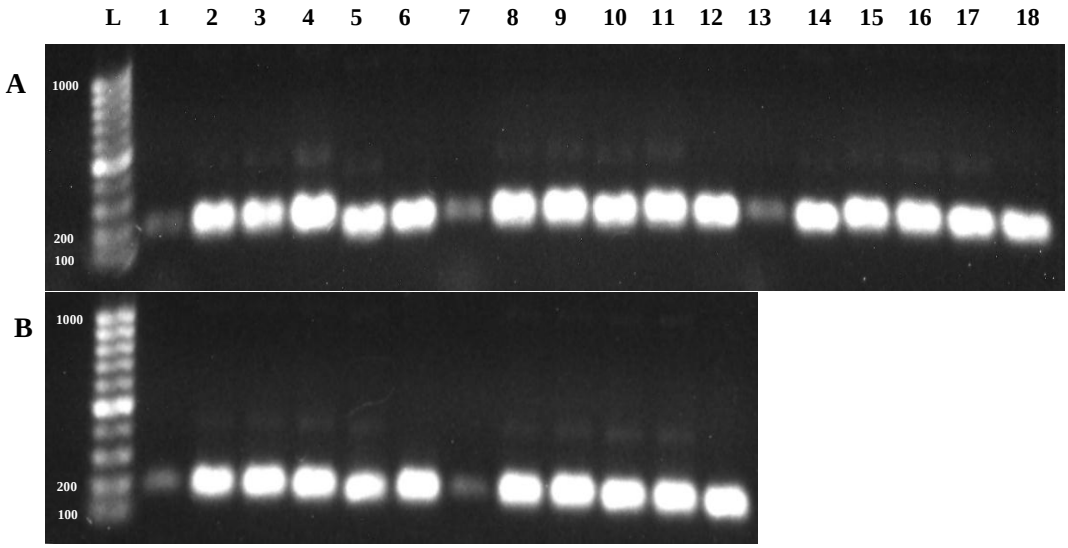

Figure 5.2: Assay of amplification specificity of Haywood-F & Kb-R2 on six different strains of *K. brevis*. In (A), 100-bp PCR DNA ladder (Lane L), annealing temperature 60 °C (Lane 1-6), 61 °C (Lane 7-12), 62°C (Lane 13-18). In (B), 100-bp PCR DNA ladder (Lane L), annealing temperature 63 °C (Lane 1-6), 64 °C (Lane 7-12).

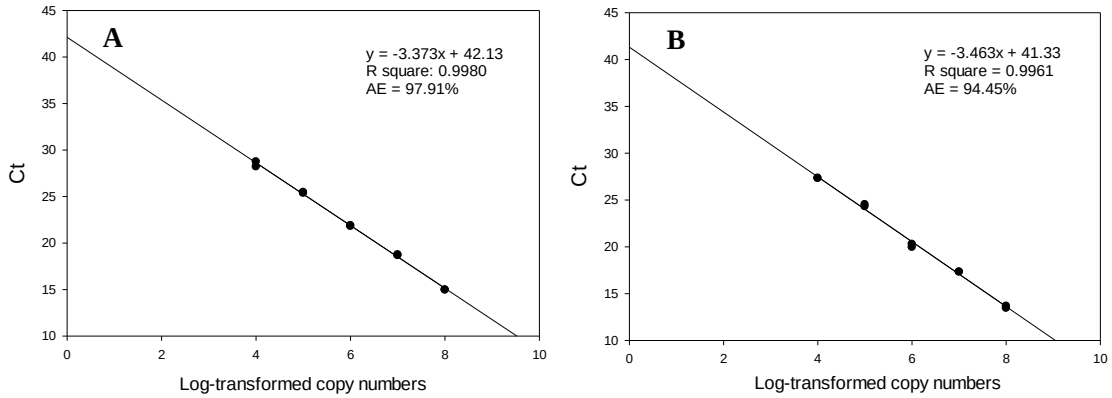

Figure 5.3: (A) Standard curves of purified 28S D1-D2 PCR products using *K. brevis* species-specific primers with annealing temperature of 62°C; (B) Standard curves of pure pGEM-3Z plasmids using M13-F & pGEM-R primers with annealing temperature of 55°C.

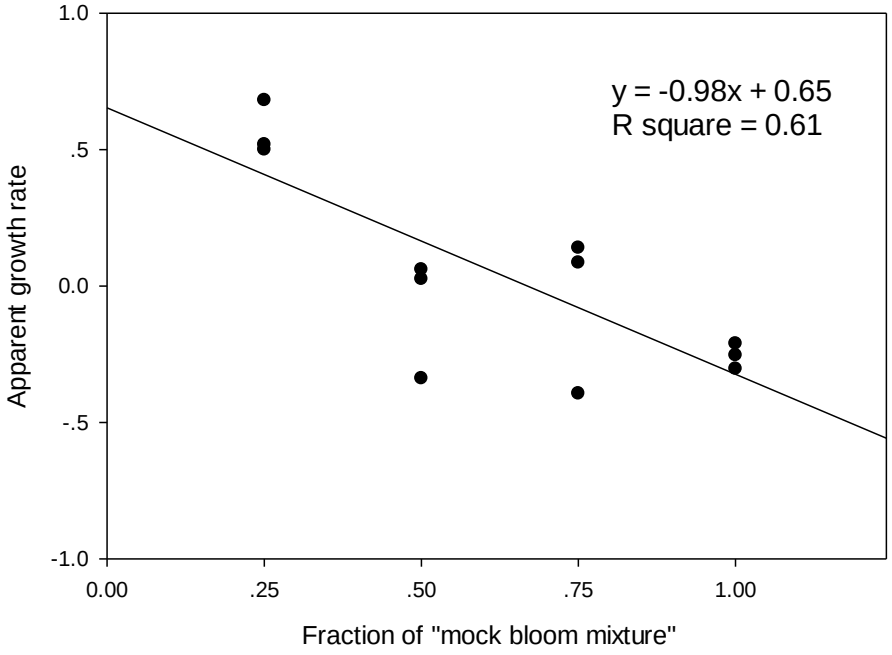

Figure 5.4: Apparent growth rate versus fraction of mock bloom mixture in dilution experiment calculated by chlorophyll *a* for the < 153 μm size fraction. The line was fitted by linear regression to the points (p = 0.0031).

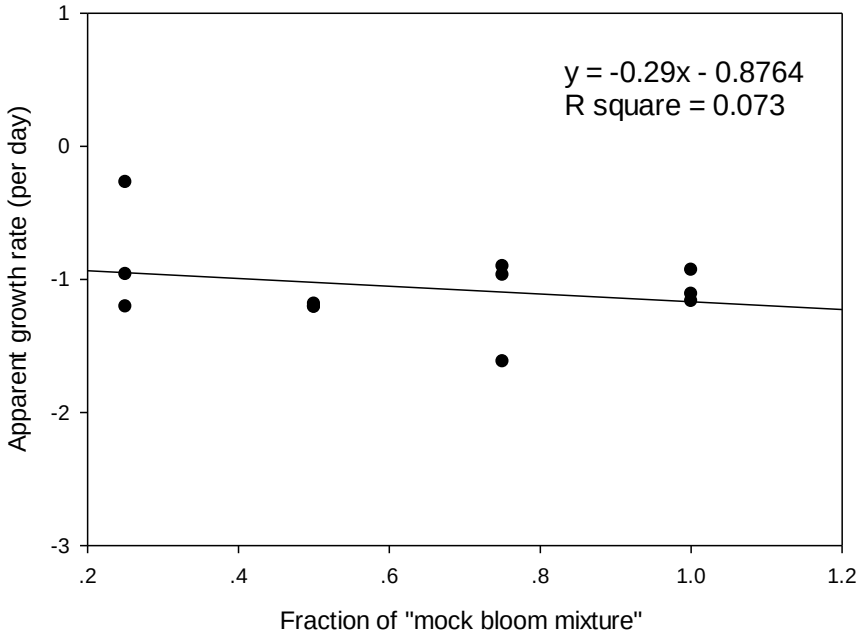

Figure 5.5: Apparent growth rate versus fraction of mock bloom mixture in dilution experiment calculated by cell densities of *K. brevis*. The line was fitted by linear regression to the points ($p = 0.40$).

Chapter 6: Conclusions

In this dissertation the cell loss processes of *K. brevis* in response to oxidative stress, high light, hypo-osmotic stress, temperature shock and grazing pressure were examined, and the potential effects of environmental stress on the decline and termination of HABs were discussed.

PERSPECTIVES ON EXTERNAL STRESS-INDUCED CELL DEATH

The application of the model oxidative stressor H_2O_2 to *K. brevis* revealed typical downstream cell death responses (Chapter 2), as many environmental stressors can trigger ROS production and ROS serves important signaling roles in cellular stress responses (Bidle, 2016). I found that acute vulnerability to PCD (within 30 mins) under oxidative stress increased as cultures aged, which may reflect a chronological decrease of cellular defense and stress acclimation abilities that have been reported at the gene expression level in *K. brevis* (Johnson et al., 2012). Prior to my dissertation the understanding of external stress-induced cell death among different growth stages in phytoplankton was limited. This information is important because it can shed light on the change in susceptibility to intrinsic cell death in algal populations during bloom development. Therefore, under a similar level of external stress PCD may be more strongly induced in aged algal populations, which agrees with the observation of PCD induction after the peak of *Alexandrium* blooms (Choi et al., 2017).

Marine phytoplankton live in a rapidly changing light environment, yet the potential for excess PAR to trigger PCD had not been investigated before my dissertation work. Theoretically, absorption of light energy beyond CO_2 assimilation capacity can result in blockage of the ETC, leading to ROS generation (Apel & Hirt, 2004; Muller et al., 2001). I hypothesized that this high-light-induced oxidative stress would trigger PCD in

microalgae. I found that autocatalytic cell death in *K. brevis* only occurred at the strongest light shock (0 to 1000 µmol m^{-2} s^{-1}). Given the intense surface light irradiance and onshore upwelling in the ocean, cell loss processes can be potentially induced in algal populations by high light stress. On the other hand, the observed dose-dependent activation of NPQ pathways may enable cells to resist or delay PCD by rapidly mitigating ROS production under certain levels of acute light stress. In the field, different intensities and timing of NPQ expression may help phytoplankton cope with natural fluctuations of light intensity, maintaining viability and enabling development of the populations.

Marine phytoplankton may also encounter drastic temperature and salinity changes. For example, during bloom season in the GoM (August to December) *K. brevis* may experience chilling events and repeated transport between coastal and offshore areas (Errera, 2013; Reyna et al., 2017; Steidinger, 1998). Nevertheless, cell death responses under hypo-osmotic and cooling stress in unicellular algae had not been described. It has also been proposed that cell death modes induced in an algal species may be determined by the type of environmental stimulus (Jiménez et al., 2009; Leist & Jäättelä, 2001; Papucci et al., 2004). In my research autocatalytic and non-autocatalytic cell death were observed after hypo-osmotic and temperature stress in *K. brevis*, respectively (Chapter 4), which further supports the diversity of cell death modes. It would be necessary to identify the genes involved in the cell death responses to different stress factors to understand what determines the stress-specific death modes. In addition, *K. brevis* exhibits robust stress acclimation ability, such that their field populations are not likely to encounter sufficient acute temperature or salinity stress alone to result in appreciable mortality under the average hydrographic conditions in western GoM during their bloom season.

Apart from abiotic stressors, microzooplankton grazing on phytoplankton has been recognized as a potential factor for cell loss during HABs (Turner, 2006), while the

difficulties of accurate enumeration of target species in the field have hindered reliable measurement of grazing pressure. In Chapter 5, a new qPCR method for quantification of *K. brevis* from environmental samples was developed which exhibits high sensitivity and specificity to *K. brevis* cells. This method does not require morphological identification and has better sensitivity than conventional microscopic cell counts. The intent is to combine this method with chlorophyll *a* extraction, in order to quantify grazing pressure on *K. brevis* vs co-occurring taxa and gain insights into the role of microzooplankton grazing on dynamics of *K. brevis* blooms.

Cell loss processes in phytoplankton populations have been closely linked to environmental stress (Bidle, 2016; Jimenez et al., 2009; Turner, 2006; Vardi et al., 1999; Zuppini et al., 2010), and my work further examined which stressors and intensities could cause significant cell death in *K. brevis*. The elucidation of environmentally-induced death responses and quantification of grazing pressure on HAB species would not only increase our understanding of the key factors that drive HABs dynamics, but also improve the accuracy of current forecasting models by including quantitative loss factors in hydrodynamic bloom simulations.

PERSPECTIVES ON MULTIPLE ROLES OF PCD CASCADE

In untreated cells, the fluctuating prevalence of ROS and caspase-like activity along the growth curve and over a diel cycle suggests the involvement of components of PCD cascade in cellular metabolism and housekeeping functions (Chapter 2). In the evolutionary history of aquatic photoautotrophs, PCD genes have existed in genomes for about 3 Ga (Summons et al., 1999; Yoon et al., 2004). The components of the PCD cascade must have some physiological benefit to unicellular algae otherwise it would have been lost from

genomes long ago. Generally, my results highlight the death and non-death roles of ROS and caspase-like activity in phytoplankton as well as the importance of understanding mechanisms controlling their intracellular accumulation. The specific metabolic activities that generate intracellular ROS and the housekeeping functions of caspase-like activity in *K. brevis* are still far from clear. Recently developed reduction-oxidation sensitive green fluorescent protein assays (roGFP) provide promising ways to track the locations and intensities of ROS production by *in-vivo* quantification of redox state in different organelles in phytoplankton (Mizrachi et al., 2019; Van Creveld et al., 2015), thereby confirming the metabolic sources of ROS. For example, a stronger roGFP oxidation level in mitochondria is expected in actively-growing cells as a result of respiration activity during the log phase (Kim et al., 2004; Portune et al., 2010; Twiner & Trick, 2000). Increasing evidence of housekeeping functions of caspase-like activity have been found in microorganisms including lysis of redundant proteins in exponentially-growing cells and acclimation to photosynthetic/iron stress in stationary phase (Bidle & Bender, 2008; Jimenez et al., 2009; Seth-Pasricha et al., 2019). My results support the potential existence of these functions in *K. brevis* based on the observed high prevalence of caspase-like activity in the corresponding growth stages. Caspase inhibitors (e.g. Ac-DEVD-CHO) can be powerful tools to further confirm these housekeeping functions in *K. brevis*. For instance, comparing the amount of targeted redundant proteins with and without the application of caspase inhibitors can provide some insights into roles of caspase-like activity in maintaining proteostasis.

PERSPECTIVES ON BLOOM DECLINE

Multiple environmental factors may drive the decline and termination of phytoplankton blooms. In the example of *K. brevis*, all environmental stimuli tested in my dissertation have the potential to induce significant cell death. In the field, co-effects of multiple stressors (e.g. high light and heat stress) can further stimulate ROS production and lead to greater damage in plant cells (Suzuki & Mittler, 2006). Under the frame of climate change, the frequencies of extreme weather conditions like flooding and freezing events are expected to be increase, which may strengthen the contribution of stress-induced cell death to bloom decline processes. For biotic impacts, bacteria isolated from the GoM have induced cell lysis of *K. brevis* in the laboratory environment (Doucette et al., 1999; Roth et al., 2008; Roth et al., 2007), although the occurrence of cell lysis in *K. brevis* blooms has not been demonstrated. Losses due to grazing by microzooplankton in the field will be measured with the developed qPCR method, however this top-down control is not expected to be the major factor driving bloom termination due to the chemical defense and nutritional inadequacy of *K. brevis* to zooplankton (Breier & Buskey, 2007; Campbell, 2012; Kubanek et al., 2007). Besides bio-chemical stress, turbulence may cause necrosis in unarmored *K. brevis*, as *Karenia* cells have low resistance to strong shear forces (Gentien et al., 2007; Lenes et al., 2013; Liu et al., 2002). Another important physical factor that may lead to bloom termination is offshore horizontal advection, which can transport populations out of a specific area and dilute cell concentrations (Lenes et al., 2012; Walsh et al., 2009). In some dinoflagellate species cyst generation has been identified as an important cell fate during bloom decline (Brosnahan et al., 2017). However, *K. brevis* cysts have not yet been found in the field (Persson et al., 2013), leaving a gap for understanding the role of life history on bloom termination and reoccurrence.

FUTURE DIRECTIONS

Overall, this dissertation provides insights into the mechanisms of intrinsic cell death in response to environmental stress in phytoplankton and develops a method to evaluate top-down controls on *K. brevis* in the field. On the other hand, this work opens some questions about the detailed cell loss pathways in phytoplankton under various environmental stress. Some future directions or questions related to cell death in microalgae include:

1. It is necessary to quantify microzooplankton grazing pressure on *K. brevis* and the proportion of *K. brevis* cells exhibiting physiological indices of cellular stress and death in the field to determine their impact on cell losses in bloom progression. This information would be valuable to determine driving factors for bloom dynamics in GoM. Additionally, these data can be incorporated into the current bloom models and provide more accurate loss terms that could better predict bloom magnitude, migration and termination once a bloom has formed.
2. In order to better understand the relationship among ROS, caspase-like activity and cell death in stressed phytoplankton cells, multiple assay reagents with different fluorescent labels should be applied on the same cells to characterize multiple cellular responses at an individual cell level. A set of staining dyes with different cellular binding locations as well as distinct florescence signals is required for applying these measurements.
3. ROS is considered to serve important roles in signal transduction in a variety of stress acclimation pathways and PCD induction in phytoplankton (Apel & Hirt, 2004). Therefore, investigating the signaling selectivity and specificity of ROS from different chemical species, intensities and sub-cellular locations would help to understand their downstream roles in cellular stress responses. The newly developed

roGFP technique may provide insights into the linkage between the redox balance in organelles and cell fates under different environmental stresses in phytoplankton cells.

4. More experimental efforts should be put dedicated to identifying the genes responsible for caspase-like activity in phytoplankton, which can facilitate the understanding of up- or downregulation of caspase-like activity under various conditions. Bidle (2016) recommended the use of *in situ* trapping of activated initiator caspases as well as genome-enabled proteomics to elucidate their expression pathways.
5. In future laboratory studies the co-effects of multiple stressors should be considered to better relate the field conditions to cell death responses and therefore bloom decline processes.

References

Affenzeller, M. J., Darehshouri, A., Andosch, A., Lutz, C., & Lutz-Meindl, U. (2009). Salt stress-induced cell death in the unicellular green alga *Micrasterias denticulata*. *Journal of Experimental Botany*, *60*(3), 939–954.

Algeciras-Schimnich, A., Barnhart, B. C., & Peter, M. E. (2002). Apoptosis-independent functions of killer caspases. *Current Opinion in Cell Biology*, *14*(6), 721–726.

Apel, K., & Hirt, H. (2004). Reactive oxygen species: Metabolism, Oxidative Stress, and Signal Transduction. *Annual Review of Plant Biology*, *55*(1), 373–399.

Azzabi, G., Pinnola, A., Betterle, N., Bassi, R., & Alboresi, A. (2012). Enhancement of Non-Photochemical Quenching in the Bryophyte *Physcomitrella patens* During Acclimation to Salt and Osmotic Stress. *Plant and Cell Physiology*, *53*(10), 1815–1825.

Berges, J. A., & Choi, C. J. (2014). Cell death in algae: physiological processes and relationships with stress. *Perspectives in Phycology*, *1*(2), 103–112.

Berman-Frank, I. (2001). Segregation of Nitrogen Fixation and Oxygenic Photosynthesis in the Marine Cyanobacterium *Trichodesmium*. *Science*, *294*(5546), 1534–1537.

Berman-Frank, Ilana, Bidle, K. D., Haramaty, L., & Falkowski, P. G. (2004). The demise of the marine cyanobacterium, *Trichodesmium spp.*, via an autocatalyzed cell death pathway. *Limnology and Oceanography*, *49*(4), 997–1005.

Bidle, K. A., Haramaty, L., Baggett, N., Nannen, J., & Bidle, K. D. (2010). Tantalizing evidence for caspase-like protein expression and activity in the cellular stress response of Archaea. *Environmental Microbiology*, *12*(5), 1161–1172.

Bidle, K. D. (2015). The Molecular Ecophysiology of Programmed Cell Death in Marine Phytoplankton. *Annual Review of Marine Science*, *7*(1), 341–375.

Bidle, K. D. (2016). Programmed Cell Death in Unicellular Phytoplankton. *Current Biology*, *26*(13), R594–R607.

Bidle, K. D., & Bender, S. J. (2008). Iron Starvation and Culture Age Activate Metacaspases and Programmed Cell Death in the Marine Diatom *Thalassiosira pseudonana*. *Eukaryotic Cell*, *7*(2), 223–236.

Bidle, K. D., & Falkowski, P. G. (2004). Cell death in planktonic, photosynthetic microorganisms. *Nature Reviews. Microbiology*, *2*(8), 643–655.

Bidle, K. D., Haramaty, L., Barcelos e Ramos, J., & Falkowski, P. (2007). Viral activation and recruitment of metacaspases in the unicellular coccolithophore, *Emiliania huxleyi*. *Proceedings of the National Academy of Sciences*, *104*(14), 6049–6054.

Bierkens, J. G. E. A. (2000). Applications and pitfalls of stress-proteins in biomonitoring. *Toxicology*, *153*(1–3), 61–72.

Bouchard, J. N., & Purdie, D. A. (2011). Temporal variation of caspase 3-like protein activity in cultures of the harmful dinoflagellates *Karenia brevis* and *Karenia mikimotoi*. *Journal of Plankton Research*, *33*(6), 961–972.

Bouchard, Josée N, & Purdie, D. A. (2011). Effect of elevated temperature, darkness and hydrogen peroxide treatment on oxidative stress and cell death in the bloom-forming toxic cyanobacterium *Microcystis aeruginosa*. *Journal of Phycology*, *47*(6), 1316–1325.

Bouchard, Josée Nina, & Yamasaki, H. (2009). Implication of nitric oxide in the heat-stress-induced cell death of the symbiotic alga *Symbiodinium microadriaticum*. *Marine Biology*, *156*(11), 2209–2220.

Boyce, M., Degterev, A., & Yuan, J. (2004). Caspases: an ancient cellular sword of Damocles. *Cell Death and Differentiation*, *11*(1), 29–37.

Brand, L. E., Campbell, L., & Bresnan, E. (2012). *Karenia*: The biology and ecology of a toxic genus. *Harmful Algae*, *14*, 156–178.

Breier, C. F., & Buskey, E. J. (2007). Effects of the red tide dinoflagellate, Karenia brevis, on grazing and fecundity in the copepod *Acartia tonsa*. *Journal of Plankton Research*, *29*(2), 115–126.

Britt, A. B. (1996). DNA damage and repair in plants. *Annual Review of Plant Physiology and Plant Molecular Biology*, *47*(1), 75–100.

Brosnahan, M. L., Ralston, D. K., Fischer, A. D., Solow, A. R., & Anderson, D. M. (2017). Bloom termination of the toxic dinoflagellate *Alexandrium catenella*: Vertical migration behavior, sediment infiltration, and benthic cyst yield. *Limnology and Oceanography*, *62*(6), 2829–2849.

Brunelle, S. A., Hazard, E. S., Sotka, E. E., & Van Dolah, F. M. (2007). Characterization of a dinoflagellate cryptochrome blue-light receptor with a possible role in circadian control of the cell cycle. *Journal of Phycology*, *43*(3), 509–518.

Bucciarelli, E., Sunda, W. G., Belviso, S., & Sarthou, G. (2007). Effect of the diel cycle on production of dimethylsulfoniopropionate in batch cultures of *Emiliania huxleyi*. *Aquatic Microbial Ecology*, *48*, 73–81.

Butow, B. J., Wynne, D., & TelOr, E. (1997). Antioxidative protection of *Peridinium gatunense* in Lake Kinneret: Seasonal and daily variation. *Journal of Phycology*, *33*(5), 780–786.

Calbet, A., Vaqué, D., Felipe, J., Vila, M., Montserrat Sala, M., Alcaraz, M., & Estrada, M. (2003). Relative grazing impact of microzooplankton and mesozooplankton on a bloom of the toxic dinoflagellate *Alexandrium minutum*. *Marine Ecology Progress Series*, *259*, 303–309.

Campbell, J. R. (2012). *The role of protozoan grazers in harmful algal bloom dynamics: tools for community and grazing analyses*. University of Texas at Austin, PhD dissertation.

Campbell, R. G., Teegarden, G. J., Cembella, A. D., & Durbin, E. G. (2005). Zooplankton grazing impacts on *Alexandrium spp.* in the nearshore environment of the Gulf of Maine. *Deep Sea Research Part II: Topical Studies in Oceanography*, *52*(19–21), 2817–2833.

Caron, D. A., Gobler, C. J., Lonsdale, D. J., Cerrato, R. M., Schaffner, R. A., Rose, J. M., … Mehran, R. (2004). Microbial herbivory on the brown tide alga, *Aureococcus anophagefferens*: results from natural ecosystems, mesocosms and laboratory experiments. *Harmful Algae*, *3*(4), 439–457.

Cassell, R. T., Chen, W., Thomas, S., Liu, L., & Rein, K. S. (2015). Brevetoxin, the Dinoflagellate Neurotoxin, Localizes to Thylakoid Membranes and Interacts with the Light-Harvesting Complex II (LHCII) of Photosystem II. *ChemBioChem*, *16*(7), 1060–1067.

Chambouvet, A., Morin, P., Marie, D., & Guillou, L. (2008). Control of Toxic Marine Dinoflagellate Blooms by Serial Parasitic Killers. *Science*, *322*(5905), 1254–1257.

Choi, C. J., & Berges, J. A. (2013). New types of metacaspases in phytoplankton reveal diverse origins of cell death proteases. *Cell Death and Disease*, 1–7.

Choi, C. J., Brosnahan, M. L., Sehein, T. R., Anderson, D. M., & Erdner, D. L. (2017). Insights into the loss factors of phytoplankton blooms: The role of cell mortality in the decline of two inshore Alexandrium blooms. *Limnology and Oceanography*, *62*(4), 1742–1753.

Cohen, G. M. (1998). Role of caspases as the executioners of apoptosis. *Toxicology Letters*, *95*, 7.

Cohen, J. H., Tester, P. A., & Forward, R. B. (2007). Sublethal effects of the toxic dinoflagellate *Karenia brevis* on marine copepod behavior. *Journal of Plankton Research*, *29*(3), 301–315.

Coyne, K., Handy, S., & Demir, E. (2005). Improved quantitative real-time PCR assays for enumeration of harmful algal species in field samples using an exogenous DNA reference standard. *Limnology and Oceanography: Methods*, *3*, 381–391.

Cui, Y., Zhang, H., & Lin, S. (2017). Enhancement of Non-photochemical Quenching as an Adaptive Strategy under Phosphorus Deprivation in the Dinoflagellate *Karlodinium veneficum*. *Frontiers in Microbiology*, *8*(March), 1–14.

Darehshouri, A., Affenzeller, M., & Lütz-Meindl, U. (2008). Cell death upon hydrogen peroxide induction in the unicellular green alga *Micrasterias*. *Plant Biology*, *10*(6), 732–745.

Daugherty, M. N. (2017). *Transcriptonmic response of Karenia brevis to environmental stress*. Texas A&M University, Master thesis.

Demmig-Adams, B., & Adams Iii, W. W. (1992). Photoprotection and other responses of plants to high light stress. *Annual Review of Plant Biology*, *43*(1), 599–626.

Denton, D., Nicolson, S., & Kumar, S. (2012). Cell death by autophagy: facts and apparent artefacts. *Cell Death & Differentiation*, *19*(1), 87–95.

Deponte, M. (2008). Programmed cell death in protists. *Biochimica et Biophysica Acta (BBA) - Molecular Cell Research*, *1783*(7), 1396–1405.

Diaz, J. M., & Plummer, S. (2018). Production of extracellular reactive oxygen species by phytoplankton: past and future directions. *Journal of Plankton Research*, *40*, 655–666.

Ding, Y., Gan, N., Li, J., Sedmak, B., & Song, L. (2012). Hydrogen peroxide induces apoptotic-like cell death in *Microcystis aeruginosa* (Chroococcales, Cyanobacteria) in a dose-dependent manner. *Phycologia*, *51*(5), 567–575.

Dingman, J. E., & Lawrence, J. E. (2012). Heat-stress-induced programmed cell death in *Heterosigma akashiwo* (Raphidophyceae). *Harmful Algae*, *16*, 108–116.

Doucette, G. J., McGovern, E. R., & Babinchak, J. A. (1999). Algicidal bacteria active against *gymnodinium breve* (Dinophyceae). I. bacterial isolation and characterization of killing activity. *Journal of Phycology*, *35*(6), 1447–1454.

Drummond, A.J., Ashton, B., Buxton, S., Cheung, M., Cooper, A., Duran, C., Field, M., Heled, J., Kearse, M., Markowitz, S. and Moir, R. (2011). Geneious. *Biomatters Ltd.*

Dunn, S. R., Thomason, J. C., Le Tissier, M. D. A., & Bythell, J. C. (2004). Heat stress induces different forms of cell death in sea anemones and their endosymbiotic algae depending on temperature and duration. *Cell Death & Differentiation*, *11*(11), 1213–1222.

Dupont, C. L., Goepfert, T. J., Lo, P., Wei, L., & Ahner, B. A. (2004). Diurnal cycling of glutathione in marine phytoplankton: Field and culture studies. *Limnology and Oceanography*, *49*(4), 991–996.

Durand, P. M., Rashidi, A., & Michod, R. E. (2011). How an Organism Dies Affects the Fitness of Its Neighbors. *The American Naturalist*, *177*(2), 224–232.

Dyhrman, S. T., Erdner, D., Du, J. La, Galac, M., & Anderson, D. M. (2006). Molecular quantification of toxic *Alexandrium fundyense* in the Gulf of Maine using real-time PCR. *Harmful Algae*, *5*(3), 242–250.

Edgar, R. S., Green, E. W., Zhao, Y., van Ooijen, G., Olmedo, M., Qin, X., … Reddy, A. B. (2012). Peroxiredoxins are conserved markers of circadian rhythms. *Nature*, *485*(7399), 459–464.

Elrad, D., Niyogi, K. K., & Grossman, A. R. (2002). A Major Light-Harvesting Polypeptide of Photosystem II Functions in Thermal Dissipation. *The Plant Cell*, *14*(8), 1801–1816.

Erdner, D. L., Percy, L., Keafer, B., Lewis, J., & Anderson, D. M. (2010). A quantitative real-time PCR assay for the identification and enumeration of Alexandrium cysts in marine sediments. *Deep Sea Research Part II: Topical Studies in Oceanography*, *57*(3–4), 279–287.

Errera, R. (2013). *Response of the toxic dinoflagellate Karenia brevis to current and projected environmental conditions*. Texas A&M University, PhD dissertation.

Evens, T. J. (2001). Photophysiological responses of the toxic red-tide dinoflagellate *Gymnodinium breve* (Dinophyceae) under natural sunlight. *Journal of Plankton Research*, *23*(11), 1177–1194.

Fleming, L. E., Kirkpatrick, B., Backer, L. C., Walsh, C. J., Nierenberg, K., Clark, J., … Baden, D. G. (2011). Review of Florida red tide and human health effects. *Harmful Algae*, *10*(2), 224–233.

Foyer, C. H., Lelandais, M., & Kunert, K. J. (1994). Photooxidative stress in plants. *Physiologia Plantarum*, *92*(4), 696–717.

Franklin, D. J., & Berges, J. a. (2004). Mortality in cultures of the dinoflagellate *Amphidinium carterae* during culture senescence and darkness. *Proceedings of the Royal Society of London. Series B: Biological Sciences*, *271*(1553), 2099–2107.

Franklin, D. J., Brussaard, C. P. D., & Berges, J. a. (2006). What is the role and nature of programmed cell death in phytoplankton ecology? *European Journal of Phycology*, *41*(1), 1–14.

Galluzzi, L., Bertozzini, E., Penna, A., Perini, F., Garcés, E., & Magnani, M. (2010). Analysis of rRNA gene content in the Mediterranean dinoflagellate *Alexandrium catenella* and *Alexandrium taylori*: implications for the quantitative real-time PCR-based monitoring methods. *Journal of Applied Phycology*, *22*(1), 1–9.

Gechev, T. S., & Hille, J. (2005). Hydrogen peroxide as a signal controlling plant programmed cell death. *Journal of Cell Biology*, *168*(1), 17–20.

Gentien, P., Lunven, M., Lazure, P., Youenou, A., & Crassous, M. . (2007). Motility and autotoxicity in *Karenia mikimotoi* (Dinophyceae). *Philosophical Transactions of the Royal Society B: Biological Sciences*, *362*(1487), 1937–1946.

Gobler, C. J., Deonarine, S., Leigh-Bell, J., Gastrich, M. D., Anderson, O. R., & Wilhelm, S. W. (2004). Ecology of phytoplankton communities dominated by *Aureococcus anophagefferens*: the role of viruses, nutrients, and microzooplankton grazing. *Harmful Algae*, *3*(4), 471–483.

Gobler, C. J., Renaghan, M. J., & Buck, N. J. (2002). Impacts of nutrients and grazing mortality on the abundance of *Aureococcus anophagefferens* during a New York brown tide bloom. *Limnology and Oceanography*, *47*(1), 129–141.

Godhe, A., Cusack, C., Pedersen, J., Andersen, P., Anderson, D. M., Bresnan, E., … Töbe, K. (2007). Intercalibration of classical and molecular techniques for identification of *Alexandrium fundyense* (Dinophyceae) and estimation of cell densities. *Harmful Algae*, *6*(1), 56–72.

Golstein, P., & Kroemer, G. (2007). Cell death by necrosis: towards a molecular definition. *Trends in Biochemical Sciences*, *32*(1), 37–43.

Gülden, M., Jess, A., Kammann, J., Maser, E., & Seibert, H. (2010). Cytotoxic potency of H2O2 in cell cultures: Impact of cell concentration and exposure time. *Free Radical Biology and Medicine*, *49*(8), 1298–1305.

Hariganeya, N., Tanimoto, Y., Yamaguchi, H., Nishimura, T., Tawong, W., Sakanari, H., … Adachi, M. (2013). Quantitative PCR Method for Enumeration of Cells of Cryptic Species of the Toxic Marine Dinoflagellate Ostreopsis spp. in Coastal Waters of Japan. *PLoS ONE*, *8*(3), e57627.

Haywood, A. J., Scholin, C. A., Marin, R., Steidinger, K. A., Heil, C., & Ray, J. (2007). Molecular detection of the brevetoxin-producing dinoflagellate *Karenia brevis* and closely related species using rRNA-targeted probes and a semiautomated sandwich hybridization assay 1. *Journal of Phycology*, *43*(6), 1271–1286.

Haywood, A. J., Steidinger, K. A., Truby, E. W., Bergquist, P. R., Bergquist, P. L., Adamson, J., & Mackenzie, L. (2004). Comparative morphology and molecular phylogenetic analysis of three new species of the genus *Karenia* (Dinophyceae) from New Zealand. *Journal of Phycology*, *40*(1), 165–179.

Heil, C. A., Bronk, D. A., Mulholland, M. R., O'Neil, J. M., Bernhardt, P. W., Murasko, S., … Vargo, G. A. (2014). Influence of daylight surface aggregation behavior on nutrient cycling during a Karenia brevis (Davis) G. Hansen & Ø. Moestrup bloom: Migration to the surface as a nutrient acquisition strategy. *Harmful Algae*, *38*(2014), 86–94.

Henrichs, D. W., Hetland, R. D., & Campbell, L. (2015). Identifying bloom origins of the toxic dinoflagellate *Karenia brevis* in the western Gulf of Mexico using a spatially explicit individual-based model. *Ecological Modelling*, *313*, 251–258.

Hetland, R. D., & Campbell, L. (2007). Convergent blooms of Karenia brevis along the Texas coast. *Geophysical Research Letters*, *34*(19), 1–5.

Hou, Y., Zhang, H., Miranda, L., & Lin, S. (2010). Serious Overestimation in Quantitative PCR by Circular (Supercoiled) Plasmid Standard: Microalgal pcna as the Model Gene. *PLoS ONE*, *5*(3).

Houot, V. (2001). Hydrogen peroxide induces programmed cell death features in cultured tobacco BY-2 cells, in a dose-dependent manner. *Journal of Experimental Botany*, *52*(361), 1721–1730.

Huntley, M., Sykes, P., Rohan, S., & Marin, V. (1986). Chemically-mediated rejection of dinoflagellate prey by the copepods *Calanuspacificus* and *Paracalanusparvus* : mechanism , occurrence and significance. *Marine Ecology Progress Series*, *28*, 105–120.

Irigoien, X., Flynn, K. J., & Harris, R. P. (2005). Phytoplankton blooms: a 'loophole' in microzooplankton grazing impact? *Journal of Plankton Research*, *27*(4), 313–321.

Jansen, S., Riser, C. W., Wassmann, P., & Bathmann, U. (2006). Copepod feeding behaviour and egg production during a dinoflagellate bloom in the North Sea. *Harmful Algae*, *5*(1), 102–112.

Jauzein, C., & Erdner, D. L. (2013). Stress-related Responses in *Alexandrium tamarense* Cells Exposed to Environmental Changes. *Journal of Eukaryotic Microbiology*, *60*(5), 526–538.

Jensen, S. I., Steunou, A., Bhaya, D., Kühl, M., & Grossman, A. R. (2011). In situ dynamics of O2, pH and cyanobacterial transcripts associated with CCM, photosynthesis and detoxification of ROS. *The ISME Journal*, *5*(2), 317–328.

Jeong, S. W., Choi, S. M., Lee, D. S., Ahn, S. N., Hur, Y., Chow, W. S., & Park, Y. (2002). Differential susceptibility of photosynthesis to light-chilling stress in rice (Oryza sativa L.) depends on the capacity for photochemical dissipation of light. *Molecules and Cells*, *13*(3), 419–428.

Jimenez, C., Capasso, J. M., Edelstein, C. L., Rivard, C. J., Lucia, S., Breusegem, S., … Segovia, M. (2009). Different ways to die: cell death modes of the unicellular chlorophyte *Dunaliella viridis* exposed to various environmental stresses are mediated by the caspase-like activity DEVDase. *Journal of Experimental Botany*, *60*(3), 815–828.

Johnson, J. G., Janech, M. G., & Van Dolah, F. M. (2014). Caspase-like activity during aging and cell death in the toxic dinoflagellate *Karenia brevis*. *Harmful Algae*, *31*, 41–53.

Johnson, J. G., Morey, J. S., Neely, M. G., Ryan, J. C., & van Dolah, F. M. (2012). Transcriptome remodeling associated with chronological aging in the dinoflagellate, Karenia brevis. *Marine Genomics*, *5*, 15–25.

Johnson, M. D., Rome, M., & Stoecker, D. K. (2003). Microzooplankton grazing on *Prorocentrum minimum* and *Karlodinium micrum* in Chesapeake Bay. *Limnology and Oceanography*, *48*(1), 238–248.

Kamiyama, T., & Matsuyama, Y. (2005). Temporal changes in the ciliate assemblage and consecutive estimates of their grazing effect during the course of a *Heterocapsa circularisquama* bloom. *Journal of Plankton Research*, *27*(4), 303–311.

Kanduc, D., Mittelman, A., Serpico, R., Sinigaglia, E., Sinha, A., Natale, C., … Farber, E. (2002). Cell death: apoptosis versus necrosis. *International Journal of Oncology*, *21*, 165–170.

Kawano, I., Oda, T., Ishimatsu, A., & Muramatsu, T. (1996). Inhibitory effect of the iron chelator desferrioxamine (Desferal) on the generation of activated oxygen species by *Chattonella marina*. *Marine Biology*, *126*(4), 765–771.

Kerr, J. F. R., Wyllie, A. H., & Currie, A. R. (1972). Apoptosis: A Basic Biological Phenomenon with Wideranging Implications in Tissue Kinetics. *British Journal of Cancer*, *26*(4), 239–257.

Kim, C. S., Lee, S. G., Kyu, L. C., Kim, H. G., & Jung, J. (1999). Reactive oxygen species as causative agents in the ichthyotoxicity of the red tide dinoflagellate *Cochlodinium polykrikoides*. *Journal of Plankton Research*, *21*(11), 2105–2115.

Kim, D., Watanabe, M., Nakayasu, Y., & Kohata, K. (2004). Production of superoxide anion and hydrogen peroxide associated with cell growth of *Chattonella antiqua*. *Aquatic Microbial Ecology*, *35*, 57–64.

Kobiyama, A., Tanaka, S., Kaneko, Y., Lim, P., & Ogata, T. (2010). Temperature tolerance and expression of heat shock protein 70 in the toxic dinoflagellate *Alexandrium tamarense* (Dinophyceae). *Harmful Algae*, *9*(2), 180–185.

Kon, N. F., Lau, W. L. S., Hii, K. S., Law, I. K., Teng, S. T., Lim, H. C., … Leaw, C. P. (2017). Quantitative real-time PCR detection of a harmful unarmoured dinoflagellate, *Karlodinium australe* (Dinophyceae). *Phycological Research*, *65*(4), 291–298.

Kon, N. F., Teng, S. T., Hii, K. S., Yek, L. H., Mujahid, A., Lim, H. C., … Leaw, C. P. (2015). Spatial distribution of toxic *Alexandrium tamiyavanichii* (Dinophyceae) in the southeastern South China Sea-Sulu Sea: A molecular-based assessment using real-time quantitative PCR (qPCR) assay. *Harmful Algae*, *50*, 8–20.

Kozlowsky-Suzuki, B., Carlsson, P., Rühl, A., & Granéli, E. (2006). Food selectivity and grazing impact on toxic *Dinophysis spp.* by copepods feeding on natural plankton assemblages. *Harmful Algae*, *5*(1), 57–68.

Krause, G. Heinrich, & Jahns, P. (2004). Non-photochemical Energy Dissipation Determined by Chlorophyll Fluorescence Quenching: Characterization and Function. In *Chlorophyll a Fluorescence* (pp. 463–495). Dordrecht: Springer Netherlands.

Krause, G H, & Weis, E. (1991). Chlorophyll Fluorescence and Photosynthesis: The Basics. *Annual Review of Plant Physiology and Plant Molecular Biology*, *42*(1), 313–349.

Krysko, D. V, Berghe, T. Vanden, Parthoens, E., D'Herde, K., & Vandenabeele, P. (2008). Chapter 16 Methods for Distinguishing Apoptotic from Necrotic Cells and Measuring Their Clearance. In *Methods in enzymology* (Vol. 442, pp. 307–341). Retrieved from https://linkinghub.elsevier.com/retrieve/pii/S007668790801416X

Kubanek, J., Snell, T. W., & Pirkle, C. (2007). Chemical defense of the red tide dinoflagellate *Karenia brevis* against rotifer grazing. *Limnology and Oceanography*, *52*(3), 1026–1035.

Kupper, F. C., Carpenter, L. J., McFiggans, G. B., Palmer, C. J., Waite, T. J., Boneberg, E.-M., … Feiters, M. C. (2008). Iodide accumulation provides kelp with an inorganic antioxidant impacting atmospheric chemistry. *Proceedings of the National Academy of Sciences*, *105*(19), 6954–6958.

Landry, M. R., & Hassett, R. P. (1982). Estimating the grazing impact of marine micro-zooplankton. *Marine Biology*, *67*(3), 283–288.

Landsberg, J. H., Flewelling, L. J., & Naar, J. (2009). *Karenia brevis* red tides, brevetoxins in the food web, and impacts on natural resources: Decadal advancements. *Harmful Algae*, *8*(4), 598–607.

Laporte, C., Kosta, A., Klein, G., Aubry, L., Lam, D., Tresse, E., … Golstein, P. (2007). A necrotic cell death model in a protist. *Cell Death & Differentiation*, *14*(2), 266–274.

Larkindale, J., & Knight, M. R. (2002). Protection against Heat Stress-Induced Oxidative Damage in Arabidopsis Involves Calcium, Abscisic Acid, Ethylene, and Salicylic Acid. *Plant Physiology*, *128*(2), 682–695.

Lauritano, C., Carotenuto, Y., Procaccini, G., Turner, J. T., & Ianora, A. (2013). Changes in expression of stress genes in copepods feeding upon a non-brevetoxin-producing strain of the dinoflagellate *Karenia brevis*. *Harmful Algae*, *28*, 23–30.

Leist, M., & Jäättelä, M. (2001). Four deaths and a funeral: from caspases to alternative mechanisms. *Nature Reviews Molecular Cell Biology*, *2*(8), 589–598.

Lenes, J. M., Darrow, B. P., Walsh, J. J., Jolliff, J. K., Chen, F. R., Weisberg, R. H., & Zheng, L. (2012). A 1-D simulation analysis of the development and maintenance of the 2001 red tide of the ichthyotoxic dinoflagellate *Karenia brevis* on the West Florida shelf. *Continental Shelf Research*, *41*, 92–110.

Lenes, J., Walsh, J., & Darrow, B. (2013). Simulating cell death in the termination of *Karenia brevis* blooms: implications for predicting aerosol toxicity vectors to humans. *Marine Ecology Progress Series*, *493*, 71–81.

Leu, K., & Hsu, B. (2005). A programmed cell disintegration of Chlorella after heat stress. *Plant Science*, *168*(1), 145–152.

Levy, O., Achituv, Y., Yacobi, Y. Z., Dubinsky, Z., & Stambler, N. (2006). Diel ' tuning ' of coral metabolism : physiological responses to light cues, 273–283.

Li, M., Li, L., Shi, X., Lin, L., & Lin, S. (2015). Effects of phosphorus deficiency and adenosine 5'-triphosphate (ATP) on growth and cell cycle of the dinoflagellate *Prorocentrum donghaiense*. *Harmful Algae*, *47*, 35–41.

Li, Z., Wakao, S., Fischer, B. B., & Niyogi, K. K. (2009). Sensing and Responding to Excess Light. *Annual Review of Plant Biology*, *60*(1), 239–260.

Liu, G., Janowitz, G. S., & Kamykowski, D. (2001). A biophysical model of population dynamics of the autotrophic dinoflagellate *Gymnodinium breve*. *Marine Ecology Progress Series*, *210*, 101–124.

Liu, Gang, Janowitz, G., & Kamykowski, D. (2002). Influence of current shear on *Gymnodinium breve* (Dinophyceae) population dynamics: a numerical study. *Marine Ecology Progress Series*, *231*, 47–66.

Liu, H., Suzuki, K., & Saino, T. (2002). Phytoplankton growth and microzooplankton grazing in the subarctic Pacific Ocean and the Bering Sea during summer 1999. *Deep Sea Research Part I: Oceanographic Research Papers*, *49*(2), 363–375.

Liu, W., Au, D. W. T., Anderson, D. M., Lam, P. K. S., & Wu, R. S. S. (2007). Effects of nutrients, salinity, pH and light:dark cycle on the production of reactive oxygen species in the alga *Chattonella marina*. *Journal of Experimental Marine Biology and Ecology*, *346*(1–2), 76–86.

Liu, W., Ming, Y., Li, P., & Huang, Z. (2012). Inhibitory effects of hypo-osmotic stress on extracellular carbonic anhydrase and photosynthetic efficiency of green alga *Dunaliella salina* possibly through reactive oxygen species formation. *Plant Physiology and Biochemistry*, *54*, 43–48.

Livak, K. J., & Schmittgen, T. D. (2001). Analysis of Relative Gene Expression Data Using Real-Time Quantitative PCR and the 2−ΔΔCT Method. *Methods*, *25*(4), 402–408.

Loebl, M., & Van Beusekom, J. E. E. (2008). Seasonality of microzooplankton grazing in the northern Wadden Sea. *Journal of Sea Research*, *59*(4), 203–216.

Lu, C., & Vonshak, A. (1999). Characterization of PSII photochemistry in salt-adapted cells of cyanobacterium *Spirulina platensis*. *New Phytologist*, *141*(2), 231–239.

Magaña, H. A., & Villareal, T. A. (2006). The effect of environmental factors on the growth rate of *Karenia brevis* (Davis) G. Hansen and Moestrup. *Harmful Algae*, *5*(2), 192–198.

Matsuyama, Y., Miyamoto, M., & Kotani, Y. (1999). Grazing impacts of the heterotrophic dinoflagellate Polykrikos kofoidii on a bloom of *Gymnodinium catenatum*. *Aquatic Microbial Ecology*, *17*, 91–98.

McKay, L., Kamykowski, D., Milligan, E., Schaeffer, B., & Sinclair, G. (2006). Comparison of swimming speed and photophysiological responses to different external conditions among three *Karenia brevis strains*. *Harmful Algae*, *5*(6), 623–636.

Mella-Flores, D., Six, C., Ratin, M., Partensky, F., Boutte, C., Le Corguillé, G., … Garczarek, L. (2012). *Prochlorococcus* and *Synechococcus* have Evolved Different Adaptive Mechanisms to Cope with Light and UV Stress. *Frontiers in Microbiology*, *3*, 1–20.

Miller-Morey, J. S., & Van Dolah, F. M. (2004). Differential responses of stress proteins, antioxidant enzymes, and photosynthetic efficiency to physiological stresses in the Florida red tide dinoflagellate, *Karenia brevis*. *Comparative Biochemistry and Physiology Part C: Toxicology & Pharmacology*, *138*(4), 493–505.

Miller, G., Suzuki, N., Ciftci-Yilmaz, S., & Mittler, R. (2010). Reactive oxygen species homeostasis and signalling during drought and salinity stresses. *Plant, Cell & Environment*, *33*(4), 453–467.

Milne, A., Davey, M. S., Worsfold, P. J., Achterberg, E. P., & Taylor, A. R. (2009). Real-time detection of reactive oxygen species generation by marine phytoplankton using flow injection-chemiluminescence. *Limnology and Oceanography: Methods*, *7*(10), 706–715.

Mizrachi, A., Graff van Creveld, S., Shapiro, O. H., Rosenwasser, S., & Vardi, A. (2019). Light-dependent single-cell heterogeneity in the chloroplast redox state regulates cell fate in a marine diatom. *ELife*, *8*, 1–27.

Moharikar, S., D'Souza, J. S., Kulkarni, A. B., & Rao, B. J. (2006). Apoptotic-like cell death pathway is induced in unicellular chlorophyte *Chlamydomonas reinhardtii* (Chlorophyceae) cells following UV irradiation: Detection and functional analyses. *Journal of Phycology*, *42*(2), 423–433.

Møller, I. M. (2001). PLANT MITOCHONDRIA AND O XIDATIVE STRESS : Electron Transport , NADPH Turnover , and Metabolism of Reactive Oxygen Species. *Annual Review of Plant Physiology and Plant Molecular Biology*, *52*, 561–591.

Müller, P., Li, X., & Niyogi, K. K. (2001). Non-Photochemical Quenching. A Response to Excess Light Energy. *Plant Physiology*, *125*(4), 1558–1566.

Murik, O., Elboher, A., & Kaplan, A. (2014). Dehydroascorbate: A possible surveillance molecule of oxidative stress and programmed cell death in the green alga *Chlamydomonas reinhardtii*. *New Phytologist*, *202*(2), 471–484.

Murik, O., & Kaplan, A. (2009). Paradoxically, prior acquisition of antioxidant activity enhances oxidative stress-induced cell death. *Environmental Microbiology*, *11*(9), 2301–2309.

Naar, J. P., Flewelling, L. J., Lenzi, A., Abbott, J. P., Granholm, A., Jacocks, H. M., … Landsberg, J. H. (2007). Brevetoxins, like ciguatoxins, are potent ichthyotoxic neurotoxins that accumulate in fish. *Toxicon*, *50*(5), 707–723.

Nakamura, Y., Suzuki, S., & Hiromi, J. (1996). Development and collapse of a *Gymnodinium mikimotoi* red tide in the Seto Inland Sea. *Aquatic Microbial Ecology*, *10*, 131–137. Retrieved from http://www.int-res.com/abstracts/ame/v10/n2/p131-137/

Nicholson, D. W., & Thornberry, N. A. (1997). Caspases: Killer proteases. *Trends in Biochemical Sciences*, *22*(8), 299–306.

Ning, S.-B., Guo, H.-L., Wang, L., & Song, Y.-C. (2002). Salt stress induces programmed cell death in prokaryotic organism Anabaena. *Journal of Applied Microbiology*, *93*(1), 15–28.

Niyogi, K. K. (1999). Photoprotection revisited: Genetic and Molecular Approaches. *Annual Review of Plant Physiology and Plant Molecular Biology*, *50*(1), 333–359.

Oda, T., Moritomi, J., Kawano, I., Hamaguchi, S., Ishimatsu, A., & Muramatsu, T. (1995). Catalase- and Superoxide Dismutase-induced Morphological Changes and Growth Inhibition in the Red Tide Phytoplankton *Chattonella marina*. *Bioscience, Biotechnology, and Biochemistry*, *59*(11), 2044–2048.

Okamoto, O.K., & Colepicolo, P. (2001). Circadian Protection against Reactive Oxygen Species Involves Changes in Daily Levels of the Manganese- and Iron-Containing Superoxide Dismutase Isoforms in *Lingulodinium polyedrum*. *Biological Rhythm Research*, *32*(4), 439–448.

Okamoto, O Keith, Robertson, D. L., Fagan, T. F., Hastings, J. W., & Colepicolo, P. (2001). Different Regulatory Mechanisms Modulate the Expression of a Dinoflagellate Iron-Superoxide Dismutase. *Journal of Biological Chemistry*, *276*(23), 19989–19993.

Papucci, L., Formigli, L., Schiavone, N., Tani, A., Donnini, M., Lapucci, A., … Capaccioli, S. (2004). Apoptosis shifts to necrosis via intermediate types of cell death by a mechanism depending on c- myc and bcl-2 expression. *Cell and Tissue Research*, *316*(2), 197–209.

Paul, J., Houchin, L., Griffin, D., Slifko, T., Guo, M., Richardson, B., & Steidinger, K. (2002). A filterable lytic agent obtained from a red tide bloom that caused lysis of *Karenia brevis* (Gymnodinum breve) cultures. *Aquatic Microbial Ecology*, *27*(1), 21–27.

Perini, F., Casabianca, A., Battocchi, C., Accoroni, S., Totti, C., & Penna, A. (2011). New Approach Using the Real-Time PCR Method for Estimation of the Toxic Marine Dinoflagellate *Ostreopsis cf. ovata* in Marine Environment. *PLoS ONE*, *6*(3), e17699.

Persson, A., Smith, B. C., Morton, S., Shuler, A., & Wikfors, G. H. (2013). Sexual life stages and temperature dependent morphological changes allow cryptic occurrence of the Florida red tide dinoflagellate *Karenia brevis*. *Harmful Algae*, *30*, 1–9.

Pfannschmidt, T. (2003). Chloroplast redox signals: how photosynthesis controls its own genes. *Trends in Plant Science*, *8*(1), 33–41.

Plakas, S. M., & Dickey, R. W. (2010). Advances in monitoring and toxicity assessment of brevetoxins in molluscan shellfish. *Toxicon*, *56*(2), 137–149.

Poli, M. A., Musser, S. M., Dickey, R. W., Eilers, P. P., & Hall, S. (2000). Neurotoxic shellfish poisoning and brevetoxin metabolites: A case study from Florida. *Toxicon*, *38*(7), 981–993.

Popels, L. C., Cary, S. C., Hutchins, D. A., Forbes, R., Pustizzi, F., Gobler, C. J., & Coyne, K. J. (2003). The use of quantitative polymerase chain reaction for the detection and enumeration of the harmful alga *Aureococcus anophagefferens* in environmental samples along the United States East Coast. *Limnology and Oceanography: Methods*, *1*(1), 92–102.

Portune, K. J., Craig Cary, S., & Warner, M. E. (2010). Antioxidant enzyme response and reactive oxygen species production in marine Raphidophytes. *Journal of Phycology*, *46*(6), 1161–1171.

Purvis, A. C. (1997). Role of the alternative oxidase in limiting superoxide production by plant mitochondria. *Physiologia Plantarum*, *100*(1), 165–170.

Ralph, P. J., & Gademann, R. (2005). Rapid light curves: A powerful tool to assess photosynthetic activity. *Aquatic Botany*, *82*(3), 222–237.

Rao, L., Perez, D., & White, E. (1996). Lamin proteolysis facilitates nuclear events during apoptosis. *Journal of Cell Biology*, *135*(6), 1441–1455.

Reyna, N. E., Hardison, A. K., & Liu, Z. (2017). Influence of Major Storm Events on the Quantity and Composition of Particulate Organic Matter and the Phytoplankton Community in a Subtropical Estuary, Texas. *Frontiers in Marine Science*, *4*, Article 43.

Roth, P. B., Twiner, M. J., Mikulski, C. M., Barnhorst, A. B., & Doucette, G. J. (2008). Comparative analysis of two algicidal bacteria active against the red tide dinoflagellate *Karenia brevis*. *Harmful Algae*, *7*(5), 682–691.

Roth, P. B., Twiner, M. J., Wang, Z., Bottein Dechraoui, M.-Y., & Doucette, G. J. (2007). Fate and distribution of brevetoxin (PbTx) following lysis of *Karenia brevis*

by algicidal bacteria, including analysis of open A-ring derivatives. *Toxicon*, *50*(8), 1175–1191.

Sanders, B. M., Martin, L. S., Nakagawa, P. A., Hunter, D. A., Miller, S., & Ullrich, S. J. (1994). Specific cross-reactivity of antibodies raised against two major stress proteins, stress 70 and chaperonin 60, in diverse species. *Environmental Toxicology and Chemistry*, *13*(8), 1241–1249.

Schieber, M., & Chandel, N. S. (2014). ROS Function in Redox Signaling and Oxidative Stress. *Current Biology*, *24*(10), R453–R462.

Scholin, C. A., Anderson, D. M., & Sogin, M. L. (1993). Two distinct small-subunit ribosomal RNA genes in the north American toxic dinoflagellate *Alexandrium fundyense* (Dinophyceae). *Journal of Phycology*, *29*(2), 209–216.

Scholin, C. A., Herzog, M., Sogin, M., & Anderson, D. M. (1994). Identification of group- and strain-specific genetic markers for globally distributed *Alexandrium* (Dinophyceae). II. Sequence analysis of a fragment of the LSU rRNA gene. *Journal of Phycology*, *30*(6), 999–1011.

Segovia, M., & Berges, J. A. (2009). Inhibition of caspase-like activities prevents the appearance of reactive oxygen species and dark-induced apoptosis in the unicellular chlorophyte *dunaliella tertiolecta*. *Journal of Phycology*, *45*(5), 1116–1126.

Seth-Pasricha, M., Bidle, K. A., & Bidle, K. D. (2013). Specificity of archaeal caspase activity in the extreme halophile *Haloferax volcanii*. *Environmental Microbiology Reports*, *5*(2), 263–271.

Seth-Pasricha, M., Senn, S., Sanman, L. E., Bogyo, M., Nanda, V., Bidle, K. A., & Bidle, K. D. (2019). Catalytic linkage between caspase activity and proteostasis in Archaea. *Environmental Microbiology*, *21*(1), 286–298.

Severin, T., & Erdner, D. L. (2019). The phytoplankton taxon-dependent oil response and its microbiome: Correlation but not causation. *Frontiers in Microbiology*, *10*(MAR), 1–14.

Shen, A., Ma, Z., Jiang, K., & Li, D. (2016). Effects of temperature on growth, photophysiology, Rubisco gene expression in *Prorocentrum donghaiense* and *Karenia mikimotoi*. *Ocean Science Journal*, *51*(4), 581–589.

Sherr, E. B., Sherr, B. F., & Hartz, A. J. (2009). Microzooplankton grazing impact in the Western Arctic Ocean. *Deep Sea Research Part II: Topical Studies in Oceanography*, *56*(17), 1264–1273.

Shi, X., Zhang, H., & Lin, S. (2013). Tandem Repeats, High Copy Number and Remarkable Diel Expression Rhythm of Form II RuBisCO in *Prorocentrum donghaiense* (Dinophyceae). *PLoS ONE*, *8*(8), e71232.

Sieracki, M. E., Gobler, C. J., Cucci, T. L., Thier, E. C., Gilg, I. C., & Keller, M. D. (2004). Pico- and nanoplankton dynamics during bloom initiation of *Aureococcus* in a Long Island, NY bay. *Harmful Algae*, *3*(4), 459–470.

Sigaud-Kutner, T. C. S., Neto, A. M. P., Pinto, E., & Colepicolo, P. (2005). Diel activities of antioxidant enzymes, photosynthetic pigments and malondialdehyde content in stationary-phase cells of *Tetraselmis gracilis* (Prasinophyceae). *Aquatic Botany*, *82*(4), 239–249.

Smith, K. F., De Salas, M., Adamson, J., & Rhodes, L. L. (2014). Rapid and accurate identification by real-time PCR of biotoxin-producing dinoflagellates from the family *Gymnodiniaceae*. *Marine Drugs*, *12*(3), 1361–1376.

Speekmann, C. L., Hyatt, C. J., & Buskey, E. J. (2006). Effects of *Karenia brevis* diet on RNA:DNA ratios and egg production of *Acartia tonsa*. *Harmful Algae*, *5*(6), 693–704.

Steidinger. (1998). Bloom dynamics and physiology of *Gymnodinium breve* with emphasis on the Gulf of Mexico. *Physiological Ecology of Harmful Algal Blooms*, *41*, 133–153.

Stoecker, D. K., Thessen, A. E., & Gustafson, D. E. (2008). "Windows of opportunity" for dinoflagellate blooms: Reduced microzooplankton net growth coupled to eutrophication. *Harmful Algae*, *8*(1), 158–166.

Strom, S. L., & Fredrickson, K. A. (2008). Intense stratification leads to phytoplankton nutrient limitation and reduced microzooplankton grazing in the southeastern Bering Sea. *Deep Sea Research Part II: Topical Studies in Oceanography*, *55*(16–17), 1761–1774.

Strom, S. L., & Morello, T. A. (1998). Comparative growth rates and yields of ciliates and heterotrophic dinoflagellates. *Journal of Plankton Research*, *20*(3), 571–584.

Summons, R. E., Jahnke, L. L., Hope, J. M., & Logan, G. A. (1999). 2-Methylhopanoids as biomarkers for cyanobacterial oxygenic photosynthesis. *Nature*, *400*(6744), 554–557.

Suzuki, K., Tsuda, A., Kiyosawa, H., Takeda, S., Nishioka, J., Saino, T., … Wong, C. S. (2002). Grazing impact of microzooplankton on a diatom bloom in a mesocosm as estimated by pigment-specific dilution technique. *Journal of Experimental Marine Biology and Ecology*, *271*(1), 99–120.

Suzuki, N., Koussevitzky, S., Mittler, R., & Miller, G. (2012). ROS and redox signalling in the response of plants to abiotic stress. *Plant, Cell and Environment*, *35*(2), 259–270.

Suzuki, N., & Mittler, R. (2006). Reactive oxygen species and temperature stresses: A delicate balance between signaling and destruction. *Physiologia Plantarum*, *126*(1), 45–51.

Sykes, P. F., & Huntley, M. E. (1987). Acute physiological reactions of *Calanus pacificus* to selected dinoflagellates: direct observations. *Marine Biology*, *94*(1), 19–24.

Taroncher-Oldenburg, G., Kulis, D. M., & Anderson, D. M. (1997). Toxin variability during the cell cycle of the dinoflagellate *Alexandrium fundyense*. *Limnology and Oceanography*, *42*(5part2), 1178–1188.

Taylor-Brown, E., & Hurd, H. (2013). The first suicides: a legacy inherited by parasitic protozoans from prokaryote ancestors. *Parasites & Vectors*, *6*(1), 108.

Taylor, R. C., Cullen, S. P., & Martin, S. J. (2008). Apoptosis: controlled demolition at the cellular level. *Nature Reviews. Molecular Cell Biology*, *9*(3), 231–241.

Thamatrakoln, K., Korenovska, O., Niheu, A. K., & Bidle, K. D. (2012). Whole-genome expression analysis reveals a role for death-related genes in stress acclimation of the diatom *Thalassiosira pseudonana*. *Environmental Microbiology*, *14*(1), 67–81.

Tilney, C. L., Shankar, S., Hubbard, K. A., & Corcoran, A. A. (2019). Is *Karenia brevis* really a low-light-adapted species? *Harmful Algae*, *90*.

Toepel, J., Welsh, E., Summerfield, T. C., Pakrasi, H. B., & Sherman, L. A. (2008). Differential Transcriptional Analysis of the Cyanobacterium *Cyanothece sp.* Strain ATCC 51142 during Light-Dark and Continuous-Light Growth. *Journal of Bacteriology*, *190*(11), 3904–3913.

Triantaphylidès, C., Krischke, M., Hoeberichts, F. A., Ksas, B., Gresser, G., Havaux, M., … Mueller, M. J. (2008). Singlet Oxygen Is the Major Reactive Oxygen Species Involved in Photooxidative Damage to Plants. *Plant Physiology*, *148*(2), 960–968.

Turner, J. T. (2006). Harmful algae interactions with marine planktonic grazers. In *Ecology of harmful algae* (pp. 259–270). Berlin, Heidelberg: Springer.

Twiner, M. J. (2000). Possible physiological mechanisms for production of hydrogen peroxide by the ichthyotoxic flagellate *Heterosigma akashiwo*. *Journal of Plankton Research*, *22*(10), 1961–1975.

Uhl, L., & Dukan, S. (2016). Hydrogen Peroxide Induced Cell Death: The Major Defences Relative Roles and Consequences in E. coli. *PLOS ONE*, *11*(8), e0159706.

Van Creveld, S. G., Rosenwasser, S., Schatz, D., Koren, I., & Vardi, A. (2015). Early perturbation in mitochondria redox homeostasis in response to environmental stress predicts cell fate in diatoms. *The ISME Journal*, *9*(2), 385–395.

Van Dolah, F. M., & Leighfield, T. A. (1999). Diel phasing of the cell-cycle in the Florida red tide dinoflagellate, *Gymnodinium breve*. *Journal of Phycology*, *35*(6), 1404–1411.

Van Dolah, F. M., Leighfield, T. A., Kamykowski, D., & Kirkpatrick, G. J. (2008). Cell cycle behavior of laboratory and field populations of the Florida red tide dinoflagellate, *Karenia brevis*. *Continental Shelf Research*, *28*(1), 11–23.

Vandersea, M. W., Kibler, S. R., Holland, W. C., Tester, P. A., Schultz, T. F., Faust, M. A., … Wayne Litaker, R. (2012). Development of semi-quantitative PCR assays for the detection and enumeration of Gambierdiscus species (Gonyaulacales, Dinophyceae). *Journal of Phycology*, *48*(4), 902–915.

Vardi, A., Berman-Frank, I., Rozenberg, T., Hadas, O., Kaplan, A., & Levine, A. (1999). Programmed cell death of the dinoflagellate *Peridinium gatunense* is mediated by CO2 limitation and oxidative stress. *Current Biology*, *9*(18), 1061–1064.

Vardi, A., Bidle, K. D., Kwityn, C., Hirsh, D. J., Thompson, S. M., Callow, J. A., … Bowler, C. (2008). A Diatom Gene Regulating Nitric-Oxide Signaling and Susceptibility to Diatom-Derived Aldehydes. *Current Biology*, *18*(12), 895–899.

Vargo, G. A. (2009). A brief summary of the physiology and ecology of *Karenia brevis Davis* (G. Hansen and Moestrup comb. nov.) red tides on the West Florida Shelf and of hypotheses posed for their initiation, growth, maintenance, and termination. *Harmful Algae*, *8*(4), 573–584.

Vavilala, S. L., Gawde, K. K., Sinha, M., & D'Souza, J. S. (2015). Programmed cell death is induced by hydrogen peroxide but not by excessive ionic stress of sodium chloride in the unicellular green alga *Chlamydomonas reinhardtii*. *European Journal of Phycology*, *50*(4), 422–438.

Waggett, R., Hardison, D., & Tester, P. (2012). Toxicity and nutritional inadequacy of *Karenia brevis*: synergistic mechanisms disrupt top-down grazer control. *Marine Ecology Progress Series*, *444*, 15–30.

Walsh, B. M., & O'Neil, J. M. (2014). Zooplankton community composition and copepod grazing on the West Florida Shelf in relation to blooms of *Karenia brevis*. *Harmful Algae*, *38*(2014), 63–72.

Walsh, J. J., Jolliff, J. K., Darrow, B. P., Lenes, J. M., Milroy, S. P., Remsen, A., … Bontempi, P. S. (2006). Red tides in the Gulf of Mexico: Where, when, and why? *Journal of Geophysical Research*, *111*(C11), C11003.

Walsh, J. J., Weisberg, R. H., Lenes, J. M., Chen, F. R., Dieterle, D. A., Zheng, L., … Landsberg, J. H. (2009). Isotopic evidence for dead fish maintenance of Florida red tides, with implications for coastal fisheries over both source regions of the West Florida shelf and within downstream waters of the South Atlantic Bight. *Progress in Oceanography*, *80*(1–2), 51–73.

Xu, K., Jiang, H., Juneau, P., & Qiu, B. (2012). Comparative studies on the photosynthetic responses of three freshwater phytoplankton species to temperature and light regimes. *Journal of Applied Phycology*, *24*(5), 1113–1122.

Yamori, W., Makino, A., & Shikanai, T. (2016). A physiological role of cyclic electron transport around photosystem I in sustaining photosynthesis under fluctuating light in rice. *Scientific Reports*, *6*(1), 20147.

Yeung, P. K. K., Kong, K. F., Wong, F. T. Y., & Wong, J. T. Y. (1996). Sequence data for two large-subunit rRNA genes from an Asian strain of *Alexandrium catenella*. *Applied and Environmental Microbiology*, *62*(11), 4199–4201.

Yoon, H. S., Hackett, J. D., Ciniglia, C., Pinto, G., & Bhattacharya, D. (2004). A Molecular Timeline for the Origin of Photosynthetic Eukaryotes. *Molecular Biology and Evolution*, *21*(5), 809–818.

Yuan, J., Mi, T., Zhen, Y., & Yu, Z. (2012). Development of a rapid detection and quantification method of *Karenia mikimotoi* by real-time quantitative PCR. *Harmful Algae*, *17*, 83–91.

Yuasa, K., Shikata, T., Kuwahara, Y., & Nishiyama, Y. (2018). Adverse effects of strong light and nitrogen deficiency on cell viability, photosynthesis, and motility of the red-tide dinoflagellate *Karenia mikimotoi*. *Phycologia*, *57*(5), 525–533.

Zhou, L., Tan, Y., Huang, L., Huang, J., Liu, H., & Lian, X. (2011). Phytoplankton growth and microzooplankton grazing in the continental shelf area of northeastern South China Sea after Typhoon Fengshen. *Continental Shelf Research*, *31*(16), 1663–1671.

Zuppini, A., Andreoli, C., & Baldan, B. (2007). Heat Stress: an Inducer of Programmed Cell Death in *Chlorella saccharophila*. *Plant and Cell Physiology*, *48*(7), 1000–1009.

Zuppini, A., Gerotto, C., & Baldan, B. (2010). Programmed cell death and adaptation: Two different types of abiotic stress response in a unicellular chlorophyte. *Plant and Cell Physiology*, *51*(6), 884–895.

Appendix A

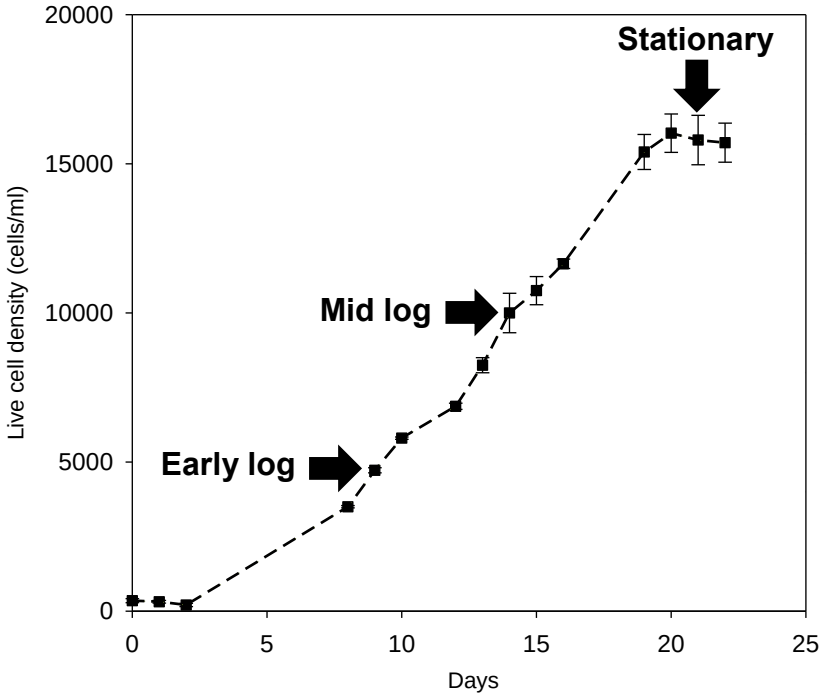

Figure A1: Cell densities of *K. brevis* cells from the "cell counts" flask under controlled environment. Black arrows indicate the day when H_2O_2 were added to early-log treatment (Day 9), mid-log treatment (Day 14) and stationary treatment cultures (Day 21). Data points show average values obtained from replicate measurement, and error bars show standard deviation of the replicates (n = 2).

Appendix B

Table B1: Osmotic stress. Percentages of cellular parameters in treatments and controls.

		ROS (%)		**Caspase-like activity (%)**		**SYTOX (%)**	
	Time (h)	Treatment	Control	Treatment	Control	Treatment	Control
35-30 psu	Time 0.5	25.15 ± 3.22	16.47 ± 2.25	28.27 ± 5.96	36.42 ± 7.43	2.79 ± 2.09	0 ± 0
	Time 6	28.96 ± 1.8	19.36 ± 3.04	30.19 ± 11.17	23.15 ± 3.44	7.75 ± 3.81	0.45 ± 0.55
35-25 psu	Time 0.5	82.58 ± 5.26	19.02 ± 5.25	59.68 ± 10.08	9.68 ± 2.52	36 ± 5.15	3.15 ± 1.35
	Time 6	57.31 ± 4.92	22.9 ± 1.98	53.19 ± 6.56	15.61 ± 6.09	37.07 ± 4.81	1.42 ± 0.86
35-20 psu	Time 0.5	94.19 ± 4.50	16.19 ± 5.04	82.64 ± 20.26	19.1 ± 4.12	84.65 ± 6.47	0.42 ± 0.51
	Time 6	77.83 ± 11.4	4.32 ± 2.15	94.74 ± 6.45	30.86 ± 5.27	85.24 ± 4.89	1.43 ± 0.56

Table B2: Cooling stress. Percentages of cellular parameters in treatments and controls.

		ROS (%)		Caspase-like activity (%)		SYTOX (%)	
	Time (h)	Treatment	Control	Treatment	Control	Treatment	Control
30-25 °C	Time 0.5	6.28 ± 1.93	11.68 ± 3.53	12.85 ± 6.21	62.83 ± 5.43	0.6 ± 0.46	2.86 ± 0.61
30-20 °C	Time 0.5	22.18 ± 3.67	18.92 ± 6.55	34.42 ± 3.17	31.86 ± 4.85	1.69 ± 0.68	1.03 ± 0.8
	Time 6	7.62 ± 1.86	6.59 ± 2.45	44.94 ± 5.19	43.66 ± 11.59	0.64 ± 0.79	1.44 ± 1.34
30-15 °C	Time 0.5	71.34 ± 2.17	10.13 ± 1.81	30.69 ± 5.53	36.78 ± 2.09	46.23 ± 7.12	2.28 ± 1.04
	Time 6	84.09 ± 3.42	6.29 ± 1.33	27.78 ± 7.61	52.22 ± 8.40	68.35 ± 7.87	2.82 ± 0.12

Table B3: Heat stress. Percentages of cellular parameters in treatments and controls.

		ROS (%)		**Caspase-like activity (%)**		**SYTOX (%)**	
	Time (h)	Treatment	Control	Treatment	Control	Treatment	Control
20-25 °C	Time 0.5	22.38 ± 5.55	9.58 ± 1.92	41 ± 1.98	40.03 ± 2.42	1.49 ± 0.87	1.15 ± 0.46
	Time 6	9.19 ± 2.6	12.68 ± 3.08	35.15 ± 5.47	38.79 ± 3.37	0.91 ± 0.71	0.6 ± 0.73
20-30 °C	Time 0.5	9.91 ± 2.12	4.53 ± 1.26	40.87 ± 4.91	39.33 ± 3.74	0.82 ± 0.48	0.39 ± 0.47
	Time 6	15.55 ± 1.82	6.47 ± 1.96	43.1 ± 4.54	36.38 ± 3.12	0.6 ± 0.49	1.11 ± 1.36
20-35 °C	Time 0.5	46.85 ± 11.13	22.21 ± 5.64	47.96 ± 2.67	39.76 ± 2.81	0.62 ± 0.76	0.31 ± 0.39
	Time 6	83.99 ± 7.46	9.17 ± 2.04	27.45 ± 5.43	41.76 ± 5.22	27.24 ± 4.31	0 ± 0

Appendix C

Spatiotemporal Genetic Structure of Regional-scale *Alexandrium catenella* Dinoflagellate Blooms explained by Extensive Dispersal and Environmental Selection

This work was completed as my master project in UT marine science department. In Summer 2016 I switched from the master's program to the PhD's program.

The paper below is reprinted from "Gao, Y., Sassenhagen, I., Richlen, M. L., Anderson, D. M., Martin, J. L., & Erdner, D. L. (2019). Spatiotemporal genetic structure of regional-scale *Alexandrium catenella* dinoflagellate blooms explained by extensive dispersal and environmental selection. **Harmful algae**, 86, 46-54", with permission from ELSEVIER. DOI: 10.1016/j.hal.2019.03.013

All the tables and figures are located at the end of this manuscript.

Abstract

Paralytic Shellfish Poisoning (PSP) caused by the dinoflagellate *Alexandrium catenella* is a well-known global syndrome that negatively impacts human health and fishery economies. Understanding the population dynamics and ecology of this species is thus important for identifying determinants of blooms and associated PSP toxicity. Given reports of extensive genetic heterogeneity in the toxicity and physiology of *Alexandrium* species, knowledge of genetic population structure in harmful algal species such as *A. catenella* can also facilitate the understanding of toxic bloom development and ecological

adaptation. In this study we employed microsatellite markers to analyze multiple *A. catenella* strains isolated from several sub-regions in the Gulf of Maine (GoM) during summer blooms, to gain insights into the sources and dynamics of this economically important phytoplankton species. At least three genetically distinct clusters of *A. catenella* were identified in the GoM. Each cluster contained representatives from different sub-regions, highlighting the extent of connectivity and dispersal throughout the region. This shared diversity could result from cyst beds created by previous coastal blooms, thereby preserving the overall diversity of the regional *A. catenella* population. Rapid spatiotemporal genetic differentiation of *A. catenella* populations was observed in local blooms, likely driven by natural selection through environmental conditions such as silicate and nitrate/nitrite concentrations, emphasizing the role of short-term water mass intrusions and biotic processes in determining the diversity and dynamics of marine phytoplankton populations. Given the wide-spread intraspecific diversity of *A. catenella* in GoM and potentially elsewhere, harmful algal blooms will likely persist in many regions despite global warming and changing environmental conditions in the future. Selection of different genetic lineages through variable hydrological conditions might impact toxin production and profiles of future blooms, challenging HAB control and prediction of PSP risk in the future.

Keywords

Alexandrium, harmful algal blooms, population structure, dispersal, environmental selection

1. Introduction

Paralytic Shellfish Poisoning (PSP) caused by the dinoflagellate *Alexandrium catenella* is a global issue that negatively impacts human health and fisheries (Hallegraeff, 1993; Van Dolah, 2007). The Gulf of Maine (GoM) is a continental shelf sea located in the northwest Atlantic where a large areas of shellfish resources are recurrently contaminated by PSP (Anderson et al., 2014a). As a consequence, the local commercial and recreational shellfishing industries regularly suffer from seafood safety issues, resulting in a loss of millions of dollars in some years. According to long-term monitoring data, *A. catenella* blooms in the western GoM usually start in late April, peak in June or mid-July with cell densities reaching or exceeding ten thousand cells per liter, and decline in late July (Li et al., 2014; Martin et al., 2014a). The life cycle of *A. catenella* includes an annual alternation between haploid vegetative cells that germinate in response to favorable conditions in early spring, and a resting stage (cyst) that is presumably formed in response to adverse environmental conditions in the field (Anderson et al., 1983; Anderson & Lindquist, 1985; Brosnahan et al., 2015). Previous physiological research on *A. catenella* in GoM revealed that strains from northern areas had higher toxin content and different toxin composition than strains from the south (Anderson et al., 1994; Maranda et al., 1985). Based on these differences in toxicity and other distinctions in bioluminescence and morphology, a northern and a southern cluster of *A. catenella* were proposed (Anderson et al. 1994). However, the dynamics of the population structure of *A. catenella* in GoM are still unclear, limiting our ecological understanding of the development and persistence of harmful algal blooms (HABs) in the region.

In recent years, many population genetics studies have observed spatiotemporal structure in a large variety of marine phytoplankton species (Alpermann et al., 2010; Casabianca et al., 2012; Godhe et al., 2016; Richlen et al., 2012), which have greatly challenged the idea that phytoplankton populations are panmictic. These observed spatial and/or temporal genetic differentiation of phytoplankton populations was attributed to three factors: (1) oceanographic connectivity: physical barriers such as circulation and benthic topography can determine dispersal pathways of planktonic cells, therefore determining the extent of gene flow between phytoplankton populations (Casabianca et al. 2012; Godhe et al. 2013; Sjöqvist et al. 2015); (2) Natural selection: environmental conditions can select for individuals with high fitness, resulting in adaptation of a population to the local environmental conditions and providing a competitive advantage of the native population over migrants (Blanquart et al., 2013; Sjöqvist et al., 2015); and (3) isolation by distance (IBD): gene flow and sexual recombination occur more frequently among geographically-close individuals, so distant populations may diverge due to limited gene flow (Hamilton, 2011).

Most previous studies about population genetics of marine HABs focused on spatial structure of phytoplankton populations across large spatial scales, and connectivity explains many instances of spatial differentiation of marine micro-algal populations (e.g. Nagai et al., 2009; Casabianca et al., 2012; Sjöqvist et al., 2015; Richlen et al., 2012). In addition to spatial structure, temporal differentiation has also been reported in several

phytoplankton groups. In diatom populations, temporal genetic structure was linked to silicate depletion (Godhe et al. 2016; Rynearson et al., 2006), possibly indicating local adaptation. In dinoflagellate populations, temporal genetic differentiation of *Gambierdiscus caribaeus* in the Greater Caribbean Region was likely affected by salinity and benthic coverage of the habitat (Sassenhagen et al., 2018). Temporal population structure has also been examined in the genus *Alexandrium*. Dia et al. (2014) monitored the temporal population differentiation of the dinoflagellate *Alexandrium minutum* in two estuaries in France and showed that interannual genetic differentiation was greater than intra-bloom differentiation. Temporal differentiation in blooms of the dinoflagellate *A. catenella* in salt ponds near GoM was observed to occur on short (< 1 month) time scales, potentially driven by different timing of excystment, parasitism and grazing (Richlen et al., 2012). During the *Alexandrium* bloom in GoM in the year 2005, temporal succession of two genetically distinct sub-populations was observed on similar time scales (Erdner et al., 2011).

In this study, we investigated the genetic dynamics of *Alexandrium catenella* blooms in the GoM by sampling over three summer months in 2007, from several sub-regions, providing good spatial coverage of the blooms. The main objectives of this investigation were to: (1) examine temporal changes in genetic composition during local *A. catenella* blooms in the GoM; (2) determine the regional genetic structure and sources of *A. catenella* populations across the GoM; and (3) test associations between environmental conditions and genetic differentiation. Based on previous research we hypothesized that barriers to panmixia (e.g.

hydrography) may weaken gene flow between northern and southern regions of the GoM and facilitate the formation of spatially-differentiated *A. catenella* sub-populations. Natural selection of adapted genotypes may cause short-term temporal genetic differentiation during local blooms in the GoM. By using microsatellite markers on *A. catenella* strains we sought to reveal the sources and dynamics of this economically important phytoplankton species in the GoM, providing insights for future bloom sustainability and toxicity under global warming and changing environmental conditions.

2. Method

2.1 Study sites

Bloom sampling focused on three sub-regions within the GoM area (Figure 1): Georges Bank (GB), Bay of Fundy (BoF) and Nantucket Shoal (NS). GB is characterized by a central bank, which is 60 meters deep and influenced by a strong clockwise gyre that retains water as long as 90 days (Brink et al., 2003). The BoF is characterized by extensive local cyst beds, a retentive hydrography (e.g. gyre), and regular nutrient inflow from tidal water masses (Anderson et al., 2014b; Martin et al., 2014a). NS is a submerged, shallow, sand and gravel ridge that acts as a topographic barrier to deep flow between the GoM and the New England continental shelf (Limeburner & Beardsley, 1982). The Main Coastal Current (MCC; Pettigrew et al., 2005) and the Gulf of Maine Coastal Plume (Keafer et al., 2005) are the dominant currents in the GoM, and they flow from the BoF in the Northeast to southern parts of the Gulf (Figure 1).

2.2 Sampling

In May 2007, an *A. catenella* bloom covered most parts of GB with cell concentrations up to 12,000 cells L^{-1}, and then declined in June with advection to NS (McGillicuddy et al., 2014). In contrast, the inshore bloom along the BoF did not develop until June, after the GB bloom had traveled to NS (Martin et al., 2014b; McGillicuddy et al., 2014).

The *A. catenella* blooms in the surface water (0-1 m depth) were sampled at several stations in GB, BoF and NS during cruises EN435 and 437 in 2007 (Figure 1). Sampling dates and number of strains per sample were shown in Table 1. Eleven samples at GB (GBA-GBK), eight samples in BoF (BFA-BFH), and three samples in NS (NSA-NSC) were collected during the bloom season. GB samples were taken around the shallow central bank from late May to early July. Strains from GBB&GBH and GBD&GBK were obtained from the exactly same locations (Figure 1). Among BoF samples, BFC and BFF were taken during cruises, while other samples were taken from field work by Jennifer Martin. BFA, BFD and BFH were sampled from Passamaquoddy Bay, while BFG was collected near the Wolves Islands, and BFB and BFE were pooled samples from Passamaquoddy Bay and the Wolves Islands. Single *A. catenella* cells were isolated by micropipette and cultured in 96-well plates as in Erdner et al., 2011. A total of 761 clonal strains were established for this study, representing 18-40 clonal strains from each sample.

2.3 DNA extraction and microsatellite genotyping

In order to extract DNA, each clonal culture was harvested when the cell density exceeded 100 cells per well. DNA was extracted from 200 µL of each culture using the Generation Capture Column Kit (Qiagen, Valencia, CA) following the manufacturer's instructions. From the thirteen microsatellite loci found by Nagai et al. (2004), the four loci Atama 15, Atama 23, Atama 27 and Atama 39 were selected for this study based on amplification success and the observed number of alleles. These same microsatellite markers have previously been employed to examine the genetic diversity and differentiation of *A. catenella* populations sampled in 2005 to 2007 from the GoM and Nauset Estuary on Cape Cod, MA, USA (Erdner et al., 2011; Richlen et al., 2012). PCR reactions contained ~5 ng of template DNA, 0.2mmol L^{-1} of each dNTP, 0.5 µmol L^{-1} of each designed primer pair, with one primer labeled with 6FAM, NED, PET, or VIC, 1x PCR buffer (10mmol L^{-1} Tris-HCl, pH 8.3, 500 mmol L^{-1} KCl, 15 mmol L^{-1} $MgCl_2$, 0.01% w/v gelatin), and 0.25 U of Ampli Taq Gold (Applied Biosystems, Foster City, CA), in 10 µL total volume. The PCR cycling conditions were as follows: 10 min at 94 °C, 10 cycles of 30 sec at 94°C, 30 sec at 60°C and 1 min at 72°C, and then 28 cycles of 30 sec at 94°C, 30 sec at the primer-specific annealing temperature (Nagai et al., 2004), and 1 min at 72°C, and a final elongation for 5 min at 72°C. In order to determine if amplification was successful, PCR products were run on a 1% TAE agarose gel. For allele size analysis, PCR products were diluted 3-5x with nuclease-free water, and 1 µL of diluted product was mixed with 0.25 µL 500 LIZ Size Standard and 8.75 µL Hi-Di Formamide, and then analyzed using an ABI 3730xi DNA Analyzer (Applied Biosystems, Foster City, CA). Allele sizes were determined using the

program FPMiner (2005; Bioinfor-Soft LLC, Beaverton, OR). Microsatellite data is available from the Mendeley Data repository, doi: 10.17632/nhwkm3nczj.1.

2.4 Microsatellite Data Analysis

2.4.1 Genetic diversity

Allele diversity (Nei 1973) was calculated based on all individuals as well as only unique genotypes in each genetic sub-cluster using POPGENE v. 1.32 (Yeh et al., 1997). Clonal diversity was defined as the ratio of the number of unique four-locus genotypes (G) to the total number of genotypes analyzed (N) with a threshold of one base to distinguish clones in Arlequin v. 3.5.1.2 (Excoffier et al., 2005). This parameter was also calculated after adjusting the sample size of each genetic sub-cluster to N=59 by using the R function "sample". Multilocus linkage disequilibrium was assessed by the Monte Carlo method in LIAN v. 3.5 with 10,000 resamplings (Haubold & Hudson, 2000), while linkage disequilibrium between pairs of loci was determined in GenePop v. 4.5 with Markov Chain parameters of 1000 dememorisation steps and 100 batches with 1000 iterations per batch (Rousset et al., 2008).

2.4.2 Inference of population structure

To identify the genetic clusters in the GoM dataset, PCAGEN was applied to run a principal components analysis (PCA) based on allele frequencies, with 10000 randomisations used to determine the significance of the inertia of each axis (Goudet, 1999).

Genetic composition and structuring were examined using Bayesian cluster analysis implemented in STRUCTURE 2.3.2 (Pritchard et al., 2000). The number of potential clusters (K) was first assessed using 10 runs performed at every K value from 1 to 10, each with a burn-in period of 100,000 steps and 200,000 Markov Chain Monte Carlo repetitions. Simulations were conducted using the admixture model with the locprior option, assuming correlated allele frequencies among populations. The calculation of the most likely value of K was performed in Structure Harvester Web v0.6.94 (Earl, 2012) by the method of ad hoc statistic $\triangle$ K (Evanno et al., 2005).

The partitioning of genetic variance within and among genetic clusters was assessed using the analysis of molecular variance (AMOVA) implemented in the software GenoDive 2.0b27 (Meirmans & Van Tienderen, 2004).

Genetic clustering of *A. catenella* populations in the GoM was further examined by performing pairwise comparisons. Wright's F_{ST} (Wright, 1949) was used to identify fixation of genetic differences, calculated in Arlequin v. 3.5.1.2 with 10,000 permutations to test for significance. The Fisher's exact test (Raymond, 1995) was used to assess differences in allele frequencies between clusters, performed in GenePop v. 4.5 using Markov Chain parameters of 1000 dememorisation steps and 100 batches with 1000 iterations per batch (Rousset et al., 2008). All p-values were Bonferroni corrected to account for multiple comparisons.

2.5 Environmental effects

Environmental data were obtained from http://grampus.umeoce.maine.edu/gomtox/gomtox.htm. We included nitrate and nitrite concentrations (µM), temperature (°C), salinity, water density anomaly measured as δT (kg m^{-3}), ammonium (µM), chlorophyll a (µg L^{-1}), phaeopigments (µg L^{-1}), silicate (µM) and phosphate (µM) from surface water of a subset of the same sampling stations as used for isolation of algal strains (GBA, GBB, GBC, GBD, GBE, GBG, GBH, GBJ, GBK and BFC) (Table 2). Environmental data were not available from the other stations, and therefore could not be included in this analysis.

To understand the impact of environmental conditions on the population structure of *A. catenella*, the relationship between genetic structure and environmental variables was tested using a distance based redundancy analysis (dbRDA) (Legendre & Andersson, 1999). Distances between samples based on the genetic data were calculated with a principal coordinate analysis (PCoA) using the R package adegenet 1.0.1 (Jombart, 2008). The relationship between the coordinates of samples from the PCoA and the environmental variables was determined by dbRDA using the R package vegan 2.4-1 (Oksanen et al., 2016).

3. Results

3.1 Genetic differentiation and population dynamics

In this study, 761 isolates were genotyped using four different microsatellite loci. Strains that had any null alleles were removed from the data set, resulting in a final set of 667 individuals. All four loci were polymorphic in all samples. There were 158 unique genotypes in the entire data set resulting in an overall clonal diversity of 0.23. Multilocus linkage disequilibrium was not detected ($I_A{}^S$=0.0069, p=0.179), nor was linkage disequilibrium between pairs of loci.

The *A. catenella* populations displayed more rapid and complicated differentiation over the course of the 2007 blooms compared with the temporal succession from early to late sub-populations as observed in the 2005 bloom across the GoM (Erdner et al., 2011). To identify genetic structure of *A. catenella* populations in the GoM, PCA implemented in the program PCAGEN was performed (Figure 2). The first two axes of the PCA were both significant and explained 38% and 30% of the total variation in F_{ST}, respectively. Three clusters of samples were identified: (1) GBB, GBF, GBG, GBH, GBI, GBK, BFA, BFE, NSA, NSB and NSC (orange samples in Figure 2); (2) GBC, BFC, BFD and BFF (blue samples in Figure 2); (3) BFB, GBJ, GBD and GBE (yellow samples in Figure 2). However, GBA, BFG and BFH (black samples in Figure 2) were in a transitional location between two of the clusters. In order to further examine the genetic differentiation among these three samples, the clustering pattern was investigated using an AMOVA. When GBA was added to Cluster (1) and BFH&BFG were added to Cluster (2), differentiation among

clusters was significant (Rct=0.022, p=0.008), but not significant within each cluster (Rsc=0.009, p=0.122). Other grouping patterns were also tested but were less supported by AMOVA based on distribution of within-cluster variation and among-cluster variation (data not shown). The PCA and AMOVA analyses indicated differentiation of the GoM dataset into three genetic clusters based on their genetic similarity, and they were re-named by the location of the majority of samples: (1) **Southern Cluster**: GBA, GBB, GBF, GBG, GBH, GBI, GBK, BFA, BFE, NSA, NSB and NSC; (2) **Northern Cluster:** GBC, BFC, BFD, BFF, BFG and BFH; (3) **Mixed Cluster:** GBD, GBE, GBJ and BFB. These genetic clusters were not entirely grouped according to geography, but instead comprised samples from different sub-regions in the GoM.

Bayesian analyses implemented in the program STRUCTURE were performed to examine the genetic composition and the relationships of samples (Figure 3). A K value of three was identified as the most likely number of "ancestral" populations in the GoM dataset using the Evanno method. The result of the STRUCTURE bar plot from "K=3" was similar to the "three-cluster" pattern described above, i.e. samples with similar proportional ancestry membership corresponded to the groupings identified by PCA and AMOVA. Subtle population structure was apparent within clusters. BFC's unique genetic composition in STRUCTURE analysis was reflected in its divergence in the PCA plot. The transitional locations of BFG and BFH in PCA analysis were also shown in STRUCTURE with mixed ancestral populations.

Pairwise F_{ST} values were calculated between the Northern, Southern and Mixed Clusters. All pairwise F_{ST} values between the genetic clusters were significant and ranged from 0.051 to 0.088 (Table 3). Additionally, the degree of differentiation based on Fisher's exact test was highly significant between these clusters. Allele frequencies from each genetic cluster were compared in detail. All loci in Southern and Northern Clusters had private alleles, whereas none were observed the Mixed Cluster. For example, of the 21 alleles detected at locus Atama15 in GoM, 8 alleles were found only in Southern Cluster while another 4 were found only in Northern Cluster. In order to understand the sources of the observed genetic differentiation, F_{ST} values based on each locus were calculated (data not shown). The divergence between Southern and Northern Cluster was driven by locus Atama27, as the differentiation was not significant based on other microsatellites loci. Specifically, allele size 162 (87%) was most common in Southern Cluster while allele sizes 162 (56%) and 160 (38%) dominated in Northern Cluster. All loci except Atama 39 were the driving force to differentiate Northern and Mixed Cluster, while only Atama 15 and Atama23 contributed significantly to the genetic differentiation between Southern and Mixed Cluster.

Within sub-regions of the GoM, significant changes in genetic composition were observed during local blooms. GB samples contained representatives from all of the three genetic clusters defined above: (1) GB-Southern: GBA, GBB, GBF, GBG, GBH, GBI and GBK; (2) GB-Mixed: GBD, GBE and GBJ; and (3) GB-Northern: GBC. The pairwise F_{ST} analysis was repeated for the sub-clusters in GB to clarify local population structure. The

results confirmed the significant differentiation of this local bloom into the three distinct sub-clusters, with F_{ST} values ranging from 0.058 to 0.134 (data not shown). To gain insights into temporal structure of the GB bloom, **early** (5/26-5/30: GBA, GBB, GBC, GBD and GBE) and **late samples** (6/16-7/3: GBF, GBG, GBH, GBI, GBJ and GBK) were investigated separately. During the early bloom period, all three genetically distinct sub-clusters described above were represented: (1) GB-Southern: GBA and GBB; (2) GB-Northern: GBC; (3) GB-Mixed: GBD and GBE. Pairwise F_{ST} comparisons among sub-clusters that included only samples from the early bloom confirmed patchy distribution of spatially differentiated clusters over the bank during this period, with F_{ST} values ranging from 0.047 to 0.137. Twenty days later, during the late bloom period, a more homogenous distribution of *A. catenella* was observed, as all samples were identified as GB-Southern except GBJ (GB-Mixed).

BoF samples also contained all three genetic clusters based on the results of PCA and AMOVA analyses of the entire data set: (1) BF-Southern: BFA and BFE; (2) BF-Mixed: BFB; and (3) BF-Northern: BFC, BFD, BFF, BFG and BFH. The pairwise F_{ST} analysis was repeated for the BoF dataset, and indicated significant differentiation of these three sub-clusters, with F_{ST} values ranging from 0.029 to 0.058.

The genetic diversity of different sub-clusters varied, however (Table 4). The Southern sub-clusters from each sub-region exhibited the lowest Ht: GB (Ht=0.49) and BoF (Ht=0.47). However, the lowest values of Ht (unique) in the respective sub-regions were

found in GB-Northern and BoF-Mixed. When strain numbers were equalized to 59, clonal diversity was higher in GB-Mixed (0.63), and distinctly lower in GB-Southern (0.46) among all sub-regions.

3.2 Environmental Correlation

Nine environmental factors were collected from ten samples in the GoM. Some samples stood out due to relatively high nutrient concentrations: GBC with 1.47 µM of nitrate and nitrite; GBD with relatively high silicate concentrations (10.53 µM); and BFC with 6.63 µM of silicate and 10.17 µM of nitrate and nitrite (Table 2).

The impact of variable environmental conditions on the population genetic structure of *A. catenella* populations was assessed using a distance-based redundancy analysis (dbRDA). Among nine environmental variables, only silicate (P=0.0068), and nitrate and nitrite (P=0.0007) concentrations emerged as factors that were significantly associated with the genetic structure (Figure 4). Silicate concentration distinguished GBD and GBE (Mixed Cluster) from the other samples, while nitrate and nitrite concentration primarily drove the divergence of GBC and BFC (Northern Cluster), although the silicate concentration in BFC was also comparatively high.

4. Discussion

This study investigated regional population genetic structure of *A. catenella* blooms distributed throughout the GoM. Spatiotemporal genetic differentiation of *A. catenella*

populations was analyzed to describe the dispersal of *A. catenella* cells in the GoM as well as the influence of environmental conditions on their population structure. At least three genetically distinct clusters of *A. catenella* were identified in the GoM based on PCA analysis, STRUCTURE plots, fixation indices of genetic differentiation, and AMOVA. Significant short-term temporal and spatial differentiation was observed within local blooms, and linked to environmental conditions. Across the region as whole, representatives of the three genetic clusters were detected at all locations, indicating significant gene flow that could arise from hydrographic connectivity and the presence of resting (cyst) stages.

Circulation around GB is characterized by a strong gyre that is expected to homogenize *A. catenella* bloom populations, however, small-scale spatial differentiation into several sub-clusters was observed throughout the bloom on this bank. The early bloom period was characterized by three spatial sub-clusters, while the late bloom period was mostly characterized by one homogeneous population. This spatiotemporal variation in population structure at GB may be influenced by many factors, among which nitrate, nitrite and silicate concentrations may play a key role (Figure 4). During most of the bloom season in GB, abundant and stable supplies of ammonium and phosphate as well as low supply of nitrite and nitrate were found all over the bank (McGillicuddy et al. 2014; Townsend et al. 2014), which coincided with the presence of GB-Southern Cluster. Hence, the *A. catenella* cells from GB-Southern Cluster were likely utilizing ammonium instead of nitrite or nitrate as primary nitrogen source. However, GB-Northern Cluster, located at the Northeast Peak of

GB, coincided with significantly higher nitrite and nitrate concentrations, which may have been derived from an inflow of nitrate and nitrite-rich deeper water masses, i.e. Warm Slope Water, onto the Bank along the Northern Flank and Northeast Peak (Hu et al., 2008). Since laboratory experiments have shown differential preference of *A. tamarense* strains for different nitrogen sources (Leong et al., 2004), high nitrite and nitrate concentrations may select for distinct *Alexandrium* strains, facilitating the prevalence of the selected alleles. Occasional increases in silicate concentration on GB may also indirectly select GB-Mixed genotypes, some of which were present at the beginning of the *A. catenella* bloom in early summer, co-existing and likely competing with the annual spring diatom bloom (Townsend et al., 2014). This distribution pattern of silicate may result from regeneration of silicate from diatom frustules produced in spring bloom (Gettings et al., 2014). Short-term variations in nutrient concentrations may thus have rapidly selected for distinct genotypes, which were present before in low concentrations, and disrupted the otherwise homogenous population structure at GB. Many previous studies have described the effect of natural selection on the change of genetic structure within short periods (Rynearson et al., 2006; Godhe et al., 2016; Sassenhagen et al., 2018). For example, changes in environmental conditions such as salinity could rapidly select favorable genotypes and therefore drive genetic differentiation of *Gambierdiscus caribaeus* in the Greater Caribbean Region (Sassenhagen et al., 2018). Succession of genetically distinct populations of the diatom *Skeletonema marinoi* was observed even within fifteen days after a decline in silicate concentrations in the Baltic Sea (Godhe et al., 2016).

NS samples were not genetically different from the dominant cluster on GB (GB-Southern), thus strong algal dispersal and gene flow strengthened by the Gulf of Maine Coastal Plume (Keafer et al., 2005) or other currents might occur between these two sub-regions. Stable genetic composition of the *A. catenella* population in NS during the sampling period may reflect overall stable local environmental conditions. However, since no information about the NS cyst bed and transport through sub-subface layers are available, the sources of NS populations still need to be explored.

The BoF is considered to retain phytoplankton cells through the Minas Basin cyclonic gyre (Aretxabaleta et al., 2009; Townsend et al., 2014) and an extensive cyst seedbed (Anderson et al., 2014b; Martin et al., 2014a), potentially restricting gene flow yet preserving high genetic diversity of algal species (Sundqvist et al., 2018). Our results showed significant temporal genetic differentiation in the BoF among samples collected at roughly the same location. This pattern may result from induction of sexual reproduction by unfavorable conditions. In *Alexandrium*, environmentally induced encystment could strengthen the effects of natural selection on dominant genotypes by removing lineages that are less successful under the prevailing conditions. At the same time, some genotypes will be favored and accelerate vegetative growth. This characteristic would facilitate the domination of the population by a few successful lineages, effectively reducing gene flow between sub-clusters (Erdner et al., 2011). The turnover rates of genetically distinct sub-clusters were as short as seven days in the BoF. Such rapid changes in population structure may facilitate the persistence of phytoplankton populations in variable marine

environments (Rynearson & Armbrust, 2005). Temporal differentiation of phytoplankton populations has been observed in several different microalgal species from many locations around the world (Godhe et al. 2016; Richlen et al. 2012; Rynearson & Armbrust, 2005). In particular, rapid (~one week) temporal differentiation in populations of the dinoflagellate *A. catenella* was also observed in Cape Cod MA (USA) salt pond systems, which may have been facilitated by early induction of sexuality and different timing of germination that preserved the genetic diversity of local populations (Richlen et al., 2012).

Environmental data were unfortunately not available from most samples from BoF for correlation analysis with the observed population structure. The only sample with available environmental data (BFC) was characterized by much higher nitrate and nitrite conditions – as was GBC – which might have selected for comparatively similar genotypes in both locations. Thus, variable nutrient concentrations might have induced the observed rapid temporal genetic differentiation of *A. catenella* populations in the BoF throughout the sampling period, which could have been facilitated by local cyst beds with high genotype diversity. In order to test this hypothesis, further research should be directed to investigating the genetic diversity of the resting cysts in the BoF.

Although GB and the BoF are located at the southern and northeastern regions of the GoM respectively, at least 400 km apart from each other, several samples from both sites were very similar to each other genetically and belonged to the same clusters, which may indicate algal dispersal across the region. Studies of the population genetic structure of the

dinoflagellate *Margalefidinium polykrikoides* across the Sea of Japan found evidence for strong dispersal and gene flow over a distance of more than 600 km, highlighting the important role of Tsushima Warm Current on the connectivity of algal populations (Nagai et al., 2009). The BoF is located upstream of the MCC, the prevailing current that flows from Northeast to southern parts of the Gulf, and the bloom in BoF is supported by an extensive local cyst bed and a retentive gyre at the mouth of the Bay. The gyre is leaky, however (Aretxabaleta et al., 2009), so there is potential for dispersal from this northern area to affect the initiation and genetic structure of distant GB blooms, for example through the transport of vegetative cells from BoF to GB during the bloom.

However, the bloom on GB was extensive in May 2007 when there was near absence of *A. catenella* in the coastal waters of the GoM including BoF (McGillicuddy et al., 2014). Furthermore, during the bloom season of that year no evidence of *A. catenella* cells was found in surface waters between Casco Bay and Cape Cod, which is the main circulation pathway connecting BoF and GB-NS (McGillicuddy et al., 2014). Additionally, Li et al. (2014) studied coastal ocean connectivity in the GoM using surface numerical particle tracking and found that the circulation significantly retained particles within the BoF in 2007. As the gyre-like circulation in the BoF may serve as a barrier reducing surface connectivity between BoF and south-western parts of the GoM in 2007, surface cells from the BoF may not be the source of cells blooming on GB. However, the transport of cells through sub-surface layers between the BoF and GB cannot be excluded due to a lack of information about this process.

Other potential explanations for observed patterns of genetic connectivity could be the formation of cyst beds on GB or inshore areas including BoF and mid-coast Maine (Anderson et al., 2014b) that contained a mix of resting stages from different genetic clusters. During summer 2005, the GoM experienced the largest *A. catenella* bloom in the preceding three decades, spanning over 700 km of coastline. In that year, temporal succession of different inshore *A. catenella* sub-populations was observed during the bloom (Erdner et al., 2011). These differentiated blooms could have resulted in the formation of cysts with high genotype diversity, allowing rapid changes in population structure through natural selection of germinating cells. Although the bloom in 2006 was smaller than in other years, numerical simulations showed a significant number of particles traveling from BoF to the western GoM that year (Li et al., 2014), which may have further enhanced genetic diversity in the downstream cyst beds. Similarly, low to moderate algal dispersal via the MCC across the GoM over many years might have contributed to mixed cysts beds throughout the region.

Previous studies have found significant numbers of *A. catenella* cysts in benthic nepheloid layers (BNLs) throughout the GoM, representing a deep interconnection between BoF, MCC and south-central regions of the gulf (Pilskaln et al., 2014). Resuspended cysts may therefore serve as bloom inoculum on GB. Although cyst concentrations in the sediments of GB were roughly two orders of magnitude smaller than in the coastal GoM (Anderson et al., 2014b; McGillicuddy et al., 2014), local germination might still contribute at least

partially to the bloom on GB. Furthermore, even low cyst concentrations might be sufficient for inoculation of a bloom due to rapid exponential growth of microalgae under favorable environmental conditions. McGillicuddy et al. (2014) also hypothesized that cysts could be transported to the bank from the adjacent deep basins by tidal pumping. Our results suggest significant dispersal and gene flow throughout the GoM, resulting in the absence of endemic populations. Meanwhile, the results described herein also highlight the need for a comprehensive cyst bed investigation including cyst abundance, genetic diversity and transport pathway across the GoM.

5. Conclusions

At least three genetically distinct clusters of *A. catenella* were identified in the GoM. Each cluster contains representatives from different sub-regions, highlighting the extent of connectivity and dispersal throughout the GoM. This shared diversity could result from cyst beds containing a mix of resting stages from different genetic clusters. The cyst beds would preserve the overall diversity of the regional *A. catenella* population and allow selection of physiologically and phenotypically different genotypes based on local conditions. Rapid temporal and spatial genetic differentiation of *A. catenella* populations, as observed in local blooms, was likely associated with natural selection through environmental conditions such as silicate and nitrate/nitrite concentrations, emphasizing an important role of the changing nutrient environment in determining the diversity and dynamics of marine phytoplankton populations. This observed short-term genetic differentiation may be indicative of patchiness of different water masses and biotic

processes during the development of the bloom. Given the wide-spread intraspecific diversity of *A. catenella* in the GoM and potentially elsewhere, blooms of this species will likely persist in many regions despite global warming and changing environmental conditions in the future. Furthermore, selection of different genetic lineages through variable environmental conditions might impact toxin production and profiles of future blooms, challenging HAB control and prediction of PSP risk with changeable toxicity effect and persistent bloom dynamics.

6. Acknowledgement

We thank David Townsend for collection and provision of environmental data of sampling stations, and Bruce Keafer, Kerry Norton and Dave Kulis for their hard work in obtaining the samples used in this study. We also gratefully acknowledge the work of captains and crews of the R/V Endeavor. This study was supported by National Science Foundation [grant numbers OCE-0430724, OCE-0850421, OCE-0911031, OCE-1314642, OCE1840381] and National Institutes of Health [grant numbers 1P50-ES012742-01, 1P50-ES021923-01, and 1P01-ES028938-01] through the Woods Hole Center for Oceans and Human Health. Funding was also provided by NOAA Grant [NA06NOS4780245, NA11NOS4780061 and NA15NOS4780181]. This is contribution *** from the US ECOHAB program.

Author Contributions

DLE, MLR, and DMA conceived and designed the work; YG, IS, DLE, MLR, and JLM acquired, analyzed, and/or interpreted the data; YG and IS drafted the work; and all authors provided critical revision for important intellectual content.

References

Alpermann, T.J., Tillmann, U., Beszteri, B., Cembella, A.D., John, U., 2010. Phenotypic variation and genotypic diversity in a planktonic population of the toxigenic marine dinoflagellate *Alexandrium Tamarense* (DINOPHYCEAE)1. J. Phycol. 46 (1), 18–32.

Anderson, D.M., Lindquist, N.L., 1985. Time-course measurements of phosphorus depletion and cyst formation in the dinoflagellate *Gonyaulax tamarensis* Lebour. J. Exp. Mar. Biol. Ecol. 86 (1), 1–13.

Anderson, D.M., Chisholm, S.W., Watras, C.J., 1983. Importance of life cycle events in the population dynamics of *Gonyaulax tamarensis*. Mar. Biol. 76 (2), 179–189.

Anderson, D.M., Kulis, D.M., Doucette, G.J., Gallagher, J.C., Balech, E., 1994. Biogeography of toxic dinoflagellates in the genus *Alexandrium* from the northeastern United States and Canada. Mar. Biol. 120 (3), 467–478.

Anderson, D.M., Couture, D.A., Kleindinst, J.L., Keafer, B.A., McGillicuddy Jr., D.J., Martin, J.L., et al., 2014a. Understanding interannual, decadal level variability in paralytic shellfish poisoning toxicity in the Gulf of Maine: the HAB Index. Deep. Sea Res. Part II Top. Stud. Oceanogr. 103, 264–276.

Anderson, D.M., Keafer, B.A., Kleindinst, J.L., McGillicuddy, D.J., Martin, J.L., Norton, K., et al., 2014b. *Alexandrium fundyense* cysts in the Gulf of Maine: long-term time series of abundance and distribution, and linkages to past and future blooms. Deep. Sea Res. Part II Top. Stud. Oceanogr. 103, 6–26.

Aretxabaleta, A.L., McGillicuddy, D.J., Smith, K.W., Manning, J.P., Lynch, D.R., 2009. Model simulations of the bay of fundy gyre: 2. Hindcasts for 2005-2007 reveal interannual variability in retentiveness. J. Geophys. Res. Oceans 114 (9), 1–15.

Blanquart, F., Kaltz, O., Nuismer, S.L., Gandon, S., 2013. A practical guide to measuring local adaptation. Ecol. Lett. 16 (9), 1195–1205.

Brink, K.H., Limeburner, R., Beardsley, R.C., 2003. Properties of flow and pressure over Georges Bank as observed with near-surface drifters. J. Geophys. Res. 108 (C11), 8001.

Brosnahan, M.L., Velo-Suárez, L., Ralston, D.K., Fox, S.E., Sehein, T.R., Shalapyonok, A., et al., 2015. Rapid growth and concerted sexual transitions by a bloom of the harmful dinoflagellate *Alexandrium fundyense* (Dinophyceae). Limnol. Oceanogr. 60 (6), 2059–2078.

Casabianca, S., Penna, A., Pecchioli, E., Jordi, A., Basterretxea, G., Vernesi, C., 2012. Population genetic structure and connectivity of the harmful dinoflagellate *Alexandrium minutum* in the Mediterranean Sea. Proc. R. Soc. B Biol. Sci. 279 (1726), 129–138.

Dia, A., Guillou, L., Mauger, S., Bigeard, E., Marie, D., Valero, M., Destombe, C., 2014. Spatiotemporal changes in the genetic diversity of harmful algal blooms caused by the toxic dinoflagellate *Alexandrium minutum*. Mol. Ecol. 23 (3), 549–560.

Earl, D.A., 2012. STRUCTURE HARVESTER: a website and program for visualizing STRUCTURE output and implementing the Evanno method. Conserv. Genet. Resour. 4 (2), 359–361.

Erdner, D.L., Richlen, M., McCauley, L.A.R., Anderson, D.M., 2011. Diversity and dynamics of a widespread bloom of the toxic dinoflagellate *Alexandrium fundyense*. PLoS One 6 (7), e22965.

Evanno, G., Regnaut, S., Goudet, J., 2005. Detecting the number of clusters of individuals using the software structure: a simulation study. Mol. Ecol. 14 (8), 2611–2620.

Excoffier, L., Laval, G., Schneider, S., 2005. Arlequin (version 3. 0): An Integrated Software Package for Population Genetics Data Analysis. pp. 47–50.

Gettings, R.M., Townsend, D.W., Thomas, M.A., Karp-Boss, L., 2014. Dynamics of late spring and summer phytoplankton communities on Georges Bank, with emphasis on diatoms, *Alexandrium spp.*, and other dinoflagellates. Deep Sea Res. Part II Top. Stud. Oceanogr. 103, 120–138.

Godhe, A., Egardt, J., Kleinhans, D., Sundqvist, L., Hordoir, R., Jonsson, P.R., 2013. Seascape analysis reveals regional gene flow patterns among populations of a marine planktonic diatom. Proceedings of the Royal Society B: Biological Sciences 280 (1773), 20131599.

Godhe, A., Sjöqvist, C., Sildever, S., Sefbom, J., Harðardóttir, S., Bertos-Fortis, M., et al., 2016. Physical barriers and environmental gradients cause spatial and temporal genetic differentiation of an extensive algal bloom. J. Biogeogr. 43 (6), 1130–1142.

Goudet, J., 1999. PCA-GEN for Windows, V. 1.2. Institute of Ecology, Univ. of Lausanne. Hallegraeff, G.M., 1993. A review of harmful algal blooms and their apparent global increase*. Phycologia 32 (2), 79–99.

Hamilton, M., 2011. Population Genetics. John Wiley & Sons. Haubold, B., Hudson, R.R., 2000. LIAN 3.0: detecting linkage disequilibrium in multilocus data. Bioinformatics 16 (9), 847–849.

Hu, S., Townsend, D.W., Chen, C., Cowles, G., Beardsley, R.C., Ji, R., Houghton, R.W., 2008. Tidal pumping and nutrient fluxes on Georges Bank: a process-oriented modeling study. J. Mar. Syst. 74 (1–2), 528–544.

Jombart, T., 2008. Adegenet: a R package for the multivariate analysis of genetic markers. Bioinformatics 24 (11), 1403–1405.

Keafer, B.A., Churchill, J.H., McGillicuddy, D.J., Anderson, D.M., 2005. Bloom development and transport of toxic *Alexandrium fundyense* populations within a coastal plume in the Gulf of Maine. Deep-Sea Research Part II: Topical Studies in Oceanography 52, 2674–2697 19–21 SPEC. ISS.

Legendre, P., Andersson, M.J., 1999. Distance-based redundancy analysis: testing multi-species responses in multifactorial ecological experiments. Ecol. Monogr. 69 (1), 1–24.

Leong, S.C.Y., Murata, A., Nagashima, Y., Taguchi, S., 2004. Variability in toxicity of the dinoflagellate *Alexandrium tamarense* in response to different nitrogen sources and concentrations. Toxicon 43 (4), 407–415.

Li, Y., He, R., Manning, J.P., 2014. Coastal connectivity in the Gulf of Maine in spring and summer of 2004-2009. Deep Sea Res. Part II Top. Stud. Oceanogr. 103, 199–209.

Limeburner, R., Beardsley, R.C., 1982. The seasonal hydrography and circulation over nantucket shoals. J. Mar. Res. 40, 371–406.

Maranda, L., Anderson, D.M., Shimizu, Y., 1985. Toxicity of *Gonyaulax tamarensis* clones from eastern North American waters. Toxic Dinoflagellates 2, 349–350.

Martin, J.L., Legresley, M.M., Gidney, M.E., 2014a. Phytoplankton monitoring in the Western Isles region of the Bay of Fundy during 2007-2013. Can. Tech. Rep. Fish. Aquat. Sci. 3105.

Martin, J.L., LeGresley, M.M., Hanke, A.R., 2014b. Thirty years - *Alexandrium fundyense* cyst, bloom dynamics and shellfish toxicity in the Bay of Fundy, eastern Canada. Deep Sea Res. Part II Top. Stud. Oceanogr. 103, 27–39.

McGillicuddy, D.J., Townsend, D.W., Keafer, B.A., Thomas, M.A., Anderson, D.M., 2014. Georges Bank: a leaky incubator of *Alexandrium fundyense* blooms. Deep. Sea Res. Part II Top. Stud. Oceanogr. 103, 163–173.

Meirmans, P.G., Van Tienderen. P.H., 2004. Genotype and genodive: two programs for the analysis of genetic diversity of asexual organisms. Mol. Ecol. Notes 4 (4), 792–794.

Nagai, S., Lian, C., Hamaguchi, M., Matsuyama, Y., Itakura, S., Hogetsu, T., 2004. Development of microsatellite markers in the toxic dinoflagellate *Alexandrium tamarense* (Dinophyceae). Mol. Ecol. Notes 4 (1), 83–85.

Nagai, S., Nishitani, G., Sakamoto, S., Sugaya, T., Lee, C.K., Kim, C.H., et al., 2009. Genetic structuring and transfer of marine dinoflagellate *Cochlodinium polykrikoides* in Japanese and Korean coastal waters revealed by microsatellites. Mol. Ecol. 18 (11), 2337–2352.

Nei, M., 1973. Analysis of gene diversity in subdivided populations. Proc. Natl. Acad. Sci. 70 (12), 3321–3323.

Oksanen, J., Blanchet, F.G., Friendly, M., Kindt, R., Legendre, P., McGlinn, D., et al., 2016. Package "Vegan"—community ecology package. R-Package Version 2.4-6.

Pettigrew, N.R., Churchill, J.H., Janzen, C.D., Mangum, L.J., Signell, R.P., Thomas, A.C., et al., 2005. The kinematic and hydrographic structure of the Gulf of Maine Coastal Current. Deep. Sea Res. Part II Top. Stud. Oceanogr. 52 (19–21), 2369–2391.

Pilskaln, C.H., Hayashi, K., Keafer, B.A., Anderson, D.M., McGillicuddy, D.J., 2014. Benthic nepheloid layers in the Gulf of Maine and *Alexandrium* cyst inventories. Deep Sea Res. Part II Top. Stud. Oceanogr. 103, 55–65.

Pritchard, J.K., Stephens, M., Donnelly, P., 2000. Inference of population structure using multilocus genotype data. Genetics 155 (2), 945–959.

Raymond, M., Rousset, F., 1995. An exact test for population differentiation. Evolution 49 (6), 1280–1283.

Richlen, M.L., Erdner, D.L., McCauley, L.A.R., Libera, K., Anderson, D.M., 2012. Extensive genetic diversity and rapid population differentiation during blooms of *Alexandrium fundyense* (Dinophyceae) in an isolated salt pond on Cape Cod, MA, USA. Ecol. Evol. 2 (10), 2588–2599.

Rousset, F., De, S., Montpellier, U., Bataillon, P.E., 2008. GENEPOP' 007 : A Complete Re-Implementation of the GENEPOP Software for Windows and Linux. pp. 103–106.

Rynearson, T.A., Armbrust, E.V., 2005. Maintenance of clonal diversity during a spring bloom of the centric diatom *Ditylum brightwellii.* Mol. Ecol. 14 (6), 1631–1640.

Rynearson, T.A., Newton, J.A., Armbrust, E.V., 2006. Spring bloom development, genetic variation, and population succession in the planktonic diatom *Ditylum brightwellii*. Limnol. Oceanogr. 51 (3), 1249–1261.

Sassenhagen, I., Gao, Y., Lozano-Duque, Y., Parsons, M.L., Smith, T.B., Erdner, D.L., 2018. Comparison of spatial and temporal genetic differentiation in a harmful dinoflagellate species emphasizes impact of local processes. Front. Mar. Sci. 5 (October), 1–13.

Sjöqvist, C., Godhe, A., Jonsson, P.R., Sundqvist, L., Kremp, A., 2015. Local adaptation and oceanographic connectivity patterns explain genetic differentiation of a marine diatom across the North Sea-Baltic Sea salinity gradient. Mol. Ecol. 24 (11), 2871–2885.

Sundqvist, L., Godhe, A., Jonsson, P.R., Sefbom, J., 2018. The anchoring effect—long-term dormancy and genetic population structure. ISME J. 12 (12), 2929–2941.

Townsend, D.W., McGillicuddy, D.J., Thomas, M.A., Rebuck, N.D., 2014. Nutrients and water masses in the Gulf of Maine–georges Bank region: variability and importance to blooms of the toxic dinoflagellate *Alexandrium fundyense*. Deep. Sea Res. Part II Top. Stud. Oceanogr. 103, 238–263.

Van Dolah, F.M., 2007. Marine algal toxins: origins, health effects, and their increased occurrence Frances M. Van Dolah. Environ. Health A Glob. Access Sci. Source 108, 133–141.

Wright, S., 1949. The genetical structure of populations. Annals of Human Genetics. Ann. Hum. Genet. 15 (1), 323–354.

Yeh, F.C., Yang, R.C., Boyle, T.B., Ye, Z.H., Mao, J.X., 1997. POPGENE, the User-Friendly Shareware for Population Genetic Analysis 10. Molecular Biology and Biotechnology Centre, University of Alberta, Canada, pp. 295–301.

Table 1: Sampling dates and number of strains per sample used in this study.

Sample	Date	# of individuals
GBA	5/26	32
GBB	5/28	31
GBC	5/28	33
GBD	5/26	36
GBE	5/30	24
GBF	6/17	30
GBG	6/16	40
GBH	6/24	30
GBI	6/24	30
GBJ	6/23	24
GBK	7/3	19
NSA	5/3	29
NSB	5/20-21	39
NSC	5/28	35
BFA	5/7	28
BFB	5/14	18
BFC	5/24	31
BFD	6/12	38
BFE	6/26	31
BFF	7/2	31
BFG	7/10	20
BFH	7/24	38

Table 2: Environmental data of samples from GoM (obtained from the University of Maine GOMTOX Data Archives http://grampus.umeoce.maine.edu/gomtox/gomtox.htm).

	Nitrate+Nitrite (µM)	Silicate (µM)	Phosphate (µM)	Ammonium (µM)	Temp (°C)	Salinity (psu)	Sigmat (kg m^{-3})	Chlorophyll a (µg L^{-1})	Phaeopigments (µg L^{-1})
GBA	0.10	0.40	0.09	0.20	8.62	32.98	25.59	3.76	0.05
GBB	0.09	0.90	0.10	0.21	9.62	32.97	25.43	2.16	0.32
GBC	1.47	1.22	0.38	0.59	8.17	33.14	25.79	4.61	0.60
GBD	0.15	10.53	0.20	1.35	9.29	33.06	25.55	5.05	0
GBE	0.09	6.83	0.09	0.40	10.62	32.80	25.12	1.82	0.13
GBG	0.09	1.13	0.11	0.72	6.99	31.95	25.02	0.80	0.67
GBH	0.62	0.95	0.10	0.61	11.57	32.81	24.97	2.11	0
GBJ	0.11	1.40	1.22	0.28	11.73	32.38	24.61	0.77	0.03
GBK	0.09	0.03	0.03	0.04	14.04	32.90	24.56	1.48	0.26
BFC	6.63	10.17	0.41	0.16	6.29	29.58	23.24	1.77	0

Table 3: Pairwise comparisons of genotypic differentiation between clusters in GoM. Lower diagonal: F_{ST} values. Upper diagonal: p-values of the Fisher's exact test. Bold characters denote significance at α=0.05 after Bonferroni correction.

	Southern cluster	Northern cluster	Mixed cluster
Southern cluster	--	**Highly sign.**	**Highly sign.**
Northern cluster	**0.051**	--	**Highly sign.**
Mixed cluster	**0.061**	**0.088**	--

Table 4: Number of strains per sub-clusters (N), number of different clonal lineages (G), overall clonal diversity (G/N), allele diversity calculated with all strains (H_t) and excluding replicated genotypes (Ht unique).

	N	G	G/N	G (N=59)	G/N (N=59)	H_t	Ht (unique)
GB-Southern	212	72	0.34	27	0.46	0.49	0.63
GB-Mixed	86	45	0.52	37	0.63	0.55	0.64
GB-Northern	31	19	0.61	19	N/A	0.52	0.5
BoF-Southern	59	35	0.59	35	0.59	0.47	0.59
BoF-Mixed	18	13	0.72	13	N/A	0.50	0.53
BoF-Northern	158	62	0.39	30	0.51	0.51	0.63
NS-Southern	103	43	0.42	33	0.56	0.45	0.59

Figures

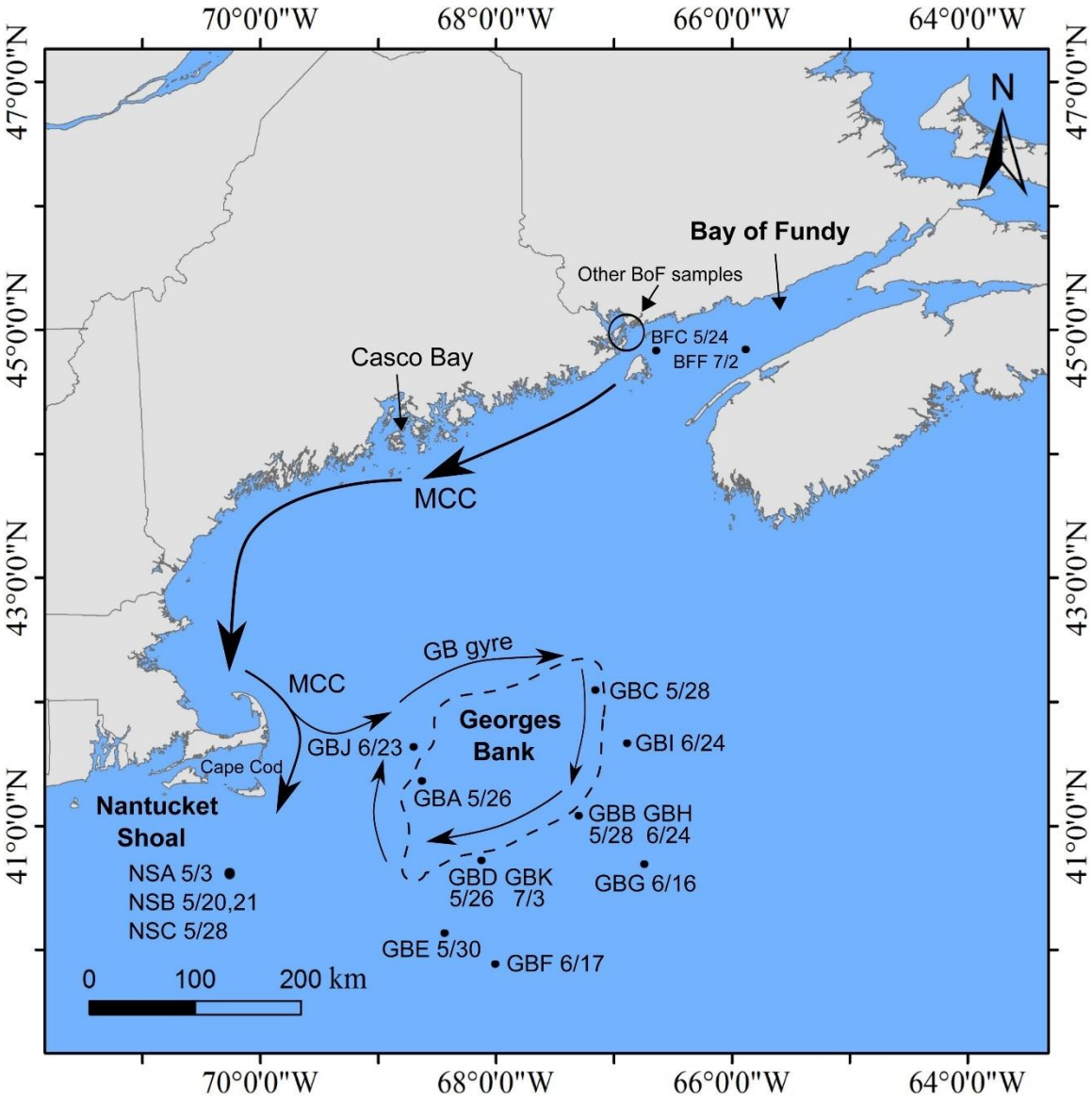

Figure 1. The location of samples in GoM. Sampling sites are indicated with black dots/circle. GB's location is shown in dashed outline, arrow lines indicate the Main Coastal Current (MCC) and GB gyre.

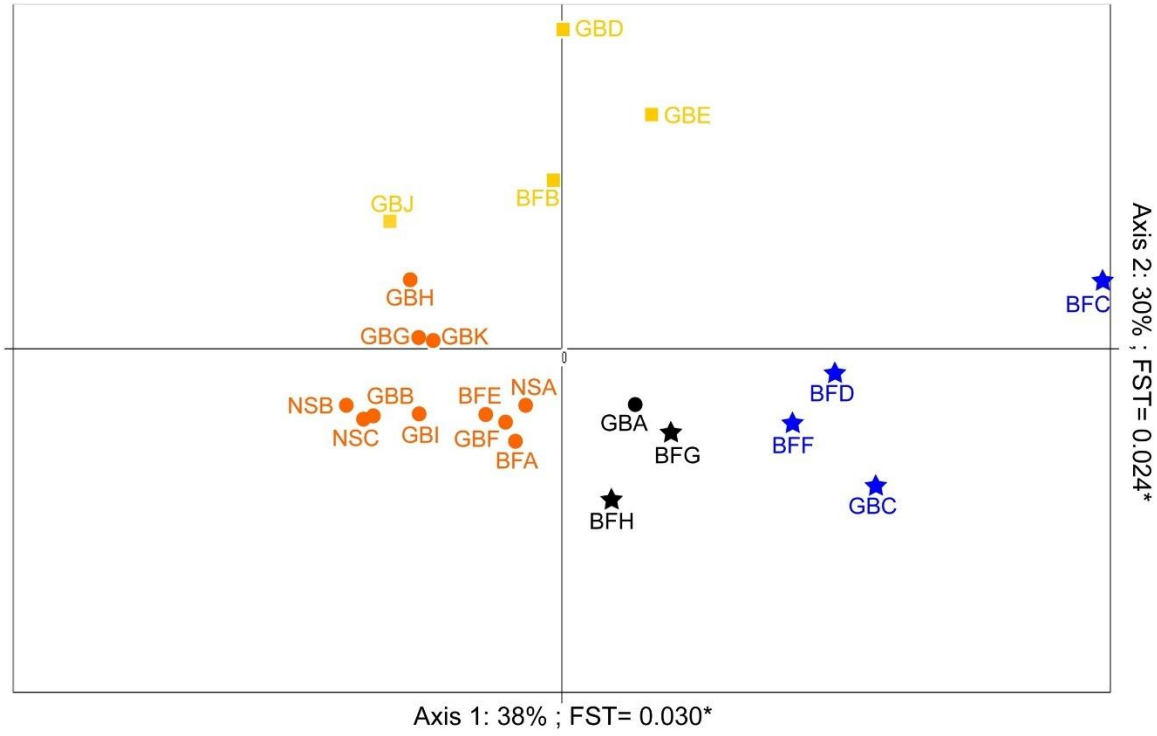

Figure 2: Principal Component Analysis (PCA) of a covariance matrix from the genetic data of **GoM**. Both axes are significant: Axis 1: percent inertia=38%, F_{ST}=0.030, p=0.004; Axis 2: percent inertia=30%, F_{ST}=0.024, p=0.000. Shapes correspond to the genetic clusters suggested by the AMOVA analyses (Circles=Southern Cluster; Stars=Northern Cluster; Squares=Mixed Cluster).

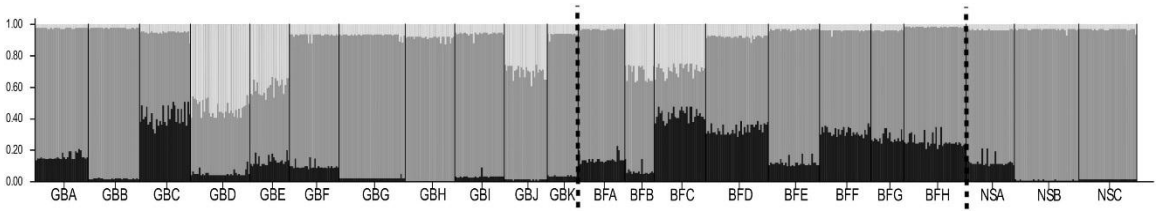

Figure 3: Population structure of **GoM** determined by Bayesian cluster analysis. Results of STRUCTURE analysis are presented for K=3. Dashed lines separate samples from different sub-regions in GoM. Colors of sample names correspond to the genetic clusters suggested by the PCA & AMOVA analyses (Orange=Southern Cluster; Blue=Northern Cluster; Yellow=Mixed Cluster).

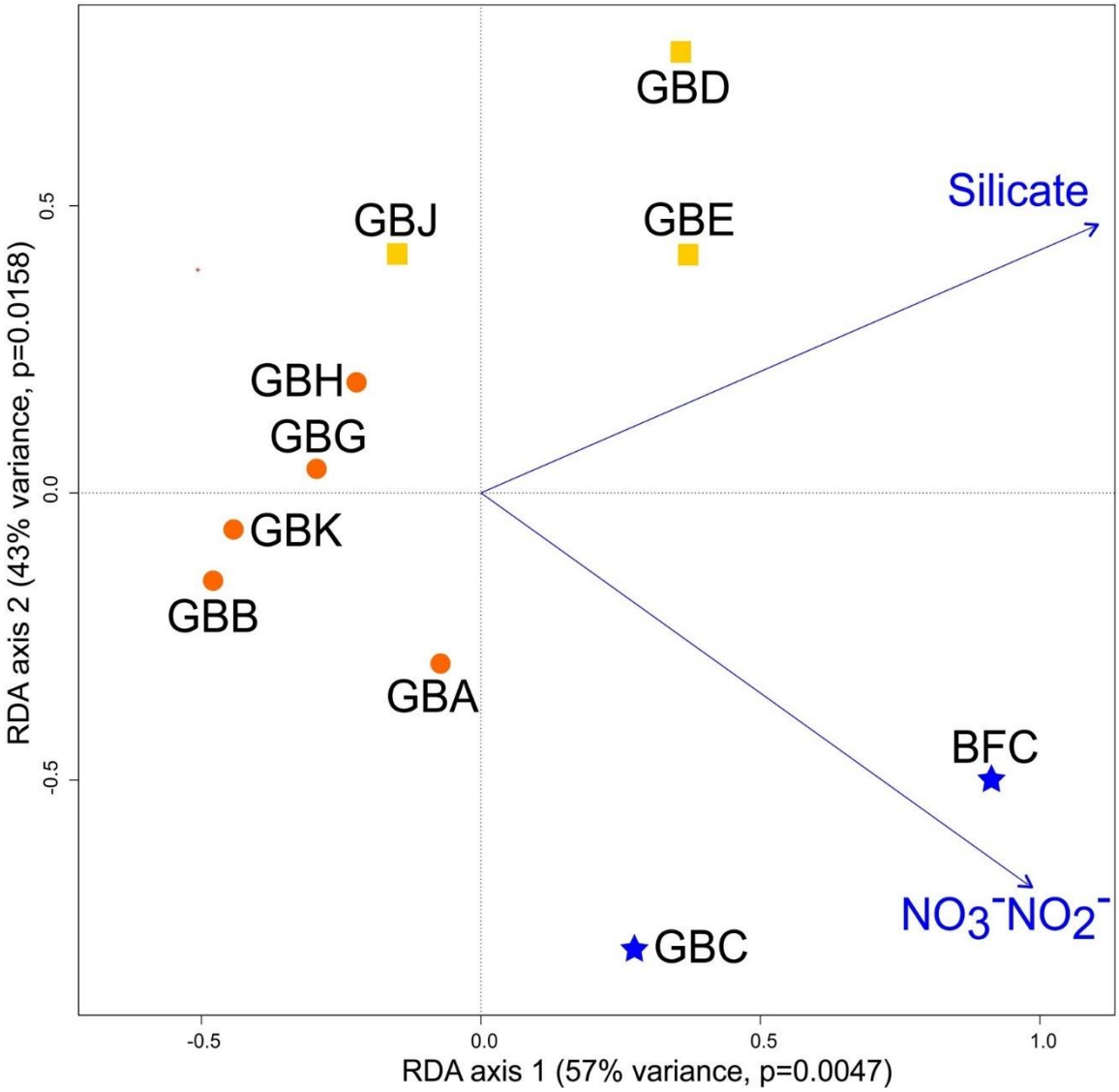

Figure 4: Environmental association analysis based on distance-based Redundancy Analysis (dbRDA). RDA plot for significant environmental factors (silicate, P=0.0068; nitrate+nitrite, P=0.0007). Colors correspond to the clusters suggested by the STRUCTURE analyses (Orange=Southern Cluster; Blue=Northern Cluster; Yellow=Mixed Cluster).